KWOOK

PROCEEDINGS

2nd WORKSHOP ON WIND ENGINEERING AND INDUSTRIAL AERODYNAMICS

28 to 30 August 1985

at
CSIRO Division of Energy Technology
Highett, (Melbourne), Victoria

ORGANIZING COMMITTEE

J D Holmes, CSIRO Division of Building Research
M C Welsh, CSIRO Division of Energy Technology
T G Hird, RMIT
J F Howell, Vipac Pty Ltd
B T Hawkins, CSIRO Division of Building Research
S A T Stoneman, University College, Swansea
K Hourigan, CSIRO Division of Energy Technology

Following the successful workshop held in July 1984, a 2nd Workshop on Wind Engineering and Industrial Aerodynamics was held from August 28 to 30, 1985. The dates were chosen to coincide with the visits to CSIRO of Dr Stewart Stoneman of University College, Swansea, and to R.M.I.T. of Dr Peter Bearman of Imperial College, London. Dr Peter Jackson from Auckland University and Dr Tony Bowen from the University of Canterbury attended the Workshop as guests of the Australian Wind Engineering Society.

The Workshop was divided into the following sessions:

Environmental Aerodynamics, including wind flow over hills and dispersion of pollutants
Wind loads on structures
Vehicle Aerodynamics
Duct flow, Jets and Combustion
Bluff body aerodynamics

The discussion sessions were recorded and are available on cassette tapes.

Aknowledgments

Acknowledgments are due to the Chief, CSIRO Division of Energy Technology, for permission to use the facilities of the Division. Vipac Pty Ltd kindly provided the cost of printing the Proceedings. The assistance of Mr R V Crowle, Ms F Geermans and Mr D Israel during the running of the Workshop are gratefully acknowledged by the Organizing Committee.

The Photographs on the front cover show:

(a) Flow visualization during acoustic resonance in a duct with baffle plates, simulating a rocket motor (courtesy of M C Welsh, CSIRO Division of Energy Technology).

(b) Flow visualization of flow around a truck (courtesy of T G Hird, RMIT).

(c) Wind tunnel models of the Askervein Hill in the A.E.S. wind tunnel, Toronto, Canada (courtesy of A J Bowen, University of Canterbury).

SPONSORS

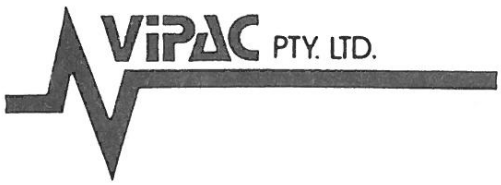

Royal Melbourne Institute of Technology
Department of Mechanical and Production Engineering

WORKSHOP ON WIND ENGINEERING
AND INDUSTRIAL AERODYNAMICS

Lecture Theatre, Division of Energy Technology
CSIRO, Highett, Victoria

PROGRAM

WEDNESDAY 28th AUGUST

9.00 a.m. Opening of Workshop
Dr D C Gibson, Chief, Division of Energy Technology

9.15 a.m. Session I. Environmental Aerodynamics
Chairman: Professor W H Melbourne, Monash University

"The Askervein Hill Experiments"
A J Bowen, University of Canterbury, New Zealand

"Wind Tunnel Studies of Turbulent Flow over a Two-dimensional Ridge"
J J Finnigan and M Raupach, CSIRO Division of Environmental Mechanics

"Codification of Topographical Effects"
P S Jackson, University of Auckland

"Terrain Blocking of Large Scale Flows"
W W Moriarty, Bureau of Meteorology

"The Wind in a Broad Valley - the LaTrobe Valley of Victoria"
P C Manins, LaTrobe Valley Airshed Study

"Plume Concentration Statistics in the Atmospheric Boundary Layer"
B L Sawford, CSIRO Division of Atmospheric Research

"The Development of a Boundary Layer in a Portable Wind Tunnel"
J H Tubb and G H Moore, Western Australian Institute of Technology

11.15 a.m. Morning Tea

11.30 a.m. Session ID - Discussion Session
Chairman: Dr P S Jackson, University of Auckland

12.30 p.m. Lunch - Division of Energy Technology Canteen

1.30 p.m. Session II - Wind Loads on Structures
Chairman: Dr A J Bowen, University of Canterbury

"Atmospheric Boundary Layer Simulation in Two Wind Tunnels"
K C S Kwok and P A McDonald, University of Sydney

"Point Pressure Measurements on Model Circular Storage Bins, Silos and Tanks"
P A McDonald, K C S Kwok, University of Sydney and J D Holmes, CSIRO, Division of Building Research

"Wind Loads on Grandstand Roofs"
W H Melbourne and J C K Cheung, Monash University

"Total Load Measurements on Attached Canopies"
E D Jancauskas, James Cook University

"Wind Loading on Porous Cladding"
J C K Cheung and W H Melbourne, Monash University

"Wind-induced Force at the Truss/Wall Connections in a Low-Rise Building"
E D Jancauskas, J A Harris, James Cook University

"Wind Loading on Tent Structures"
P S Jackson, University of Auckland

3.30 p.m. Afternoon Tea

3.45 p.m. Session IID - Discussion Session
Chairman: Dr J F Howell, VIPAC

5.30 p.m. General Meeting - Australian Wind Engineering Society
Chairman: Dr J D Holmes, CSIRO

7.00 p.m. Drinks at Brighton Savoy Motel

7.30 p.m. Dinner in Wellington Room, Brighton Savoy Motel

THURSDAY 29th AUGUST

9.00 a.m. Session III - Vehicle Aerodynamics
Chairman: Dr J W Saunders, RMIT

"A Review of Some Problems in Road Vehicle Aerodynamics"
P W Bearman, Imperial College, London

"Correlation Between Scale Model Wind Tunnel Tests and Full Scale Fuel Consumption"
T G Hird and S Watkins, RMIT

"An On-Road Testing Procedure for Determining Underbody Pressure Distributions on Vehicles"
P Cenek and J W Docherty, Central Laboratories, Ministry of Works and Development, New Zealand

"The Wind Environment Experienced by Moving Vehicles"
S Watkins, RMIT

"Automotive Engine Cooling System Design with Particular Reference to Air Circuit Components"
C Y L Chan and P I Cooper, CSIRO, Division of Energy Technology

"Effect of Ram Air and Fan Air on Automotive Heat Exchanger Performance"
P I Cooper and C Y L Chan, CSIRO, Division of Energy Technology

11.00 a.m. Morning Tea

11.15 a.m. Sessions IIID - Discussion Session
Chairman: Dr P W Bearman, Imperial College

12.30 p.m. Lunch

1.30 p.m. Session IV - Duct Flow, Jets and Combustion
Chairman: Dr P I Cooper, CSIRO, Division of Energy Technology

"Acoustic Properties of Plates in Tandem"
S A T Stoneman, University College, Swansea, U.K., M C Welsh, CSIRO and R Parker, University of Swansea

"Duct Resonance in High Pressure Ratio Thrust Augmenting Ejectors"
A M Abdel-Fattah, Aeronautical Research Laboratories

"The Start-up Behaviour of a Gas-turbine-ejector-long-stack System"
M Somogyi and G E Pleasance, Herman Research Laboratories State Electricity Commission of Victoria

"Measurements of Reynolds Stresses in Duct Flow by Hot Wire Anemometry"
J D Hooper, CSIRO, Division of Mineral Engineering

"Pressure Fluctuation Transmission in Small Diameter Tubes - Comparison of Theory and Experiment"
J D Holmes and R E Lewis, CSIRO, Division of Building Research

3.30 p.m. Afternoon tea

3.45 p.m. Session IVD - Discussion Session
Chairman: Dr J D Hooper, CSIRO, Division of Mineral Engineering

5.30 p.m. Session close

FRIDAY 30th AUGUST

9.00 a.m. Session V - Bluff Body Aerodynamics
Chairman: Dr S A T Stoneman, University College, Swansea

"Effects of Wind Tunnel Blockage on Streamwise Surface Pressures"
P J Saathoff and W H Melbourne, Monash University

"Flow Over a Blunt Flat Plate"
L W Welch, K Hourigan and M C Welsh, CSIRO, Division of Energy Technology

"Pressures on Surface-mounted Rectangular Plates"
J D Holmes, CSIRO, Division of Building Research

"The Interaction of Shear Layers with Obstacles in a Flow"
B R Morton, Monash University

"Numerical Simulation of Separated and Reattached Flows: Effect of Acoustic Field on Heat Transfer"
K Hourigan and M C Thompson, CSIRO, Division of Energy Technology

"Aeroelastic Analysis of Sails"
P S Jackson, University of Auckland

11.00 a.m. Morning Tea

11.15 a.m. Session VD - Discussion Session
Chairman: Professor B R Morton, Monash University

12.30 p.m. Lunch

1.30 p.m. Session VID - General Discussion Session
Chairman: Mr M C Welsh, CSIRO Division of Energy Technology

3.30 p.m. Closure of Workshop

4.00 p.m. Airport transport available

THE ASKERVEIN HILL EXPERIMENTS

A.J. Bowen*

Summary

A co-operative full-scale experiment to measure the wind flow and turbulence characteristics over a low smooth hill is described and some typical field results presented. This field experiment together with associated numerical prediction and wind-tunnel modelling programmes,have provided an excellent data set for the study of boundary-layer flow over low hills.

Introduction

This paper reports on the Askervein Hill project which was established in June 1982 as Task VI of the International Energy Agency Programme of Research and Development on Wind Energy Conversion Systems (Study of local Wind Flow at Potential WECS Hill Site). The participants in the project are Canada (Operating Agent), Denmark, Germany, New Zealand and the United Kingdom. The objective is to improve our understanding of the boundary-layer flow over relatively low smooth hills by carrying out a major co-operative field experiment to measure in detail, the spatial characteristics of mean wind and turbulence over a typical wind-turbine hill site. A suitable hill called Askervein was previously located in the Outer Hebrides and a preliminary field test was carried out in September-October 1982 with the main field study one year later. Full details of these two co-operative field experiments and the accumulated data are given in [1] and [2].

These data will also be used to assess the accuracy of a number of supplementary wind-tunnel model tests (some of which have already been reported in [3],[4]) and a numerical prediction model [5],[6] developed at AES, Canada. A series of journal papers is being prepared to cover the field, model and numerical activities. By an intercomparison of these data, it is hoped to refine the numerical and wind-tunnel modelling techniques to ensure that they adequately simulate the full-scale flow. The techniques can then be applied to other sites with confidence avoiding the necessity for complex and costly full-scale measurements. The accumulated field and model data and the experience gained will also be invaluable for other wind engineering applications, particularly for the prediction of wind loading on structures at exposed hill sites.

Askervein Hill Site and Field Tests

Askervein is an isolated hill of elevation 126 m ASL located near the west coast of the island,South Uist in the Outer Hebrides, Scotland. The smooth hill is elliptical in plan with a 2 km long major axis orientated near the NW-SE direction and a 1 km long minor axis. A 2 m contour interval map of Askervein is shown in Figure 1. To the west of the hill, from which sector the majority of the winds blew during the field tests, there is a flat uniform fetch of 3 to 5 km covered by heather, grass and low rocks to the coastline. The estimated surface roughness length, $Z_o \simeq 0.03$ m. The western foot of the hill has an approximate elevation of 10 m giving a hill height $h = 116$ m for winds from this sector. A typical value of $L = 220$ m, defined as the distance from the hilltop to the upstream point where the elevation is half its maximum, may be taken for this sector, giving a value of $h/L \simeq 0.53$. The summit of the hill is marked as HT on Figure 1 and a second position called Centre Point (CP) was chosen as an additional reference point marking the centre of the wind-tunnel models. A Base Station (BS) was established near the foot of the hill to assist the field activities, while an upstream Reference Site (RS) (not shown) was located about 3 km to the SSW of the hill for detailed measurements of the undisturbed wind flow prior to its modification by the hill.

*Department of Mechanical Engineering, University of Canterbury, Christchurch, New Zealand.

The preliminary 1982 field test was mainly concerned with mean-flow measurements whilst the main 1983 test recorded both turbulence and mean-flow data. On both occasions 50 m towers were deployed on the hilltop (HT) and at the upwind reference site (RS). These masts supported sonic, propeller and cup anemometers to measure vertical profiles. In addition to some 30 m and 16 m towers, about fifty 10 m posts and towers were deployed along the lines A, AA and B indicated in Figure 1, carrying one cup anemometer each at a height of 10 m. In the 1983 field test, line A was instrumented with 3 component propeller anemometers for detailed turbulence measurements. Airsonde and Tala kite profiles provided additional profiles for heights above 50 m. During the main 1983 test intensive measurements were taken over a two week period for wind directions in the 140° - 285° sector with 10 m mean wind speeds at RS between 5 and 15 m/s. Over this period, 95 hours of mean wind and 30 hours of turbulence data were successfully recorded [2].

Results and Discussion

Some typical field data are presented here to indicate the extent of some changes to the mean flow and turbulence due to the presence of the hill. Figure 2 shows the mean velocity and horizontal RMS turbulence velocity $\sigma_h(\sim\sigma_u)$ profiles above HT compared with the undistorted upstream profiles at RS. The data were taken using cup anemometers during Askervein '82 [1] with a wind direction of 235°, nearly normal to the major hill axis.

Current understanding of the effects of smooth low 2D hills on the mean wind flow is largely based on the analytical theory presented by [7]. A useful measure of the modification to the mean flow speed is given by the fractional speed-up ratio,

$$\Delta S = [U(\Delta Z) - U_o(\Delta Z)]/U_o(\Delta Z) = \text{Amplification} - 1$$

where $U(\Delta Z)$ is the local mean velocity at a height ΔZ above the local terrain and $U_o(\Delta Z)$ is the undisturbed upstream velocity at the same height ΔZ. A recent paper [8] reviews simple prediction rules for estimating the maximum values of ΔS near the surface over a hill. Using these rules for Askervein for the field test conditions gives a maximum ΔS value = 1.8 h/L ~1.0 at HT which agrees quite well with the measured ΔS profile in Figure 2. This large increase in velocity is directly responsible for the general decrease in turbulence intensity (shown in Figure 2 as the fractional change in turbulence intensity $\Delta\tilde{T}$, defined in the same manner as ΔS above). However there is also a substantial decrease in σ_u evident in Figure 2 as predicted by [9] and others using rapid distortion theory, but the expected increase in σ_u in an inner-layer close to the hill top surface where there is a substantial increase in shear stress, is not clear. Figure 3 presents data for a typical run during Askervein '83 [2] showing the variation of conditions over the hill along line A at a constant height ΔZ = 10 m above the hill surface. The large increases in turbulence on the lee side are probably associated with flow separation.

Preliminary comparisons between the full scale, the wind tunnel and numerical modelling test results have been very encouraging and will be the subject of further publications.

Acknowledgements

The Askervein experiments were conducted as a collaborative effort involving groups from six organisations in five countries, all of whom contributed in various ways to the success of the programme and are too numerous to mention here. However the generous guidance and support from Dr H.W. Teunissen and Dr P.A. Taylor at the Atmospheric Environment Service, Canada where the author spent his recent study leave working on the Askervein experiments, are gratefully acknowledged.

References

[1] Taylor, P.A. and Teunissen, H.W. 1983: 'Askervein '82 Report on the September/October 1982 Experiment to Study Boundary-Layer Flow over Askervein, South Uist'. Atmospheric Environment Service Report MSRB-83-8.
[2] Taylor, P.A. and Teunissen, H.W. 1984: 'The Askervein Hill Project: Report on the September/October 1983 Main Field Experiment'. Atmospheric Environment Service Report MSRB-84-6.
[3] Teunissen, H.W. and Shokr, M.E. 1985: 'The Askervein Hill Project: Wind-tunnel simulation (smooth model) at length scale 1:1200'. Atmospheric Environment Service Report MSRB-85-.
[4] Bowen, A.J. and Teunissen, H.W. 1985: 'The Askervein Hill Project: Wind-tunnel simulation at length scale 1:2500'. Atmospheric Environment Service Report MSRB-85-.
[5] Walmsley, J.L., Salmon, J.R. and Taylor, P.A. 1982: 'On the application of a model of boundary-layer flow over low hills to real terrain'. Boundary-Layer Meteorol. 23, 17-46.
[6] Taylor, P.A., Walmsley, J.L. and Salmon, J.R. 1983: 'A simple model of neutrally stratified boundary-layer flow over real terrain incorporating wave number-dependent scaling'. Boundary-Layer Meteorol., 26, 169-189.
[7] Jackson, P.S. and Hunt, J.C.R. 1975: 'Turbulent wind flow over a low hill'. Quart,J.R.Meteorol. Soc., 101, 929-955.
[8] Taylor, P.A. and Lee, R.J. 1984: 'Simple guidelines for estimating wind speed variation due to small scale topographic features'. Climatological Bulletin 18 (2), 3-32.
[9] Britter, R.R., Hunt, J.C.R.and Richards, K.J. 1981: 'Airflow over a two-dimensional hill: studies of velocity speed-up, roughness effects and turbulence'. Quart. J.R. Meteorol. Soc., 107, 91-110.

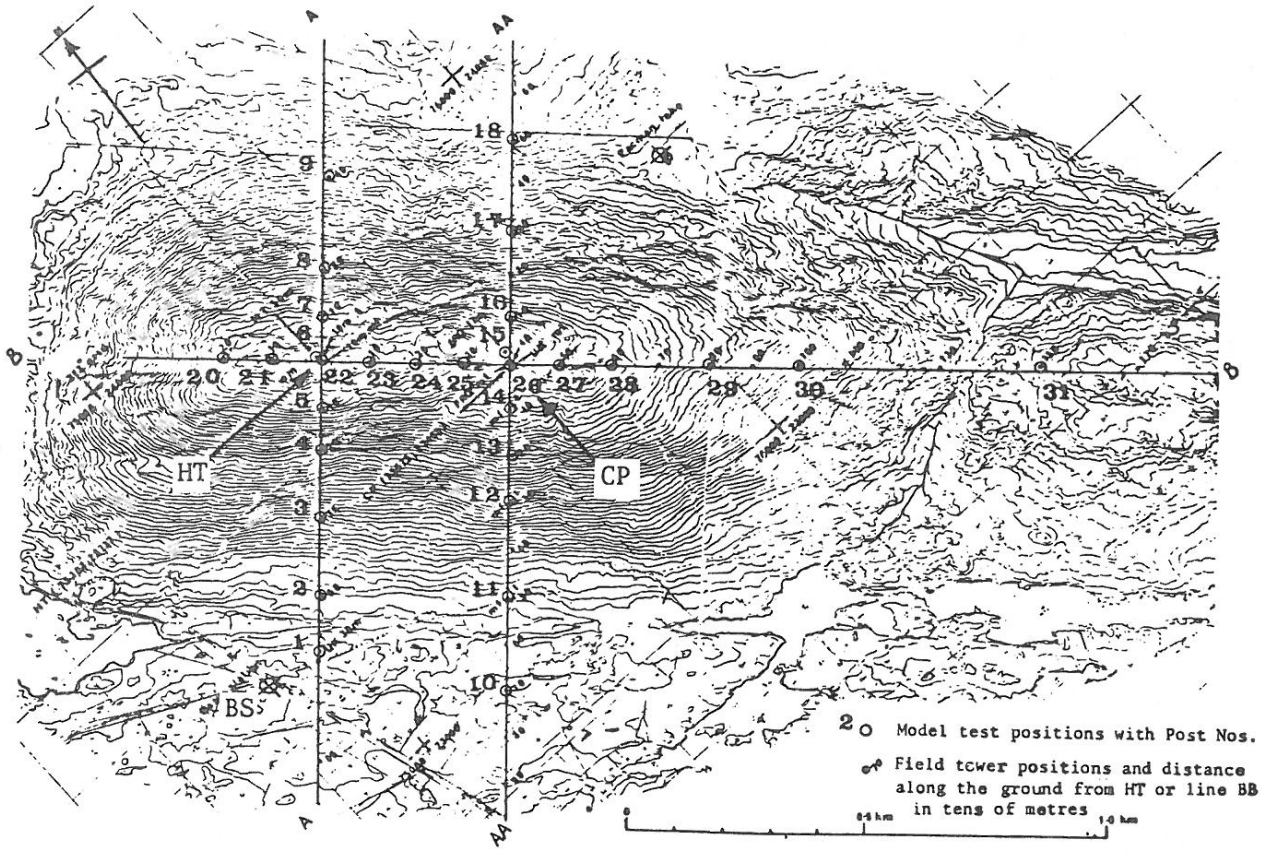

Figure 1. High resolution contour map of Askervein Hill (Contour interval 2m).

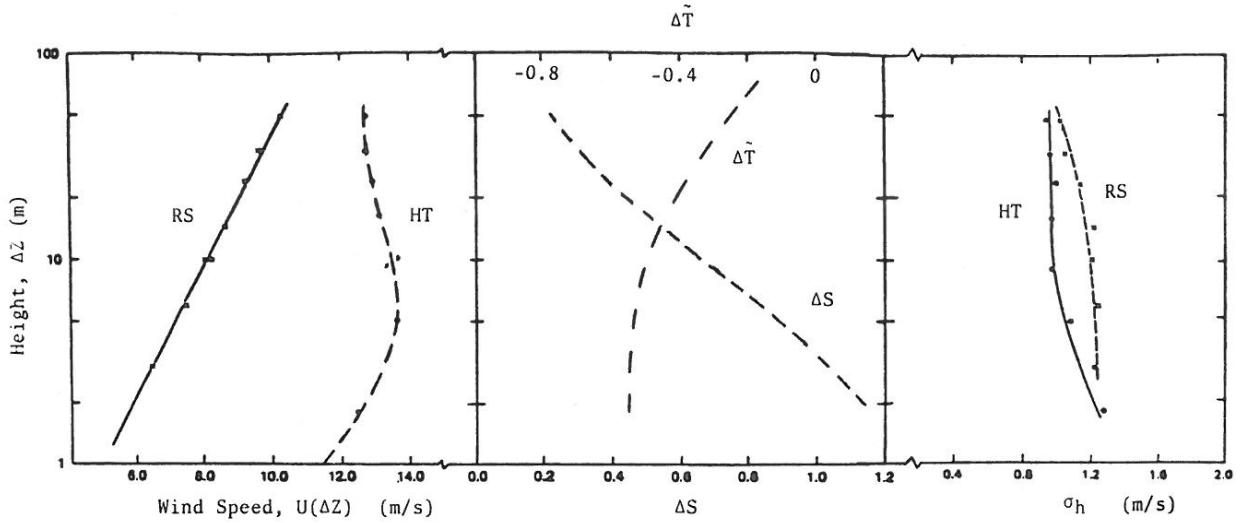

Figure 2. Typical field results from cup anemometerson 50 m towers at RS and HT from Askervein '82 for wind direction 235°, showing profiles of mean wind speed $U(\Delta Z)$, fractional speed-up ratio ΔS, standard deviation of the horizontal wind speeds σ_h and the fractional change in turbulence intensity $\Delta\tilde{T}$.

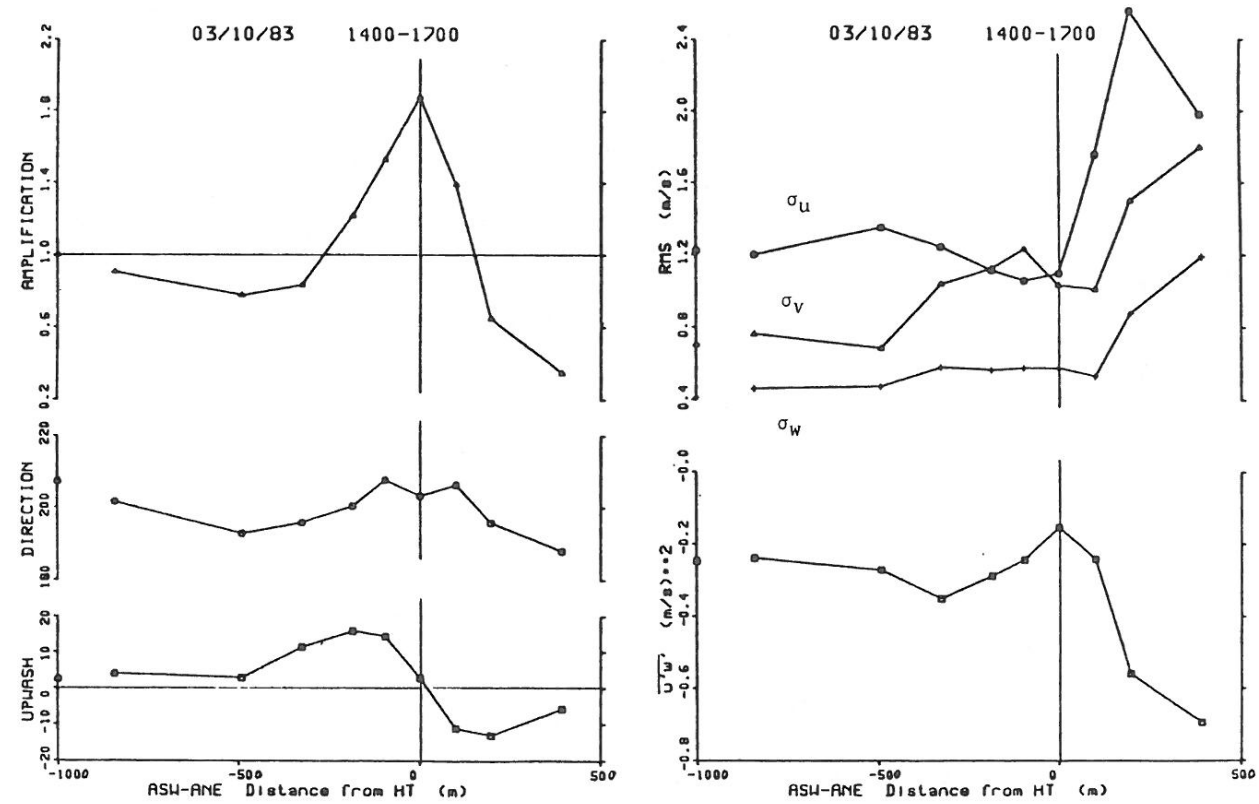

Figure 3. Variations of normalised wind speed (Amplification = ΔS + 1), direction, upwash angle, σ_u, σ_v, σ_w, and $-\overline{u'w'}$ at ΔZ = 10 m along line A during Askervein '83, run TU03A, wind direction 210°.

CODIFICATION OF TOPOGRAPHICAL EFFECTS

P S Jackson[1]

Introduction

Wind loading codes account for the effects of topography in many different ways. Some allow for an increase of speed of up to 20%, others have a more precisely defined 'escarpment rule' - the remainder either caution that topographical effects can be significant or ignore them altogether. However the last ten years have seen a great flurry of measurements of wind flow over hills, and it is now obvious that the allowance for speedup in loading codes is inadequate. It is not entirely obvious how to improve this situation, but this paper discusses some recent progress.

Loading codes should always be based on realistic physical models, and most studies of wind flow over hills have been interpreted in terms of the theory due to Jackson and Hunt (1975). In general this theory gives surprisingly good agreement with numerical, full-scale and wind-tunnel measurements, so as the flow structure proposed by the theory is quite simple it would seem to be the obvious starting point for development of design rules. The basic idea is that the flow has two discrete regions - a thin 'inner layer' next to the surface in which changes in shear stress are significant, and a much thicker 'outer layer' in which they are not important so that the velocity perturbation there can be predicted from potential theory. The pressure gradient generated by this outer flow also acts on the inner layer, where the velocities are much lower and therefore much more susceptible to pressure gradients. The induced changes in speed near the surface can thus be a large fraction of the incident speeds at the same height.

Maximum Speedup

There are several ways of quantifying this speed change. The ratio most favoured in the literature is the 'fractional speedup';

$$S = \{u(x, \Delta z) - U_o(\Delta z)\} \; / \; U_o(\Delta z)$$

where u is the speed at a *local* height of Δz above the surface. In regions where the pressure gradient is small (as at hill crests) one might expect the flow to be logarithmic close to the surface - that is, to be nearly in local equilibrium - which case S reduces to a constant. In practice this does seem to be the case, and this property of tending to a constant near the surface is the reason for the popularity of S as a speed-up parameter. One alternative is the 'nondimensional speedup'

$$\Delta u \frac{h}{L} = \{u(x,\Delta z) - U_o(\Delta z)\} \; / \; U_o(L)$$

where L is the hill length. This ratio is based on the scaling for the outer layer and is therefore independent of the method used for turbulence closure in the inner layer. However the problem is that actually *both* the above measures are relevant, but they apply in different regions of the flow. This can quite clearly be seen in Figure 1 (taken from Jackson, 1979) which is a numerical simulation of flow over a rounded ridge.

---

[1]Department of Mechanical Engineering, University of Auckland

For $Z = \Delta z/L > 0.05$ the curves for different values of surface roughness z_o collapse to a single curve for Δu, whereas near the surface the profiles are obviously all logarithmic with intercepts governed by z_o and therefore would collapse to a single curve for S. The height at which the changeover in flow structure occurs depends on the height of the inner layer, l, predicted by Jackson and Hunt (JH) from

$$l/z_o \ln(l/z_o) = 0.32\ L/z_o. \qquad (1)$$

There has been considerable argument over this length. This particular formula predicts some measurements quite well (Bradley, 1980) but is often found to overpredict the apparent inner layer thickness (Taylor *et al*, 1982). In Figure 1 the Δu curves peak at heights almost exactly half those given by this method. In practice the depth l can be quite large. For $L \sim 1$km and z_o in the range 1 - 1000mm the length l varies from 30m to 75m, so clearly the inner layer is often deep enough to immerse structures completely. It therefore seems sensible to start a design rule for *maximum* speedup based on the constant-value property for S near the surface. Taylor and Lee (1985) have quite recently proposed the following near-surface values for fractional speedup;

$$S_{max} = \begin{cases} 2.0\ h/L & \text{for 2-D ridges} \\ 0.8\ h/L & \text{for 2-D escarpments} \\ 1.6\ h/L & \text{for 3-D axisymmetric hills,} \end{cases} \qquad (2)$$

where here L is taken as the horizontal distance in which the hill falls to half its peak height h. Again there are several possible definitions of hill length, but this one seems to be winning in the literature. The numerical coefficients here have been selected by Taylor and Lee as average values of speedup obtained from measurements and numerical predictions.

This linear dependence of speedup on slope originally emerged from the JH theory and appears to be maintained right up to hill slopes at which separation begins (about 0.4 for ridges). Obviously once separation begins speedup does not continue to increase indefinitely with slope, and Taylor and Lee suggest an upper limit of 1.2 for S_{max}.

Spatial Variation of Speedup

A similar proposal for speedup has been made by BRE (1984) as;

$$S = 2\ s\ h/L \qquad (3)$$

where s is a 'speed increment coefficient' with a maximum value of 1.0 which takes account of positions other than that of maximum speedup. Here L is the *total* length of the slope, so this formula predicts only half the speedup of Taylor and Lee and is therefore too low. (Note that the working formula as given in the BRE document omits the h/L factor.) However the general formulation of this expression is a good one, but much more research is needed regarding the distribution of s for different hill shapes (the BRE reference uses some early wind-tunnel results).

The decrease in speedup with height (included in the s factor) is not easy to predict because different length scales are important at different heights from the ground. It seems clear that the flow near the hill crest is affected most by the 'sharpness' of the crest (hence the definition of L used by Taylor and Lee), but higher up the local topographical detail becomes less significant and the speed changes are more likely to be controlled by, say, the overall hill volume. This hypothesis is tested in Figure 2, where the outer flows from several numerical experiments are

plotted using a length scale L_v which gives each hill the same volume as the Witch of Agnesi, as follows:

Hill	Shape	Cross-sectional area	L_v
Witch	$(1 + x/L)^2$	π h L	L
cosine	$(1 + \cos \pi x/L)/2$	h L	L/π
Gaussian	$\exp(-(x/L)^2)$	h L $\sqrt{\pi}$	$L/\sqrt{\pi}$
triangular	$(1 \pm x/L)$	h L	$L/\sqrt{\pi}$

Here S_{max} is the limiting value of S near the surface at the crest, and the ratio S/S_{max} is plotted against height directly above the crest using the vertical scale $\Delta z/L_v$ in each case. This can be seen to produce a reasonably good collapse of the data to a single curve given approximately by -

$$S/S_{max} = (1 + 1.2 \Delta z/L_v)^{-2} \qquad (4)$$

The general form of this expression is suggested by the exact solution for the Witch of Agnesi in the outer region. A construction which is reasonably accurate at all heights is then;

$$S/S_{max} = \begin{cases} 1.0 & \text{for } \Delta z/l < 0.5 \\ \text{eqn (4)} & \text{for } \Delta z/l > 0.5 \end{cases} \qquad (5)$$

where l is given by equation (1). Although the JH theory would suggest that Δ u and not S would be the appropriate ratio for heights well above the surface, a code version would be confusing if more than one speedup were defined. Unfortunately it seems likely that it will then be necessary to use more than one definition of hill length, as shown above, but again more study of this point is needed.

There are several projects under way on full-scale and model-scale measurements of wind flow over hills. The Kettles Hill experiment carried out by the Canadian Atmospheric Environment Service is a good example (Taylor, *et al*, 1983, Teunissen *et al*, 1982). The results show very good agreement between full-scale measurements and numerical and wind-tunnel simulations. A similar experiment on a much grander scale is now under way at Askervien, and again preliminary AES wind-tunnel results show good agreement. It therefore seems likely that within even one more year there will be much more information available about the parameters discussed above (though it is perhaps equally probable that these experiments will raise more questions than they answer).

References

Bradley, E F (1980); *'An experimental study of the profiles of wind speed, shearing stress, and turbulence at the crest of a large hill'*; Quart J Roy Meteor Soc, 106, 111 - 124.

Building Research Establishment (1984); *'The assessment of windspeed over topography'*; BRE Digest 283.

Deeves, D M (1980); *'Computation of wind flow over two-dimensional hills and embankments'*; J Wind Eng and Ind Aero, 6, 89 - 111.

Jackson, P S and J C R Hunt (1975); *'Turbulent wind flow over a low hill'*; Quart J Roy Met Soc, 101, 929 - 955.

Jackson, P S (1970); *'The influence of local terrain features on site selection for wind energy generating systems'*; University of Western Ontario, Boundary Layer Wind Tunnel Lab Rep BLWT-1-1979.

Taylor, P A and R J Lee (1985); *'Simple guidelines for estimating wind speed variations due to small scale topographic features'*; submitted to Atmosphere Ocean.

Taylor, P A, R F Meikle, J R Salmon, H W Teunissen (1983) *'The Kettles Hill experiment - site description and mean flow resutls'*; Atmospheric Environment Service Rep ARQB-83-002-L.

Teunissen, H W, I R McLean and R G J Flay (1982); *'Wind-tunnel simulation of the planetary boundary layer over an isolated hill'*. Proc 4th Int Symp Wind Energy Systems, Stockholm, BHRA, U K.

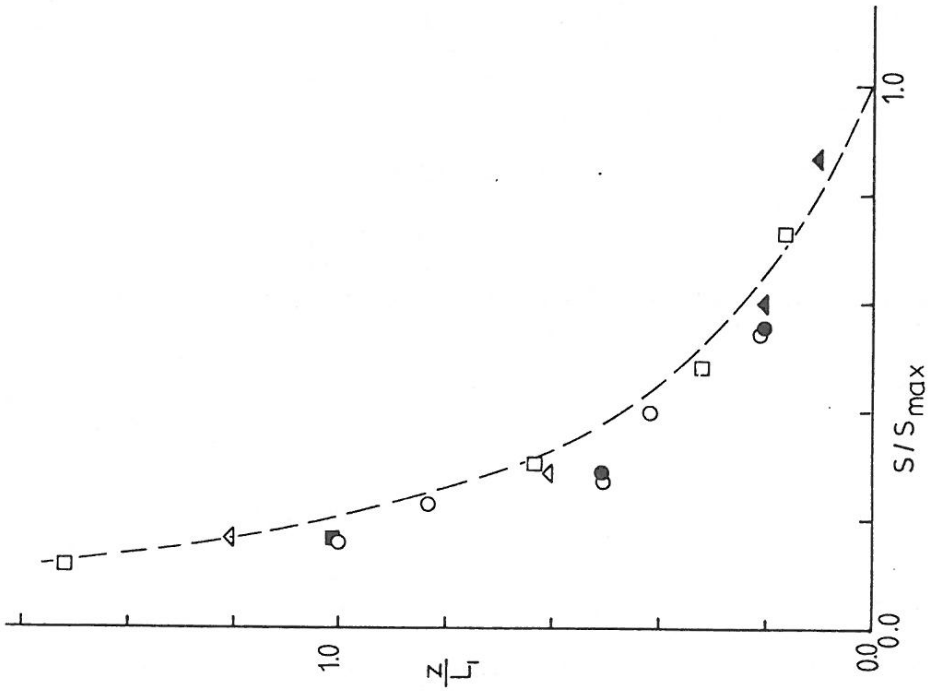

Figure 2 Change of speedup with scaled height above crest.
(Deaves - o Fig 3, △ Fig 6 ;
Jackson - □ Fig 2.23, ●▲ Fig 2.20)

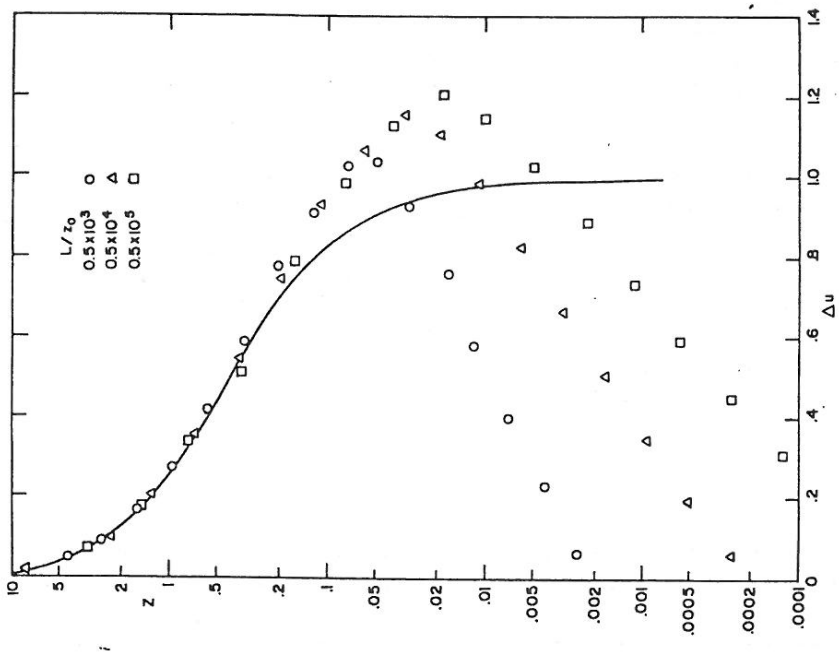

Figure 1 Nondimensional speedup over Witch of Agnesi
($^{h}/_{L}$ = 0.3, using Taylor numerical model)

TERRAIN BLOCKING OF LARGE SCALE FLOWS

W.W.Moriarty*

Introduction

When a stable wind stream approaches an obstacle there is a slowing down of the lower layers, and if the combination of obstacle height, vertical stability, and wind speed is right there is a layer near the ground which is "blocked" entirely from crossing the obstruction. This type of phenomenon may occur with obstructions over a range of scales.

A number of investigations have been conducted into this effect, using theoretical, numerical modelling, physical modelling, and/or observational approaches. Some studies have described aspects of the associated flow patterns, and some have attempted to determine the pre-requisite physical conditions. A number of authors have focussed in particular on the Froude Number of the flow ($F = U/(NH)$, U being the speed of the wind approaching the obstacle, N the Brunt-Vaisala frequency, and H the obstacle height), giving critical values for this quantity above which blocking will not occur (1,2,3,4, 5). However, there has been little agreement about this critical Froude No., the values given ranging from $1/\pi$ (1) to 2.3 (2).

In this paper we will be concerned with blocking produced by large mountain ranges, which has associated effects in the blocked layer not observed on smaller scales. As part of the blocking mechanism a low level mesoscale pressure ridge is formed on the windward side of the mountains, and this results in a distortion of the horizontal air flow (6). If the mesoscale ridge lasts for more than a few hours, a corresponding mesoscale flow may be set up, resulting in a low level wind maximum in the layers below mountain top, parallel to the range. Measurements made in the Antarctic (7) and in California (8) suggest that this wind maximum may extend over 100 Km windward from the mountain range, and when there is a totally blocked layer this may also reach over 100 Km upwind. At times there is a flow away from the mountains in the lowest layers.

To the east and south of Albury-Wodonga there is an arc of mountains, at distances varying from about 120 to 80 Km, which is of similar height to the mountains considered in the above mentioned work in the Antarctic and California. During an investigation of the air dispersion meteorology of the area (9) a number of upper air measurements were made under conditions with a north-westerly upper wind and apparent blocking in the low layers. In this paper these measurements and some concurrent measurements of surface winds by a network of anemographs will be considered, together with some of their implications.

The Observations

All except one of the upper air wind and temperature profile measurements available for this study were made early in the morning, close to sunrise. Fig. 1 shows the results in a typical case. Three layers may be distinguished,

* Head Office, Bureau of Meteorology, Melbourne, Australia.

corresponding to three of the layers found by Manins and Sawford (5) in their study of a flow blocked as it crossed a small valley (100 m deep). In the lowest layer there was a southeasterly flow with a strong inversion, showing the characteristics of a drainage wind. The surface winds over the whole Albury-Wodonga area on such mornings in fact showed the typical drainage wind flow pattern. Above the surface drainage flow was a layer of northeasterly to northerly winds. This layer would correspond to the near-stagnant blocked layer of Manins and Sawford, but due to the larger scale and longer duration of the blocking a mountain parallel wind had developed as in the cases discussed by Schwertweger (7) and Parish (8). Above this again there was the large scale flow. Manins and Sawford distinguished a layer of "sweeping wind" between the blocked layer and the ambient flow. This was a wind descending into the valley they were considering, below the level of the flanking hills. At Albury-Wodonga it did not prove possible to distinguish such a sweeping wind, partly perhaps because the flow was ascending a range rather than crossing a valley, but also because on the scale involved the corresponding vertical changes in the wind (if any) would have been hard to distinguish from vertical changes in the ambient flow.

The direction shears at the transition from the drainage wind layer to the blocked layer (A-A in Fig. 1), which usually occurred near the top of the surface inversion, and from the blocked layer to the ambient wind (B-B), were often quite sharp, as noted by Manins and Sawford in their case.

Profile measurements like that shown in Fig. 1 were made on 20 mornings. The thickness of the lowest drainage layer varied between 200 and 500 m, but was commonly close to 300 m. The thickness of the blocked layer was more variable, its top ranging from 500 m to 1700 m. Details are given in Table 1.

During the day following a morning with blocked flow the surface wind would sometimes develop to a general southeasterly to easterly flow over the whole Albury-Wodonga area; sometimes there would be general light and variable winds once the drainage flow ceased; sometimes there would develop a light easterly to northeasterly flow over part or all of the area; and sometimes there would develop a stronger northeasterly to northerly or northwesterly surface flow. The last of these developments corresponded to break down of the blocking pattern. The others would indicate different patterns of flow within the blocked layer. It is not proposed to consider this matter further here, except to note that there were a few occasions (not including any of the days with upper air observations) when blocking appeared to break down over part of the study area but not all of it.

Froude Numbers

To calculate Froude numbers from the available upper air measurements it was necessary to decide on: the effective height of the obstructing mountains; a method for estimating the speed of the ambient wind approaching the mountains; a method for estimating the effective vertical gradient of potential temperature; which air layers should be considered. It was taken that the arc of high mountains to the east and south were the cause of blocking, these being at an appropriate distance and of an appropriate height to produce such an effect, according to the observations of Schwertweger and of Parish. The effective height of these mountains was taken as 2000 m above sea level, or 1850 m above ground level at Albury-Wodonga. It was found that in most cases the winds between say 1500 and 2000 m were fairly steady with height, so their speed was taken as that of the incident wind. Finding the effective vertical gradient of potential temperature was a more difficult problem, as this gradient frequently varied considerably within the height ranges considered, and these variations

might be presumed to have an important effect on the air motion over obstacles. As a first trial it was decided to use an average value, taken from the observed profile, from the bottom of the layer being considered to the height of the obstruction i.e. to 1850 m. Froude numbers were calculated for three types of layer. In the early morning profile each day the drainage wind layer would have a temperature structure so modified by nocturnal cooling as to bear no relation to the original blocking mechanism. Hence it was decided to calculate a Froude number omitting this layer, that is, the number was calculated for the layer from the top of the drainage flow up to the mountain top. This layer should give a Froude number corresponding to blocking. Secondly, a Froude number was calculated for the layer above the top of the blocked layer i.e. for the layer from the top of the blocked layer up to mountain top. This layer should give a Froude number corresponding to absence of blocking. Thirdly a Froude number was calculated for the whole layer from ground level to mountain top for the time of daily maximum temperature, or, if there was break down of blocking during the day, for the time of this break down. For this last mentioned calculation it was necessary to assume that the upper winds had not changed from the early morning values , and that the temperature structure had not changed either except for an upward warming of the lowest layers from the ground. It might be expected that the third Froude number on a day of continuing blocking would correspond to blocking, and that on a day of blocking break down it would be close to the critical value.

It was found that all of the early morning blocked layers except two had Froude numbers less than or equal to 0.5, these having F values of 0.62 and 0.52. All of the morning layers above the blocking had Froude numbers greater than 0.5 except three, which had F values of 0.41, 0.44, and 0.48. There were nine days on which break down of blocking occurred, and in all cases the Froude number for the time of break down was between 0.47 and 0.55. On all the other days (except one when there was a frontal passage) the Froude number at the time of maximum temperature was less than 0.5. The results, then, point fairly strongly to a critical Froude number close to 0.5, a value found by Baines (3) using an hydraulic modelling technique, but by no other investigators.

The heights found for the top of the blocked layer showed a weak relationship to F (Fig.2). Katabayashi (2) also found a relationship, and Baines, examining a flow approaching a ridge with a gap, found a relationship between F and the level below which the flow was sluggish (blocked?). Since the arc of mountains near Albury-Wodonga has a significant gap near Omeo, Baines' relationship is shown in Fig. 2 for comparison.

Conclusion

Much work is needed to elucidate the behaviour of the air in regions where the flow is blocked by an obstruction, and in particular to resolve the conflict between different determinations of the Froude number which characterises the transition from a flow regime without blocking to one with blocking.

Acknowledgements

The measurements on which this discussion is based were made during an air dispersion survey of the Albury-Wodonga area conducted by the Bureau of Meteorology on behalf of the Albury-Wodonga Development Corporation.

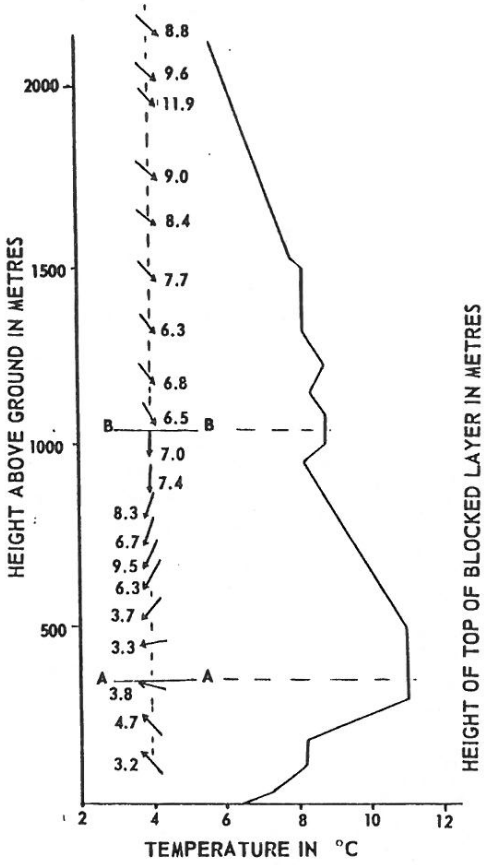

Figure 1. Profile of temperature and wind at sunrise on 16-9-79 at Albury-Wodonga. The wind speeds are given in m/s. Each wind is an average for the layer down to the next reading.

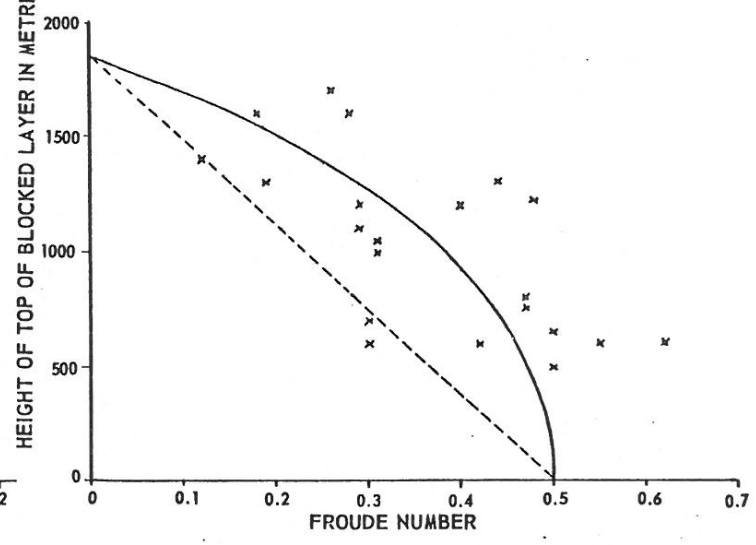

Figure 2. Height of the top of the morning blocked layer at Albury-Wodonga as a function of the Froude number for the layer extending from the top of the drainage layer (A-A in Fig.1) up to mountain top (1850 m). The dashed line gives a relationship found by Baines (3) between the Froude no. and the height of the top of the almost stagnant layer when a wind stream approaches a barrier with a narrow gap.

References

1. T.W.Kao, The phenomenon of blocking in stratified flow, J. Geoph. Res. 70, 815-822, 1965.
2. K. Katabayashi, Wind tunnel and field studies of stagnant flow upstream of a ridge, J. Met. Soc. Japan, 55, 193-203, 1977.
3. P.G.Baines, Observations of stratified flows past three-dimensional barriers, J. Geoph. Res. 84 C12, 7834-7838, 1979.
4. R.C.Bell and R.Thompson, Valley ventilation by cross winds, J. Fluid Mech. 96, 757-767, 1980.
5. P.C.Manins and B.L.Sawford, Mesoscale observations of upstream blocking, Q.J. Roy. Met. Soc. 108,427-34, 1982.
6. R.B.Smith, Synoptic observations and theory of orographically disturbed wind and pressure, J. Atmosph. Sc. 39, 60-70, 1982.
7. W. Schwertweger, Meteorological aspects of the drift of ice from the Weddell Sea towards the mid-latitude westerlies, J. Geoph. Res. 84, 6321-27, 1979.
8. T.P.Parish, Barrier winds along the Sierra Nevada Mountains, J. Appl. Met. 21, 925-30, 1982.
9. W.W.Moriarty, Winds, temperatures and air dispersion over the Albury-Wodonga area, Bureau of Meteorology Bulletin 52, Aust.Govt. Pub. Service, Canberra, 1985.

THE WIND IN A BROAD VALLEY - THE LATROBE VALLEY OF VICTORIA

P.C. Manins*

Introduction

Data on wind direction and speed at chimney top are essential for wind loading design and for determination of the chimney height necessary to meet air quality objectives. In Victoria, the latter requirement is detailed in a recently released procedure (EPAV 1985). For strong winds, small chimneys and flat terrain there is little difficulty in determining a representative wind at a height of 10m above ground level and extrapolating these wind data to the heights of interest. However, for the Latrobe Valley and the tall stacks of the State Electricity Commission of Victoria extrapolation techniques often fail in all but strong winds.

The Latrobe Valley is situated near the southern extremity of the Great Divinding Range and runs east-west some 100 km. It is approximately 30 km wide with the floor at an elevation of 50 to 100m (Fig.1). The Range to the north rises to typically 1000m with a coastal range to the south rising to typically 500m. The Valley opens out to the sea to the east, and is only weakly delineated to the west, with the floor rising to 200m near Warragul.

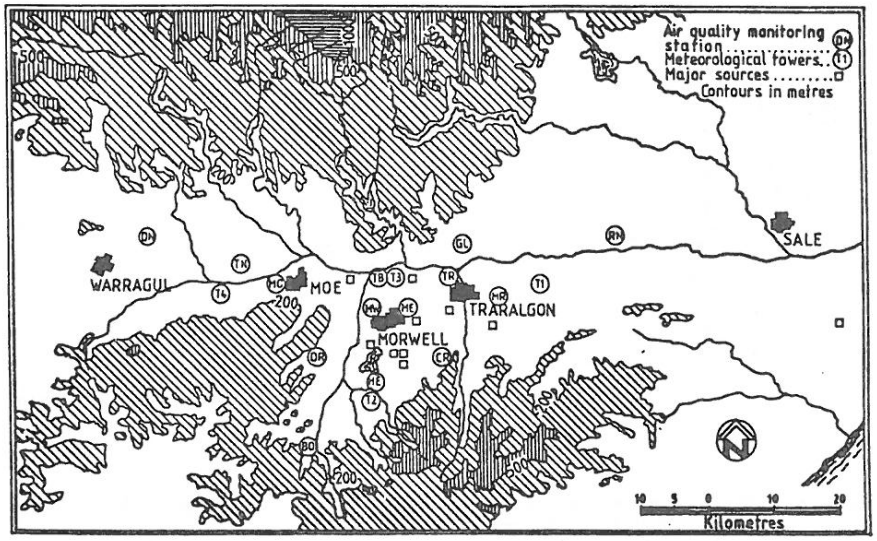

Figure 1. Latrobe Valley Air Monitoring Network.
Air Quality Stations: DN Darnum North; DR Driffield; BO Boolarra; HE Hazelwood Estate; CR Clarkes Road; GL Glengarry; TN Trafalgar North; MW Morwell West; TB Thoms Bridge; RN Rosedale North; MR Minniedale Road; MO Moe; TR Traralgon; ME Morwell East. Meteorological Towers: T1 Flynn; T2 Yinnar; T3 Thoms Bridge; T4 Trafalgar.

To help meet Airshed Study objectives regarding air quality climatology and pollutant dispersion modelling, the Latrobe Valley Air Monitoring Network has been progressively installed over the period 1979 to 1983. It consists of 14 surface air quality stations and 4 110m meteorological towers which log data (Table 1) each minute under the control of a central computer. These data are processed and stored on magnetic tape. The primary data file consists of validated 1h average values, but 1 min values in raw form are also available. Each parameter at any station or tower can be interrogated at any time from one of four remote terminals. The air quality instruments are checked amd calibrated automatically at midnight, and all instruments are regularly serviced and undergo periodic reference calibrations by SEC and EPA staff (Laws-Herd 1984).

Other data include radiosonde ascents from Minniedale Road for the periods April 1975 to April 1977 and December 1983 to March 1986, and acoustic sounder data, both facsimile and Doppler, for various periods. Four 2-week

* Latrobe Valley Airshed Study Project Director, c/o EPA, 5th floor, 240 Victoria Parade, East Melbourne, 3002, Australia.

intensive study periods comprising the Latrobe Valley Plume Tracking Experiment are presently underway (June 1984, March 1985, August 1985, February 1986) and these are giving additional upper air data, including direct measurements by aeroplane, of plume properties.

Table 1. LVAMN Measurements

(a) Air Quality Stations

Parameter	Height above Ground (m)	Stations
Nitrogen Oxide	3	All
Nitrogen Dioxide	3	All
Sulphur Dioxide	3	All
Ozone	3	Most
Carbon Monoxide	3	Towns only
Airborne Particulate Matter	3	All
Dry Bulb Temperature[1]	1	All
Wet Bulb Temperature[1]	1	All
Wind Speed	10.4[2]	All
Wind Direction	10.4[2]	All
Total Solar Radiation	2	Some
Ultra Violet Radiation	2	Some
Hi Vol Dust Sampler	2	All

(b) Meteorological Stations

Parameter	Height above Ground (m)[3]			
Air Temperature	10	25	50	110
Wind Speed	"	"	"	"
Wind Direction	"	"	"	"
Vertical Velocity	"	"	"	"
Dew Point Temperature	"			"
Rain Fall	Ground level			
Solar Radiation	"			
Net Radiation	"			
Soil Heat Flux	"			
Soil Temperature	"			

1. Stephenson's Screen. 2. Average, except Minniedale Road (13.1m), Moe (15.7m), Traralgon (15.8m).
3. Morwell West levels are 4,8,16,35m.

Winds Climatology

Consider, for example, the cumulative wind rose for all hours shown in Fig.2. The prevailing wind is westerly due, in part, to the phenomenon of channelling of the synoptic wind field. For strong winds extrapolation to around 1000m may be sufficiently accurate for some purposes, but upper level wind direction is crucial in determining air pollutant impact on particular localities and, as Fig.3 shows, this can be quite different on many occasions in the early morning.

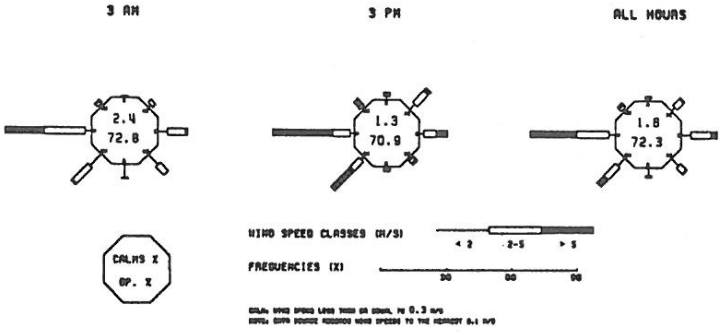

Figure 2. Cumulative wind rose for all hours obtained at Minniedale Road Air Quality Station for the period September 1979 to February 1985.

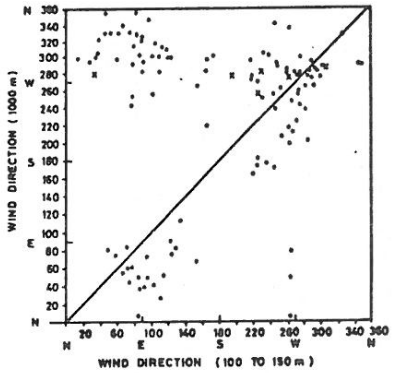

Figure 3. Relationship between wind direction in the layer 100 to 150m, and the wind direction at 1000m above the Minniedale Road Station at approximately 0800h over the period 1975-1977.

As discussed by Hoy (1985), the morning wind directions shown in Fig.3 at the levels of 1000m and 100m disagree by at least ±90° on 32% of occasions. The majority of these show typically upper-level north-westerly winds with lower-level easterly winds. Hoy concluded from his study that a three-level flow pattern is suggested on these occasions, with slope or drainage flows in the height range 10m to possibly 100m, an intermediate low-level easterly flow pattern above these from about 100m to possibly as much as 700m, and the large scale flow becoming predominant above this level. The low-level easterly flow is generally isolated from the overlying north-westerly wind by a temperature inversion and the strength of the flow is proportional to the synoptic pressure gradient.

There is no obvious single reason for the strong changes of wind direction with height shown in Fig.3. Hoy (1985) contends that it is usually associated with a lee trough - turning at lower levels due to Coriolis restoring force downwind of a long ridge, the Great Dividing Range. However, the dependence on pressure gradient indicates a role for mesoscale interaction with topography and surface roughness as well. Laboratory studies (Manins 1983) have indicated that a mesoscale eddy in the lee of the Range may also contribute on occasions when the ambient thermal stratification is signficant, much as it does for Melbourne during some easterly winds (Spillane 1978; EPAV 1985).

Thermal Influences

Consideration of upper air data from the first and second campaigns of the Plume Tracking Experiment (winter, June 1984; summer, March 1985 respectively) has shown that the degree of observed wind shear with height in the Latrobe Valley is strongly influenced by, but not determined completely by, the ambient thermal stability and this in turn depends on the strength of the upper-level winds and the time of day (Fitzgerald 1984).

At the risk of over-simplifying the picture, the conditions can be described in terms of a Froude Number, $F = U/NH$, where U is wind speed at about 1000m, N is the buoyancy frequency (a measure of the thermal stability, say between 100m and 1000m) and H is the height of the Range above Valley floor. F expresses the relative importance of wind mixing (U) to stabilization due to thermal stratification (NH). Thus if the conditions are characterised by large F the wind will be channelled by the topography, and wind-related problems are readily describable. If F is small, the airflow pattern is complex in the Valley and changes strongly with time of day when solar heating causes boundary layer growth. Air pollution problems will be difficult, with possibilities of fumigation of pollutants trapped aloft during the mornings and recirculation of pollutants in the Valley mesoscale flows during the day.

Conclusion

The Latrobe Valley Airshed Study has produced a long time-series of surface wind data at 19 stations and up to 3 km above the ground at a special-purpose radiosonde station. The winds observed are complex due to interaction of the flow with thermal stratification and the terrain. The data set and supporting documents are available for research use.

References

EPAV 1985. Plume Calculation Procedure an approved procedure under Schedule E of the State Environment Protection Policy (The Air Environment). Environment Protection Authority of Victoria. Publication 210.

EPAV 1985. The Impact of Emissions from Newport D Power Station on air quality. A Report by the Melbourne Airshed Study. Environment Protection Authority of Victoria. June 1985 320pp ISBN 0-7241-2973-1.

Fitzgerald, W.R. 1984. Editor: Study of plume dispersion characteristics. NERDDP Project 704 Progress report for 1984. State Electricity Commission of Victoria. Research and Development Report No. NP/84/007.

Hoy, R.D. 1985. Upper winds and mesoscale easterly flows in the Latrobe Valley. Preprint.

Laws-Herd, K. 1984. The Latrobe Valley Air Monitoring Network: Criteria pollutant measurements and results. Proceedings of the Eighth International Clean Air Conference. Ed: H.F. Hartmann, J.N. O'Heare, J. Chiodo and R. Gillis. Melbourne, Australia, 7-11 May 1984, v2, 471-484.

Manins, P.C. 1983. Nocturnal air circulation in the Latrobe Valley. Clean Air (Aust.), 17, 29-32.

Spillane, K.T. 1978. Atmospheric characteristics on high oxidant days in Melbourne. Clean Air (Aust.), 12, 50-56.

PLUME CONCENTRATION STATISTICS IN THE ATMOSPHERIC BOUNDARY LAYER

B.L. Sawford*

Introduction

The concentration at a fixed point in a turbulent plume is highly variable, with standard deviation comparable to or greater than the mean value, significantly skewed and is zero for a significant fraction of the time. A complete description of the concentration field thus requires knowledge of the variance, skewness and higher moments in addition to the mean. Indeed, Barry [1] and more recently Chatwin [2] argue that we should be concerned with the frequency distribution of concentration.

This more complete description is of practical importance because (i) it is necessary in order to describe and predict short-term high exposures to air pollution; (ii) the concentration variance is a direct measure of the statistical uncertainty in measurements or predictions of the mean; (iii) the rate of turbulent chemical reactions depends on the reactant concentration covariance; (iv) assessment of the hazard risk from leakage of flammable gases depends on the instantaneous concentration field.

In this paper we examine the relative effects of large- and small-scale (compared with the plume) turbulent motions on concentration statistics by comparing conditional or "in-plume" statistics (zero readings excluded) and unconditional statistics for a set of concentration measurements made in ground-level plumes in the atmosphere.

2. Conditional/Unconditional Relationships

Once the fraction of non-zero readings (the intermittency, I) in a (concentration) time series is known, there exist very simple relationships between conditional and unconditional statistics and for many purposes the zeros represent redundant information. We are interested in the frequency distribution, $P(\theta)$, defined as the probability that the concentration, C, equals or exceeds θ and the nth concentration moment,

$$\overline{C^n} = -\int_0^\infty \theta^n \, dP(\theta) \quad .$$

Using subscript "p" to denote conditional or "in-plume" statistics, we have

$$P(\theta) = I \, P_p(\theta) \tag{1}$$

and

$$\overline{C^n} = I \, \overline{C_p^n} \tag{2}$$

The first few normalized central moments, the intensity of concentration fluctuations, $i = \sigma/\bar{C}$; the skewness, $S = \overline{(C-\bar{C})^3}/\sigma^3$ and kurtosis, $K = \overline{(C-\bar{C})^4}/\sigma^4$, where σ is the standard deviation, are of greatest interest.

* CSIRO Division of Atmospheric Research, Melbourne, Australia

Data Description and Analysis

Details of the field experiments from which the data derive have been given by Sawford et al. [3]. The basic data consist of approximately 1h time series of 6s average concentration measured at a fixed point downwind of the source. The lateral distance, y, of the receptor point from the mean-plume centreline and the 1h mean-plume dispersion, σ_y, were determined from the mean-plume crosswind concentration profile measured from bag samplers. All experiments were carried out during a period of a year in day-time neutral to unstable conditions.

Spurious small but non-zero readings due to baseline drift and noise were eliminated by subtracting a threshold value from each reading and treating resultant negative values as zero. Because baseline anomalies varied from run to run (according to signal strength etc) different thresholds were chosen for each record but were typically $\sim 0.1\ \bar{C}$.

From these data, representative unconditional frequency distributions were determined by the simple regression analysis described by [3]. Other concentration statistics were calculated in the usual way.

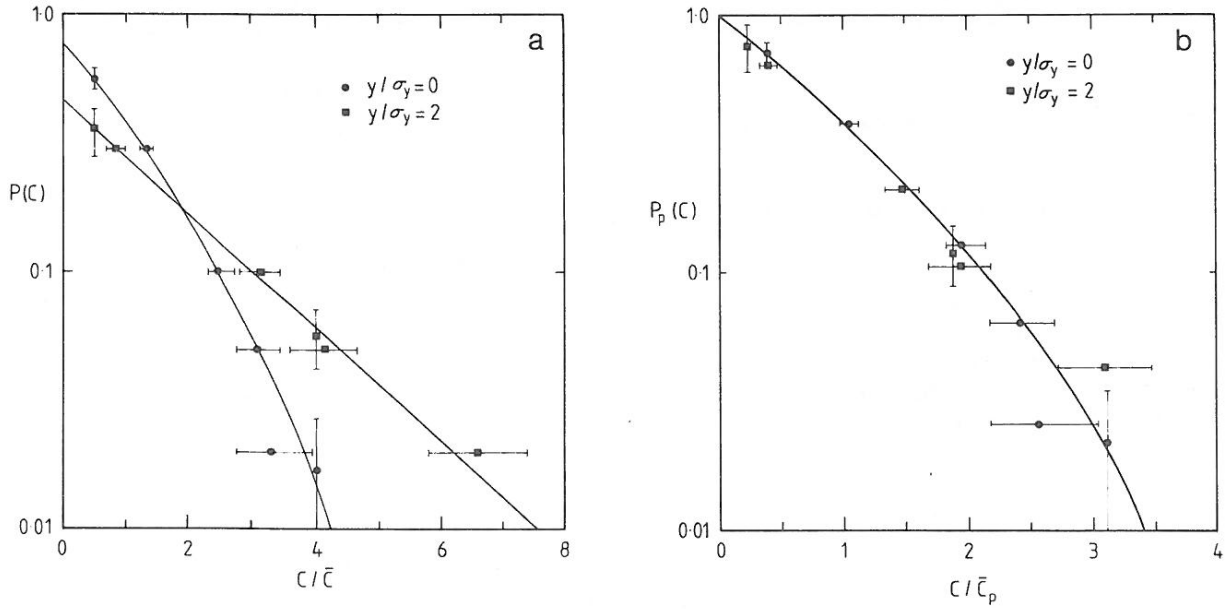

Fig.1. Unconditional (a) and conditional (b) frequency distributions for 6s average concentration at $y/\sigma_y = 0$ and 2.

Results

Figure 1(a) shows unconditional frequency distributions for 6s concentrations 25m down-wind of the source on the plume centreline, $y/\sigma_y = 0$, and near the edge of the plume, $y/\sigma_y = 2$. The error bars represent 95% confidence limits. As noted by [3], the centreline and plume edge distributions are markedly different. Figure 1(b) shows the same distributions transformed to conditional form using (1) and (2) with intermittencies estimated from Figure 1(a). In this form the plume-edge and centreline data collapse remarkably well and it is no longer entirely clear whether the difference in the shape of the distributions apparent in Figure 1(a) is significant.

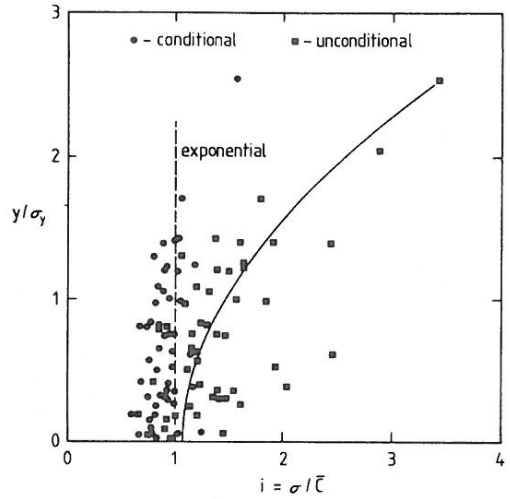

Fig.2. Unconditional and conditional intensity of fluctuations for 6s average concentration as a function of y/σ_y.

Perhaps a clearer picture of the variability in the data is conveyed by Figure 2 which shows the intensity of fluctuations for all the 6s concentration records. The trend for i to increase with y/σ_y for unconditional statistics was noted by [3] and is consistent with a wide range of laboratory [4] and field [5] measurements. As for the frequency distribution, the variation with y/σ_y is greatly diminished, if not entirely eliminated, for conditional statistics. Note that not only is this "explained" variation reduced but so is the unexplained variation or "scatter". Similar conclusions hold for the skewness.

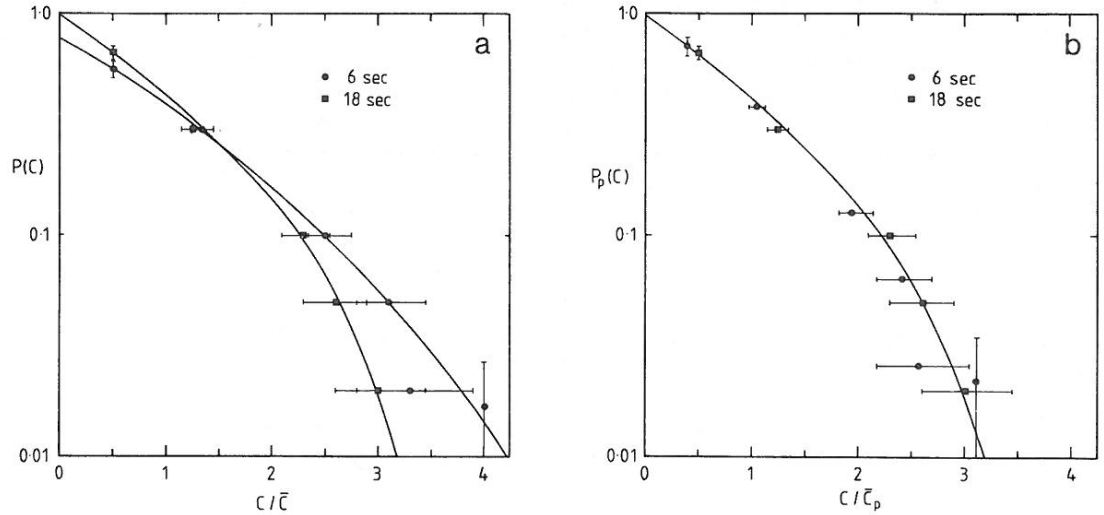

Fig.3. Effect of averaging time on unconditional (a) and conditional (b) frequency distributions for $y/\sigma_y = 0$.

The effect of averaging time on the unconditional frequency distribution is shown in Figure 3(a). As expected, increased averaging decreases the proportion of high relative concentrations and increases the intermittency. However, Figure 3(b) shows that increased averaging has a much weaker effect on the conditional frequency distribution. The reason is not that "in-plume" fluctuations are unaffected by averaging, but rather that $\bar{C}_p$ is also reduced so that the effect on i_p is reduced. It is also likely that much of the "in-plume" variation (which Jones [6] has shown to occur on very small scales) has already been smoothed by the 6s averaging.

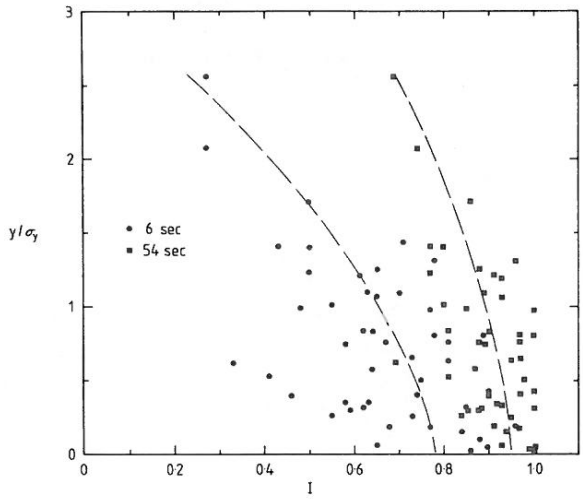

Fig.4. Intermittency as a function of y/σ_y and averaging time.

In a sense, Figure 4 complements Figures 1-3 in that it confirms that the variation which is removed by conditional sampling is reflected in the intermittency. As expected, and in agreement with wind tunnel [4] and other field [5] data, intermittency decreases with y/σ_y and increases with averaging time. It also carries most of the scatter apparent in the unconditional statistics in Figure 2.

Conclusions

Analysis of concentration statistics in ground-level plumes in the atmosphere has shown that much of the variation (both explained and unexplained) resides in the intermittency. In-plume or conditional statistics are much less variable. Broadly speaking, intermittency is determined by eddies large compared with the plume while the in-plume structure sampled by conditional statistics is due to smaller eddies. Therefore it may be profitable (or even necessary) to treat explicitly the effect of large scales of the flow and to model only in-plume concentration statistics. Since large-scale effects appear to dominate, for many purposes precise modelling of the in-plume statistics may not be critical.

References

1. P.J.Barry, 'Stochastic Properties of Atmospheric Diffusivity', AECL-5012. Atomic Energy of Canada Ltd., Chalk River, Ontario, Canada, KOJIJO, 1975.

2. P.C.Chatwin, 'The Use of Statistics in Describing and Predicting the Effects of Dispersing Gas Clouds', J.Haz.Materials, 6, 213-230, 1982.

3. B.L.Sawford, C.C.Frost, and T.C.Allan, 'Atmospheric Boundary-layer Measurements of Concentration Statistics from Isolated and Multiple Sources. Bound.Layer Meteor., 31, 249-268, 1985.

4. J.E.Fackrell, and A.G.Robins, 'Concentration Fluctuations and Fluxes in Plumes from Point Sources in a Turbulent Boundary Layer, J.Fluid.Mech., 117, 1-26, 1982.

5. S.R.Hanna, 'The Exponential Probability Density Function and Concentration Fluctuations in Smoke Plumes. Bound.Layer Meteor., 29, 361-375, 1984.

6. C.D.Jones, 'On the Structure of Instantaneous Plumes in the Atmosphere, J.Haz.Materials, 7, 87-112, 1983.

THE DEVELOPMENT OF A BOUNDARY LAYER IN A PORTABLE WIND TUNNEL

J H Tubb* & G H Moore*

1. INTRODUCTION

The Western Australian Department of Agriculture has a soil conservation research programme which is attempting to determine the economics of soil loss due to different farming practices.

The characteristics of a portable wind tunnel constructed for erosion studies is described in Section 2.

Proposed modifications to the portable wind tunnel have been carried out in a Plint TE44 wind tunnel and the results are described in Section 3.

1.1 Notation

d : surface roughness, cm

Z_o : height in cm where velocity is zero

U_∞ : bulk velocity, ms^{-1}

U_z : velocity ms^{-1} at height z

U_* : drag velocity, ms^{-1}

σ_u : root mean square velocity, ms^{-1}

2. PORTABLE WIND TUNNEL

2.1 Introduction

Five years ago Carter and Marsh (1980) decided to build an open circuit wind tunnel similar to the trailer mounted tunnel constructed by Armbrust and Box (1967) at the US Department of Agriculture Field Station at Big Spring, Texas. The design was modified to suit the Western Australian research programme and the general arrangement of the basic tunnel is shown in FIG. 1.

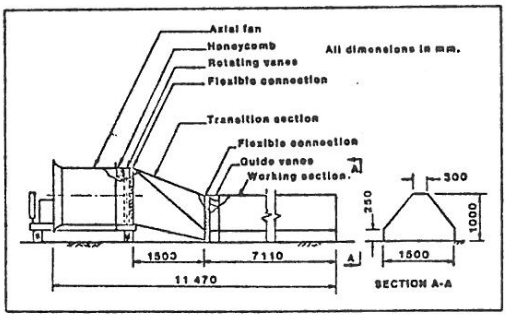

FIG. 1. Schematic Arrangement of the Portable Wind Tunnel

2.2 Wind Tunnel Components

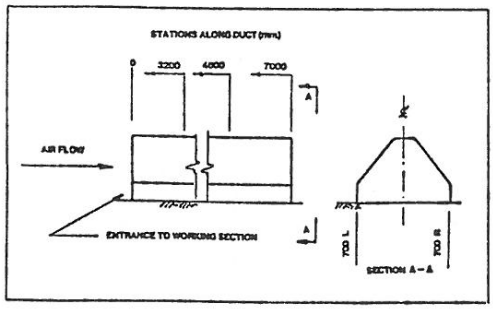

FIG. 2. Traverse Stations

A wind speed of 100 kmh^{-1} was required on the centre line of the duct. The tunnel has been described by Carter, Moore and Marsh (1985). A logarithmic-linear velocity relationship up to the centre line of the duct was required. The driving unit was a diesel engine coupled to a simple single-stage axial fan unit. The cross sectional area of the working section was approximately one square metre and the shape, shown in FIG. 2, was selected to increase ground coverage.

* Western Australian Institute of Technology

Turbulence (gust) generators in the form of seven rotating vanes were installed vertically across the outlet from the fan unit. These vanes may be fixed or rotating.

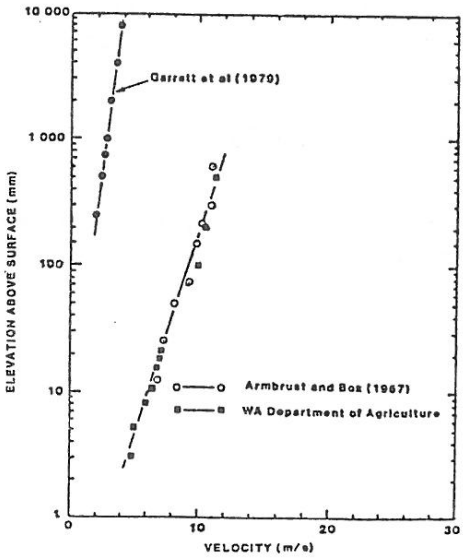

FIG. 3. Natural and Tunnel Wind Profiles

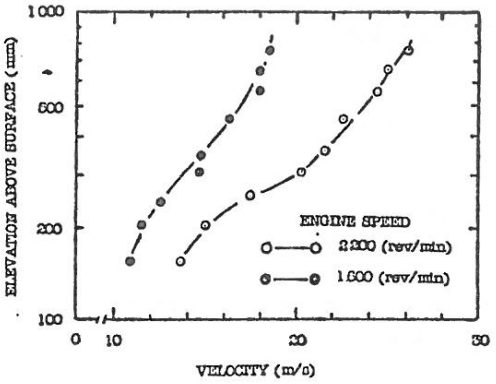

FIG. 4. Velocity Profiles just Upstream of Station, 0-0, on the Centre Line of the Duct. (Without Honeycomb Straightener)

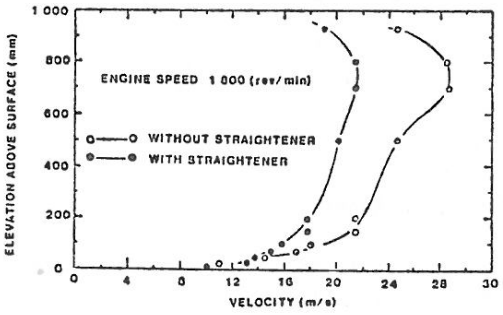

FIG. 5. Velocity Profiles at High Speed over a Cut Lawn Surface with and without Honeycomb Straightener at Station 7000.

2.3 Wind Tunnel Characteristics

The general variation of velocity with height in the tunnel was as shown in FIG. 3 together with a natural wind profile obtained by Garratt et al (1979).

Velocity profiles at the entrance to the working section are shown in FIG. 4.

The profile generated showed the influence of the "flow down" transition section on the inlet profile to the working section and indicated the need for further work in this area. The effect of the honeycomb straightener is shown in FIG. 5. The honeycomb removed an undesirable bulge in the upper part of the working section velocity profile.

Typical working section profiles over 10 mm roughness are shown in FIG. 6.

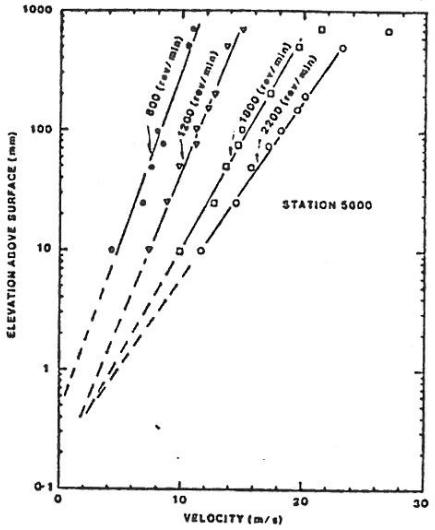

FIG. 6. Relationship between Drag Velocity and Engine Speed

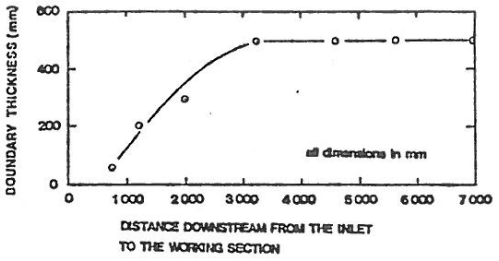

FIG. 7. Development of a Boundary Layer along the Working Section of the Tunnel

The development of a straight log-linear velocity profile with distance from the inlet to the end of the working section is shown in FIG. 7.

2.4 Initial Tunnel Performance

This wind tunnel designed for comparative field studies of ground covers and soil erodibility, has been successful in this type of research. Flow conditions similar to those obtained in the field have been achieved along approximately 60% of the working section. The tunnel does have an undesirable swirl component.

2.5 Current Work

Velocity traverses using a NPL Pitot-static tube with a precision manometer were performed in the tunnel. The tunnel was fitted with certain flow conditioning devices. These devices consisted of a trip and associated ramp situated at the beginning of the tunnel working section. The use of a 25 mm trip and associated ramp in fact did induce a more stable and developed boundary layer. This can be seen from FIGs. 8 and 9 where the straight line log-linear profile is evident FIG. 8, and the value of von Kármán constant is shown to be $\doteq$ 0.4, which is the accepted value FIG. 9.

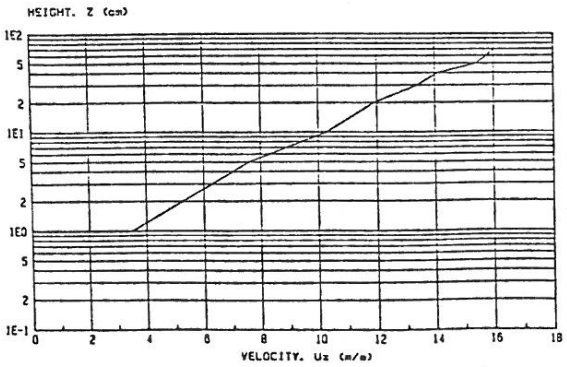

FIG. 8. Friction Velocity Graph 1400 rpm - with trip with ramp

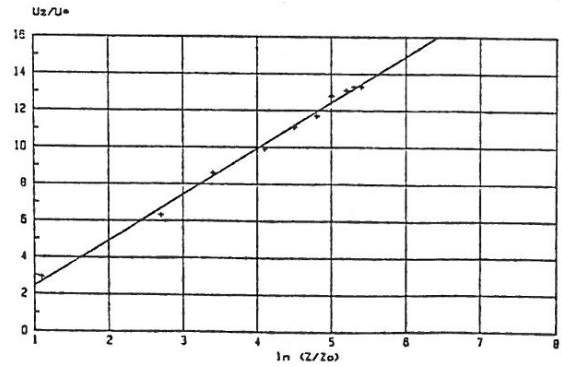

FIG. 9. Logarithmic Law Graph 1400 rpm - with trip with ramp

FIG. 10 shows the velocity matrix again at the end of the tunnel. This matrix was used to obtain lines of equal velocity. This shows the tunnel to be plagued with secondary flow effects which are to be expected in the corners of this tunnel.

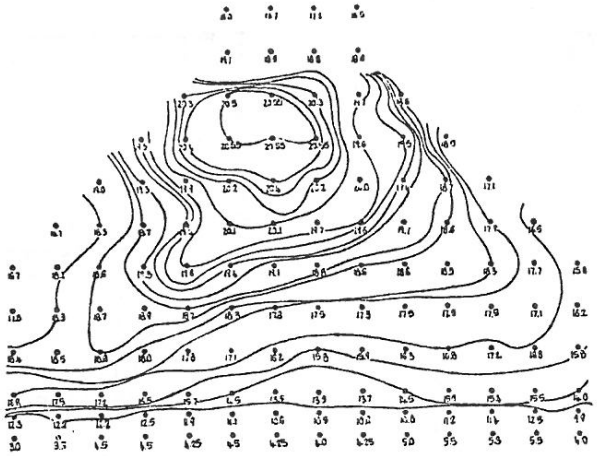

FIG. 10. Velocity Contours at exit from Tunnel.

3.0 PROPOSED MODIFICATIONS CARRIED OUT IN THE PLINT WIND TUNNEL

The Plint TE44 Wind Tunnel is an aerodynamic tunnel manufactured by Plint and Partners, England. Modifications to the tunnel included a trip with associated rough surface. A number of traverses were performed using a Disa hot-wire anemometer coupled to a HP86 microcomputer.

The boundary layer development for these flow conditioning devices are described using the straight line log-linear profile, a boundary layer profile and the value obtained for von Kármán constant. von Kármán's constant was $\doteqdot$ 0.4, and the value obtained for σ_u/U_* in the constant stress layer was 2.35.

Graphs relating to these may be seen in FIGs. 11, 12 and 13 respectively. These criteria provided typical values for constants and shapes for graphs showing the boundary layer to be fully developed and in equilibrium.

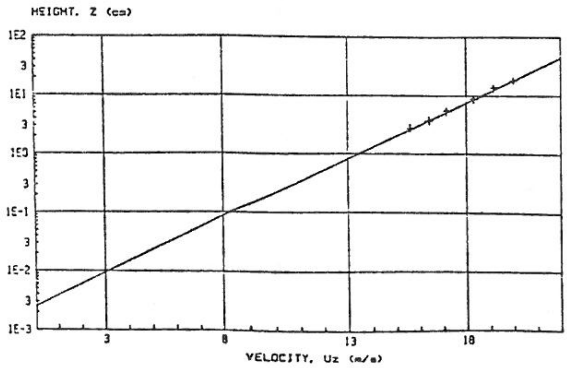

FIG. 11. Friction Velocity Graph
End of Rough Surface
20.02 m/s.

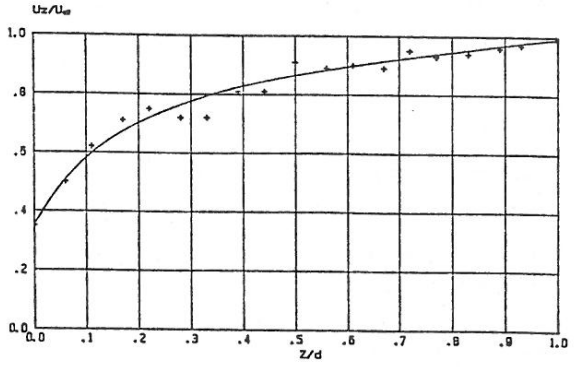

FIG. 12. Turbulent Boundary Layer Profile
End of Rough Surface
20.02 m/s.

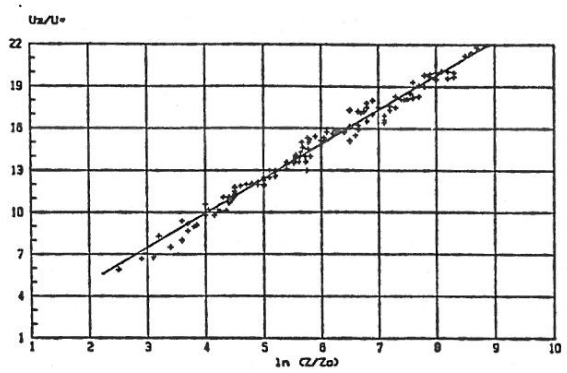

FIG. 13. Logarithmic Law Graph - all Surfaces and Velocities.

4. CURRENT RESEARCH WORK IN THE DEPARTMENT OF MECHANICAL ENGINEERING

The following projects are being carried out in the Department of Mechanical Engineering.

(a) Turbulence levels in the portable wind tunnel.

(b) Efficiency of saltation gauges.

(c) Improved methods of measuring drag velocity under soil blowing conditions.

(d) Alternative methods of collecting samples from saltation gauges.

(e) Flow patterns and efficiency for two air elutriators and saltation gauges.

Gusting produced by rotating vanes will always cast doubts on readings and results obtained under soil blowing conditions. Research is necessary to devise instrumentation to operate in this hostile environment.

REFERENCES

Carter, D and Marsh, B a'B (1980). "A Portable Wind Tunnel for Erosion Research". National Soils Conference, Sydney.

Armbrust, D V and Box, J E (1967). "Design and Operation of a Portable Soil Blowing Tunnel". US Dept Agr. ARS 41 : 131.

Carter, D, Moore, G H and Marsh, B a'B (1985). "Flow Characteristic of a Portable Wind Tunnel". Technical Report Division of Resource Management, WA Department of Agriculture (In Press).

Garratt, J R, Francey, R J, McIlroy, I C, Dyer, A J, Helmond, I, Bradley, E F and Denmead, O T (1979). "The International Turbulence Comparison Experiment" (Australia 1976). "Micrometeorology Support Data". CSIRO Div Atmospheric Physics Tech Pap No.37.

ATMOSPHERIC BOUNDARY LAYER SIMULATION IN TWO WIND TUNNELS

by K.C.S. Kwok[1] and P.A. Macdonald[2]

Introduction

In the past 12 months, attempts were made to simulate in the Boundary Layer Wind Tunnel (BLWT) and the 7 ft x 5 ft Low Speed Aeronautical Wind Tunnel (Aero WT) suitable 1/100 model of wind flow over category 2 open country terrain. These wind models are used in the study of wind loads on low to medium rise structures such as the Aylesbury house and circular storage bins, silo and tanks. This paper describes the simulation technique used and the turbulent boundary layer flow characteristics, and discusses the limitations of the simulated wind models.

Wind tunnel arrangements

The conventional augmented growth method was used in the BLWT. It consisted of a 0.3 m high fence and carpeted tunnel floor. Hot wire measurements were taken at 15 m downstream of the fence and at 3 lateral positions.

In the Aero WT, 4 triangular spires 0.9 m high and 0.12 m at the base, and carpeted floor wereused. Measurements were taken at 2.25 m downstream from the spires and at 3 lateral positions.

Results and comments

Since there are only minor differences between measurements taken at the three lateral positions, only the results obtained at the centre-line of both wind tunnels are presented and discussed here. The mean wind speed profile, longitudinal, lateral and vertical turbulence intensity profiles, normalised Reynolds stress profile, and longitudinal turbulence spectrum in the BLWT are presented in Figure 1, and those in the Aero WT are presented in Figure 2.

In the BLWT, the mean wind speed profile follows closely the logarithmic profile and the power law profile (with an exponent $\alpha = 0.15$) for flow over a category 2 open country terrain, up to a height of 1 m. The logarithmic profile is based on a roughness length z_o of 0.02 m (full scale) as suggested by Melbourne (1981) for a category 2 open country terrain. In the Aero WT, reasonably good agreement with the logarithmic and power law profiles was obtained in the lower part of the boundary layer, up to about 0.3 - 0.4 m.

The turbulence intensity profiles can be compared with the code model (AS 1170, Part 2, 1983), the more accurate Deaves and Harris model (Deaves and Harris, 1978), and values suggested in ESDU 74031. In the BLWT, slightly lower values were recorded in the longitudinal turbulence intensity profile. At a height of 0.1 m (10 m in full scale), the lateral turbulence intensity is about 85% of the longitudinal value, and the vertical turbulence intensity, about 55%. These values are consistent with those suggested in ESDU 74031. In the Aero WT, there is quite a good agreement in the longitudinal turbulence intensity profile up to a height of about 0.3 - 0.4 m. At a height of 0.1 m (10 m in full scale), the lateral turbulence intensity is about 80% of the longitudinal value, and the vertical turbulence intensity, about 65%. It is noted that there is a noticeable peak in the vertical turbulence intensity profile at a height of

---

[1]Senior Lecturer and [2]Research Student, School of Civil and Mining Engineering, University of Sydney

about 0.2 m. This is believed to be introduced by the simulation method used and it may have a significant effect on roof loads for low-rise structures.

In the atmospheric boundary layer, the Reynolds stress or turbulent shear stress normally remains constant with height, or decreases slowly with an increase in height. In the BLWT, the Reynolds stress profile is nearly constant with height up to about 0.6 m. The concentrated Reynolds stress contained in the shear layer originating from the 0.3 m high fence has largely disappeared at 15 m downstream of the fence. In the Aero WT, the Reynolds stress profile exhibits a very prominent peak at a height of about 0.2 m which has a value of approximately twice the value close to the floor. The raised Reynolds stress level is thought to have some influence on the flow separation process, in particular separation and reattachment on roofs.

A geometric length scale ratio can be established by comparing the longitudinal turbulence spectrum with the Harris-Von Karman spectrum. Two length constants, L (10 m) = 800 m (ESDU 74031) and 1500 m (Counihan, 1975), were used in the Harris-Von Karman equation. In the BLWT, a geometric length scale of 1/100 is quite appropriate. The integral length scale at a height of 0.1 m was about 0.55 m or 55 m at 1/100 scale. This corresponds closely to the value of about 70 m suggested in ESDU 74031.

In the Aero WT, there is a significant mismatch in the longitudinal turbulence spectrum (if a 1/100 scale is adopted), by a factor of about 3. It has been suggested (e.g. Surry, 1982) that for the measurement of unsteady loads on low to medium rise structures, relaxation of model scale by a factor of up to 2 to 3 appears justifiable. Nevertheless, it should be noted that there is significantly more high frequency small scale turbulence which, as suggested by Melbourne (1980), may have a significant effect on the rate of shear layer growth and reattachment, and on the local unsteady loads on roofs of low-rise structures. The integral length scale at a height of 0.1 m was about 0.18 m or 18 m at 1/100 scale. This is considerably smaller, by a factor of about 4, than the value of 70 m suggested in ESDU 74031. The turbulence scale in the low frequency range is important in the determination of overall or large-area loads. However, the effect of a distorted length scale is believed not to be significant provided that the integral length scale is as large as and preferably larger than the typical model dimension.

Conclusions

Results of extensive boundary layer measurements in the Boundary Layer Wind Tunnel showed that a 0.3 m fence and 15 m carpeted fetch can be used to generate a satisfactory 1/100 scale wind model of flow over a category 2 open country terrain.

In the 7 ft x 5 ft Low Speed Aeronautical Wind Tunnel, the use of spires and a short 2.25 m carpeted fetch provided satisfactory simulation of the wind speed profile and turbulence intensity profiles. However, the simulation of the Reynolds stress profile and the matching of the turbulence length scales were less satisfactory. Nevertheless, the wind model should be adequate for the measurement of mean and unsteady wind loads on low to medium rise structures such as circular storage bins, silos and tanks.

References

1. Counihan, J., Adiabatic atmospheric boundary layers. A review and analysis of data from the period 1880-1972, Atmospheric Environment, Vol. 9, No. 10, October, pp. 871-905.

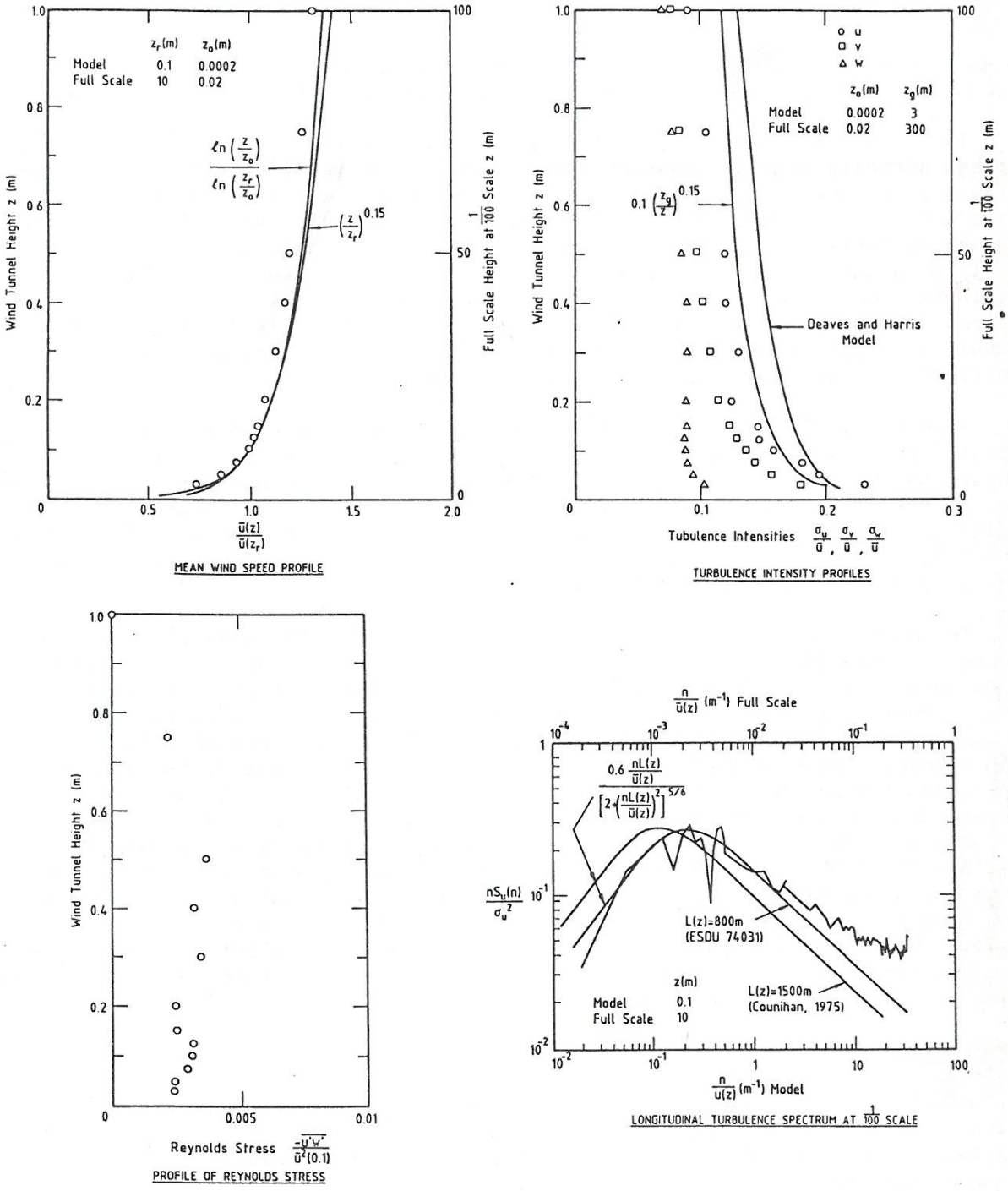

Fig.1 - Boundary layer flow characteristics, Boundary Layer Wind Tunnel

2. Deaves, D.M. and Harris, R.I., A mathematical model of the structure of strong winds, CIRIA Report 76, 1978.

3. Engineering Sciences Data Unit, ESDU Data Item 74031, 1974.

4. Melbourne, W.H., Turbulence effects on maximum surface pressures - a mechanism and possibility of reduction, Proc. 5th International Conference on Wind Engineering, Vol. 1, 1980, Pergamon Press, pp. 541-551.

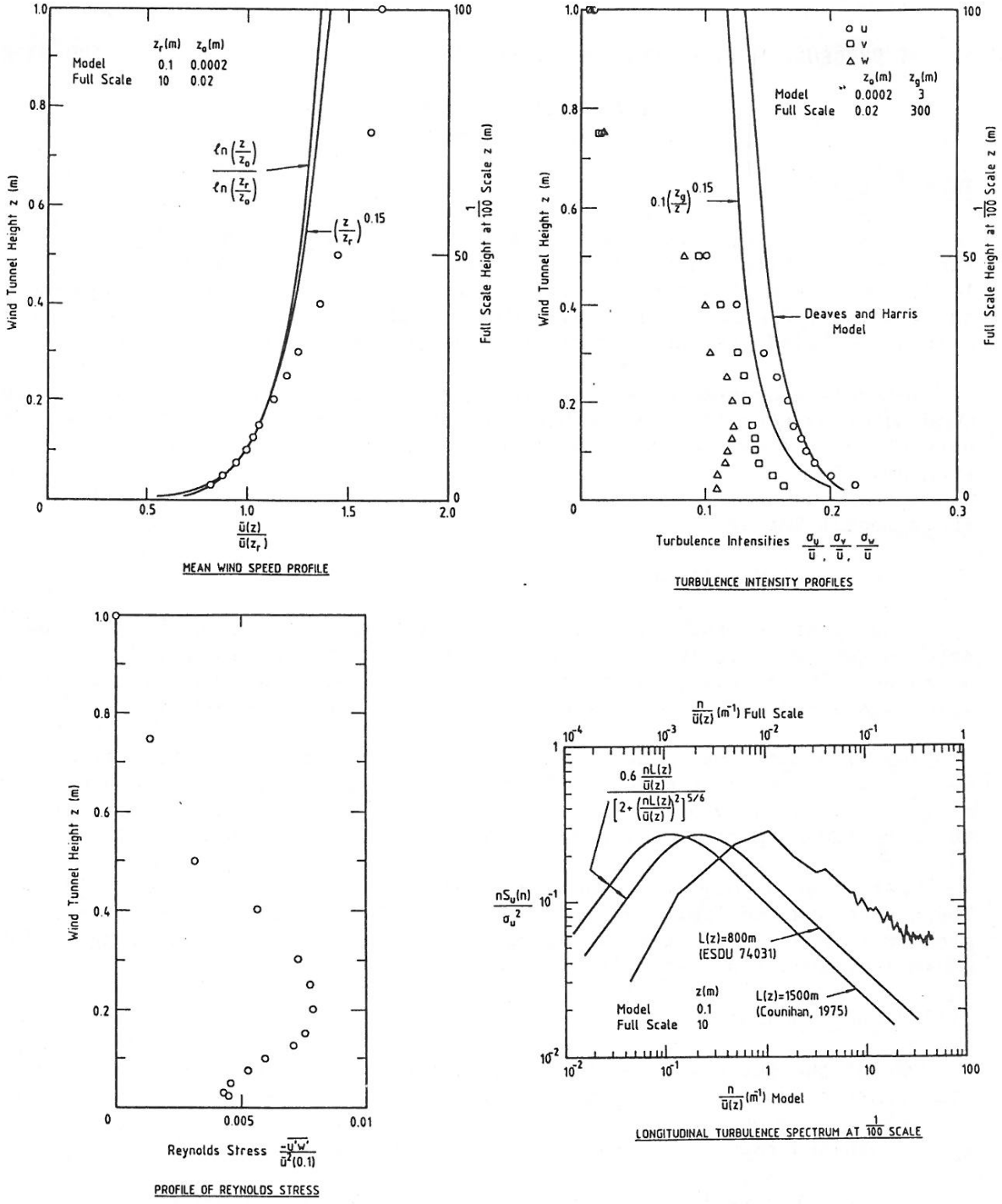

Fig.2 - Boundary layer flow characteristics, 7ft x 5ft Low Speed Aeronautical Wind Tunnel

5. Melbourne, W.H., Towards an engineering wind model, Course Notes on the Structural and Environmental Effects of Wind on Buildings and Structures, Monash University, May 1981.

6. Standard Association of Australia, SAA Loading Code Part 2 - Wind Forces, AS 1170 Part 2, 1983.

7. Surry, D., Consequences of distortions in the flow including mismatching scales and intensities of turbulence, Wind Tunnel Modelling for Civil Engineering Applications, Cambridge University Press, 1982, pp. 137-186.

POINT PRESSURE MEASUREMENTS ON MODEL CIRCULAR STORAGE BINS, SILOS AND TANKS

P.A. Macdonald[1], K.S.C. Kwok[2],
J.D. Holmes[3]

Introduction

A number of failures of cylindrical structures, such as bins, silos and tanks, has highlighted the limited data, and lack of understanding on the wind loading of these structures (1). In terms of design, the Australian wind loading code AS1170 part 2 - 1983 provides no indication of the expected internal or external wind pressure distribution on such structures.

Recently a program of wind tunnel model tests was initiated to determine the wind loads on circular storage bins, silos and tanks. This paper reports results of point pressure measurements obtained in the first phase of the test program.

Experimental Set Up

(i) Wind tunnel Modelling

Results of the turbulent boundary layer simulation in the 7' x 5' Low Speed Aeronautical Wind Tunnel have been reported by Kwok and Macdonald (2) in this workshop. The boundary layer simulation was found to adequately represent a 1/100 scale model of flow over a category 2 open country terrain.

The silo model was made of perspex and constructed in tight-fitting segments. Nine different model configurations were tested which included models of three different aspect ratios (H/D = 0.5/1, 1/1, 2/1) each being tested with three roof configurations (no roof, flat roof and 25°pitch conical roof).

Test Reynolds numbers of between 2.5×10^5 and 3.4×10^5 were achieved. These exceeded the limiting value of 2×10^5 (with a turbulence intensity of greater than 4%) suggested by Cheung and Melbourne (3) for modelling of full scale configurations with circular features.

(ii)Pressure Measurements

One of the perspex segments was fitted with 50 pressure tappings spaced at 7.2° centres around the circumference. This segment was positioned to take pressure measuements at various heights on the model. The 25° pitched conical roof contained rows of 5 pressure tappings spaced at 36° centre.

A single Honeywell 163 pressure transducer was connected to the pressure tappings via a 48 port Scanivalve and 400 mm of PVC tubing. The tubing's pressure transmission response was damped by a single small bore restrictor achieving a flat frequency response up to approximately 130 Hz. The signal output from the transducer was low-pass filtered at 200 Hz before being digitized.

A microcomputer was used to digitally sample at a rate of 1000 Hz for 10 seconds, from which the mean, standard deviation, maximum and minimum coefficient of pressure were obtained and referenced to the dynamic wind pressure at

---

[1]Research Student and [2]Senior Lecturer, School of Civil and Mining Engineering, University of Sydney
[3]CSIRO, Division of Building Research.

silo wall height. Measurements were repeated four times for each tapping and the average calculated. For open topped silo models, internal pressures were also measured.

Results and comments

Figures 1 - 3 present the variation of mean pressure coefficient with the angle θ from the stagnation line, for the three different aspect ratios and the roof configurations. The pressure distributions over the 25° pitch conical roof are also presented, in the form of mean pressure coefficient contours.

Significant trends observed in the results include:-

1) The maximum positive pressure decreases as aspect ratio increases (1.0 to 0.8).
2) The maximum negative pressure increases as aspect ratio increases (-1.0 to -1.7).
3) The windward region of positive pressure extends to between 30° and 40° from the stagnation line, marginally decreasing as aspect ratio increases.
4) When the negative internal pressure of the open topped silo is considered the region of windward positive pressure increases to between 50° and 60°.
5) Flow separation occurs at approximately 130° after which $\bar{C}p$ remain relatively constant.

Pressure measurements taken on the 25° pitch conical roof showed a largely symmetrical pressure distribution. Relatively high negative pressures were recorded near the leading edge, believed to be caused by reattachement of the separated shear layers. High negative pressures were also recorded near the centre of the roof.

Peak maximum and minimum, and standard deviation pressure coefficients were recorded at each pressure tapping. Figure 4 is a typical graph for a flat roof silo with an aspect ratio 2:1. The graph shows the large variation in wind pressure at any one point and hence the need for a measurement program to determine the critical structural loading, in particular the critical buckling load.

In general there were good agreements with results by Sabransky (4) and others. Minor differences, such as the maximum negative pressure occurring at approximately 80°, rather than 90° and separation occurring at 140°, may be attributed to the different wind tunnel and the lower Reynolds Number used by Sabransky (4).

Conclusion

Results from the experimental program allowed the assessment of the wind tunnel simulation and other experimental technique to be made.

Results of $\bar{C}p$ showed a good agreement with previous work and extended data to include the dependence of the mean wind pressure distribution on aspect ratio and roof configuration. A family of curves to define $\bar{C}p$ as a function of aspect ratio, roof configuration and θ is being considered for inclusion in AS 1170 for general design purposes.

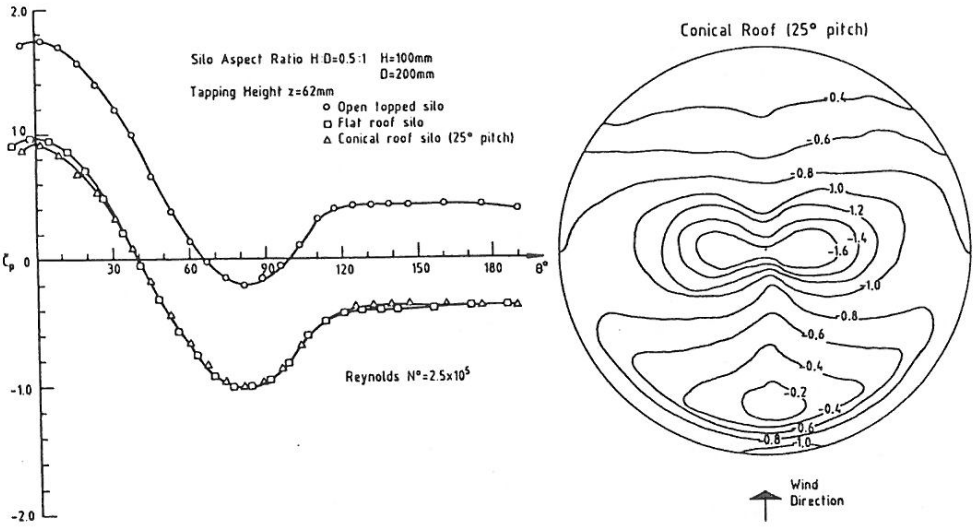

Fig. 1 - Mean Pressure Distributions (h:d=0.5:1)

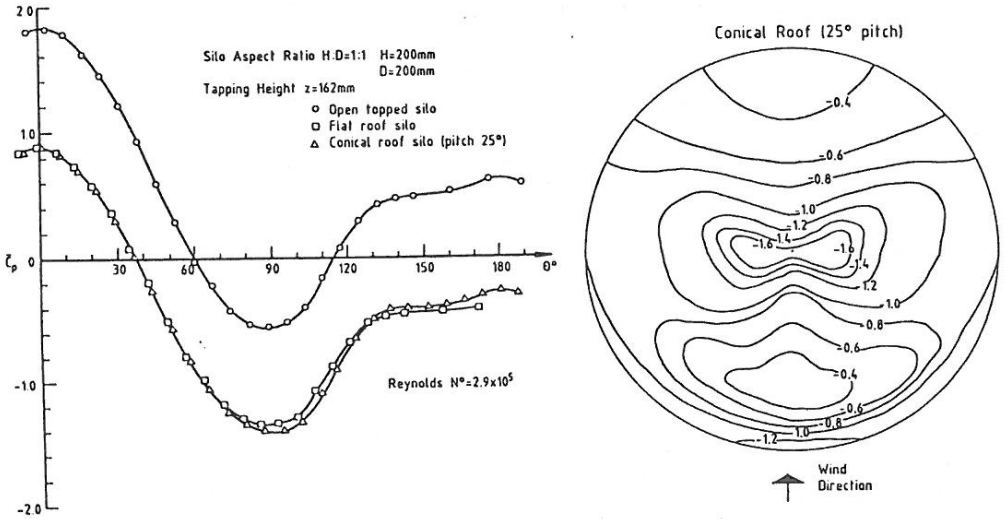

Fig. 2 - Mean Pressure Distributions (h:d=1:1)

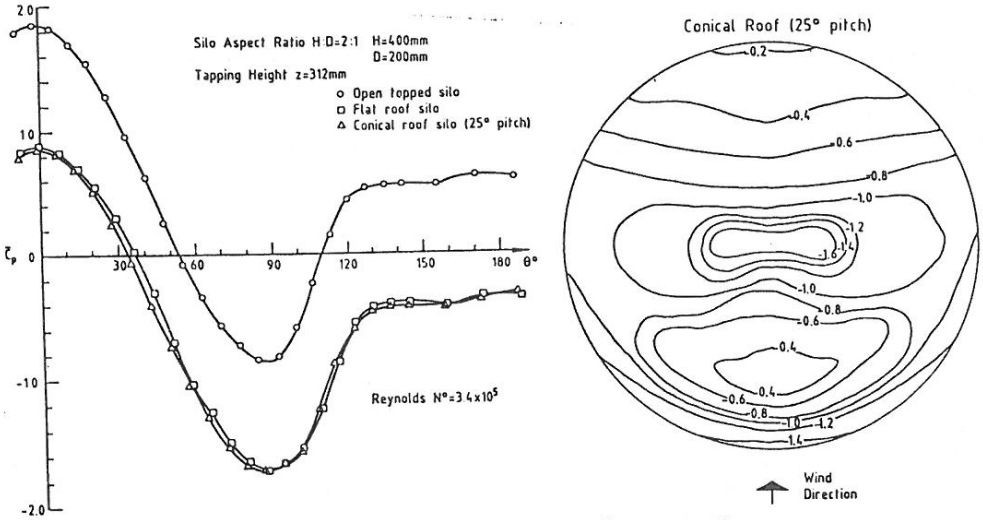

Fig. 3 - Mean Pressure Distributions (h:d=2:1)

References

1. Kwok, K.C.S. (1985), Wind loads on storage bins, silos and tanks, Proc. Joint U.S.-Australian Workshop on Loading, Analysis and Stability of Thin-Shell Bins, Tanks and Silos, Sydney, March, pp. 48-53.

2. Kwok, K.C.S and Macdonald, P.A. (1985), Simulation of turbulent boundary layer flow in two wind tunnels, Workshop on Wind Engineering and Industrial Aerodynamics, Melbourne.

3. Cheung, J.C.K. and Melbourne, W.H. (1983), Turbulence effects on some aerodynamic parameters of a circular cylinder at supercritical Reynolds Numbers. Journal of Wind Engineering and Industrial Aerodynamics, Vol. 14, pp. 399-410.

4. Sabransky, I.J. (1984), Wind pressure distribution on cylindrical grain Storage Silos. Master of Engineering Science thesis, Dept. of Civil Engineering, Monash University.

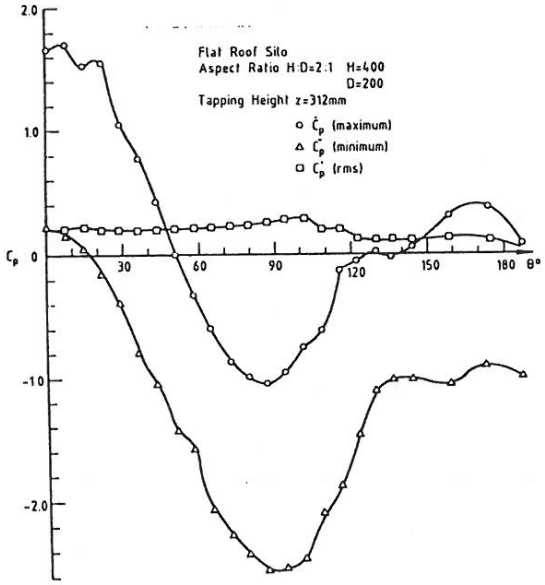

Fig. 4 - Maximum, minimum and standard deviation pressure coefficients (h:d=2:1)

WIND LOADS ON GRANDSTAND ROOFS

W.H. Melbourne and J.C.K. Cheung*

Introduction

Melbourne [1] speculated on the cause of high negative peak pressures which occur under the separation bubble near the leading edge of flat roofs or near streamwise surfaces generally, in turbulent flow. In further study, Melbourne [2] illustrated the strong dependence on turbulence and in particular showed that by venting the leading edge (to prevent the very early reattachment phenomenon which was seen to be correlated with the occurrence of the highest negative pressures), the pressures and overall wind loading on the roof could be substantially reduced. One of the most relevant applications of a vented leading edge was seen to be on grandstand roofs, which are very wind sensitive structures. Cook [3] used this approach on a cantilevered grandstand roof, and in model measurements showed that a 25% reduction in mean pressures could be achieved by using a slotted leading edge. It remained still to show that a slotted leading edge could substantially reduce the dynamic response of such a cantilevered grandstand roof. In 1985 the opportunity arose to put the idea into action on a roof for the new Parramatta Oval Grandstand, and accordingly an aeroelastic model of this roof system was built and tested in the 450 kW Boundary Layer Wind Tunnel at Monash University. Subsequently, the model was used to explore a number of configurations to optimise the slot configuration and to determine generalised equivalent static loads on a cantilevered roof system, which is the subject of this paper.

The Grandstand Roof Model

The aeroelastic model was built to a scale of 1/100 and was tested in a 1/100 scale model of the natural wind boundary layer over suburban terrain (z_o=0.020). The basic dimensions of the cantilvered roof are given in Figure 1, along with definitions of the leading edge slot configuration. The model beams were made of Sugar Pine, and the roof deck was made of Balsa, and discrete masses were added to bring up the required mass distribution.

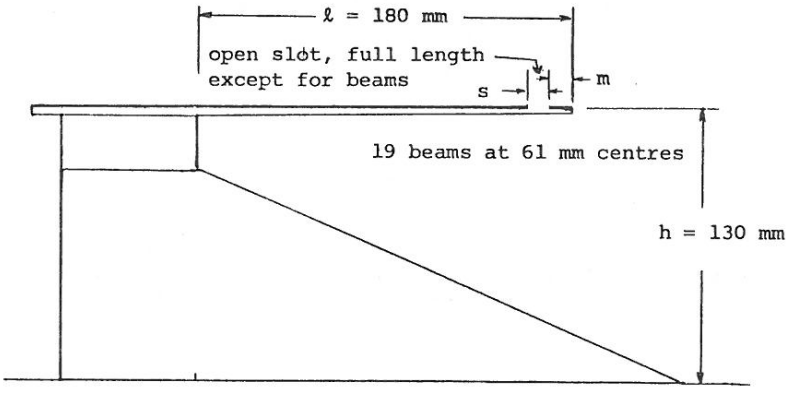

Figure 1. Dimension of 1/100 scale aeroelastic model of the grandstand cantilevered roof.

The aeroelastic scaling of the beams was based on keeping $\rho \bar{V}^2 L^4/EI$ constant in model and full scale and in which the model/full scale ratios (subscript r) were

length	$L_r = 1/100$	density	$\rho_r = 1$
velocity	$V_r \approx 0.7$	Youngs modulus	$E_r \approx 0.040$
time	$T_r = L_r/V_r \approx 0.014$	Second moment of area	$I_r \approx 12 \times 10\text{-}8$

* Department of Mechanical Engineering, Monash University, Melbourne, Australia

The deflection, in full scale terms, of the tip of the beams under a triangular load distribution, i.e. starting at a load of F Nm^{-1} at the leading edge reducing linearly to zero at the cantilever root, was 78 x 10^{-6} m per unit F Nm^{-1}. The use of a triangular load distribution will be discussed later. The stiffness of the edge beam was such that the influence of a triangular load distribution of one beam on the adjacent beams was as follows.

Measurements of the displacement of the leading edge of the roof were made directly through small calibrated strain gauged links which added negligble stiffness to the canopy system.

The model roof was also fitted with pressure tappings to permit the measurement of pressures above and below the roof with reference to freestream static pressure, and to measure pressures above the roof with reference to the pressure below the roof at the same location.

The Loading Process

The response of a cantilevered roof to wind action is complex as can be seen by a trace of the leading edge displacement given in Figure 2. The response is a combination of low frequency response, which can be observed, even at model scale, as being like a wave, often running along the leading edge from one end to the other, and on which a beam resonant component is superimposed. The low frequency response is driven in a quasi-steady manner by the pressure distribution which might typically vary from $\underline{C}_p^{\wedge} = -6$ at the leading edge to $C_p^{\wedge} = -3$ at the trailing edge (Peak C_F based on $\bar{V}_h$). The load from the resonant response is from the inertial load distribution; for a constant mass per unit length and linear mode the load distribution is triangular, but as the mode is very much that of a cantilever, (exponent could even be 2.0), and even with a reducing mass per unit length approaching the leading edge, the inertial load distribution is likely to be very much more peaked than triangular. Overall, for the purposes of determining an equivalent static load, it is suggested that a triangular load distribution is likely to be the best simple approximation of the effective load from the combined effects of the pressure driven low frequency response and the high frequency resonant response.

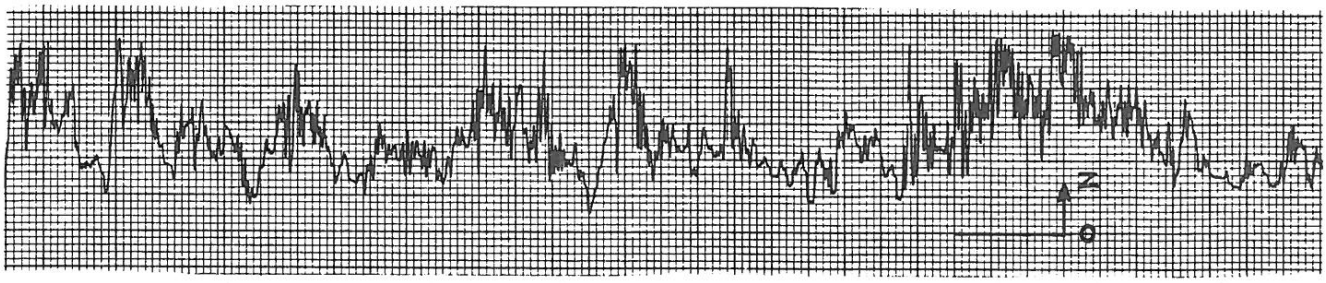

Figure 2. Trace of vertical displacement of the leading edge showing the skewed distribution, low frequency wake pressure components, and high frequency first mode beam resonance component.

Model Measurements

Tip displacements as a function of wind speed and direction were measured on a number of beams for various canopy configurations. The results are plotted in non-dimensional form as C_F versus $\bar{V}_h/n\,\ell$ where

$C_F = F/\frac{1}{2}\rho\ \bar{V}_h^2 b$

ℓ is length of cantilever beam

F is force per unit length of beam at the leading edge of a triangular load distribution which would give a displacementa z.

b is width of roof per beam (i.e. defining tributory area)

$\bar{V}_h$ is mean wind speed at the top of the beam

ρ is air density

s is the first model frequency of the beam

C_F is numerically equal to the leading edge pressure coefficient defining the triangular load distribution which, if applied statically, would give the same leading edge displacement.

These effective pressure coefficients may be converted to those based on a 3-second mean maximum gust wind speed by multiplying by $\bar{V}^2/\hat{V}^2$. These tests were conducted in a model wind turbulent boundary layer where at the height of the roof $\sigma_V/\bar{V} = 0.25$,

$$\text{which from } \hat{V} = \bar{V}\left(1 + g\frac{\sigma_V}{\bar{V}}\right) \text{ for } g = 3.7 \text{ gives } \left(\frac{\bar{V}^2}{\hat{V}^2}\right) = 0.27 .$$

For example, a peak coefficient of $\hat{C}_p = 7.0$ is equivalent to using $C_p = 7.0 \times 0.27 = 1.9$ in a quasi-steady code such as the Australian Wind Loading Code AS1170.

Examples of mean, standard deviation and peak effective pressure coefficients are given in Figures 3 and 4 for a range of slot configurations. These measurements were made over a full scale equivalent time of one hour.

Conclusions

Design loads for large cantilevered roofs are significantly greater than specified by AS1170. Incorporation of a slot along the leading edge was shown to reduce response, and hence design loads, by up to 30%.

References

1. W.H. Melbourne, 'The relevance of codification to design', Proc. 4th Int. Conf. on Wind Effects on Buildings and Structures, 785-790, 1975.

2. W.H. Melbourne, 'Turbulence effects on maximum surface pressures - a mechanism and possibility of reduction', Proc. 5th Int. Conf. on Wind Engineering, 541-552, 1979.

3. N.J. Cook, 'Reduction of wind loads on a grandstand roof', Jnl. Wind. Eng. and Industrial Aerodynamics, 10, 373-380, 1982.

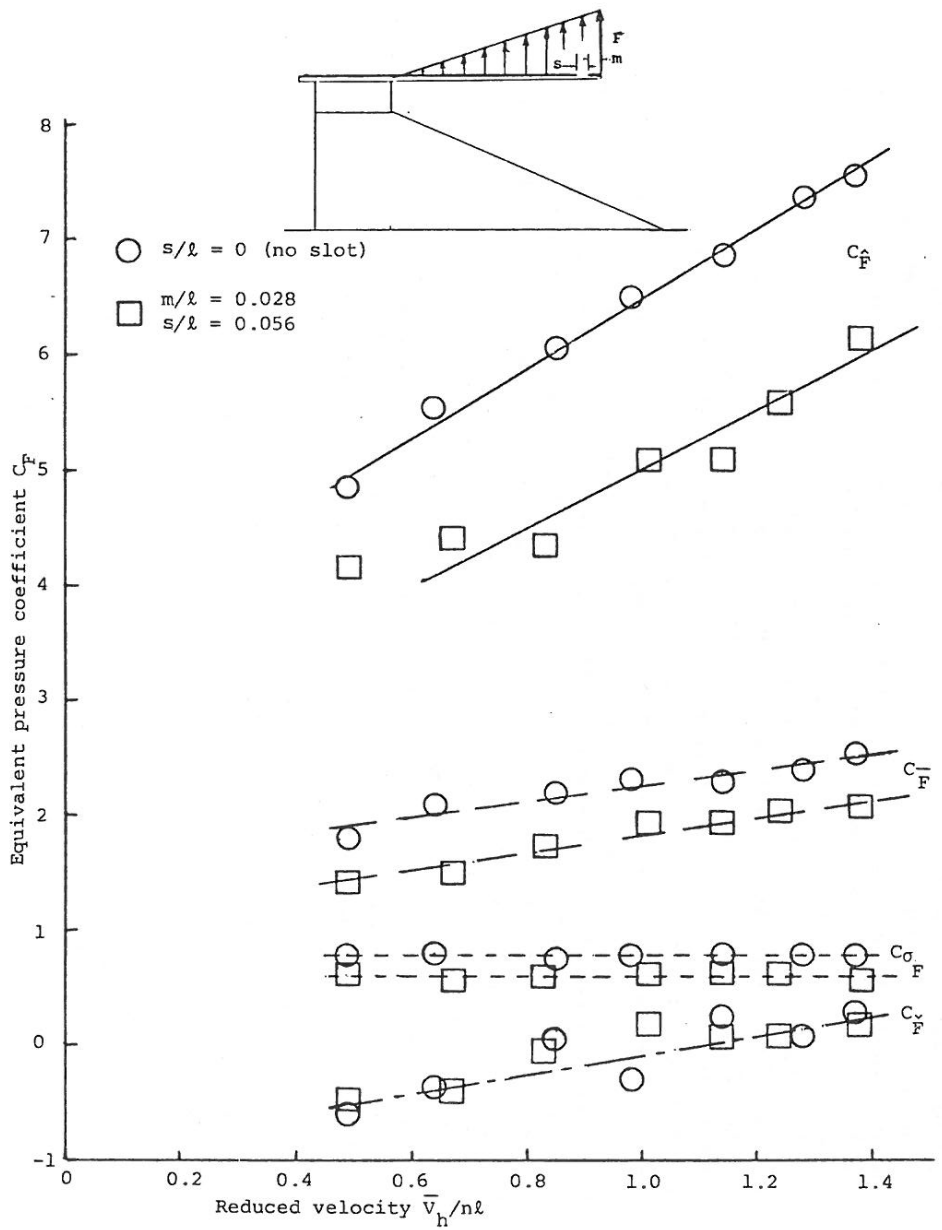

Figure 3. Leading edge response in terms of the equivalent pressure coefficient at the leading edge of a triangular distribution.

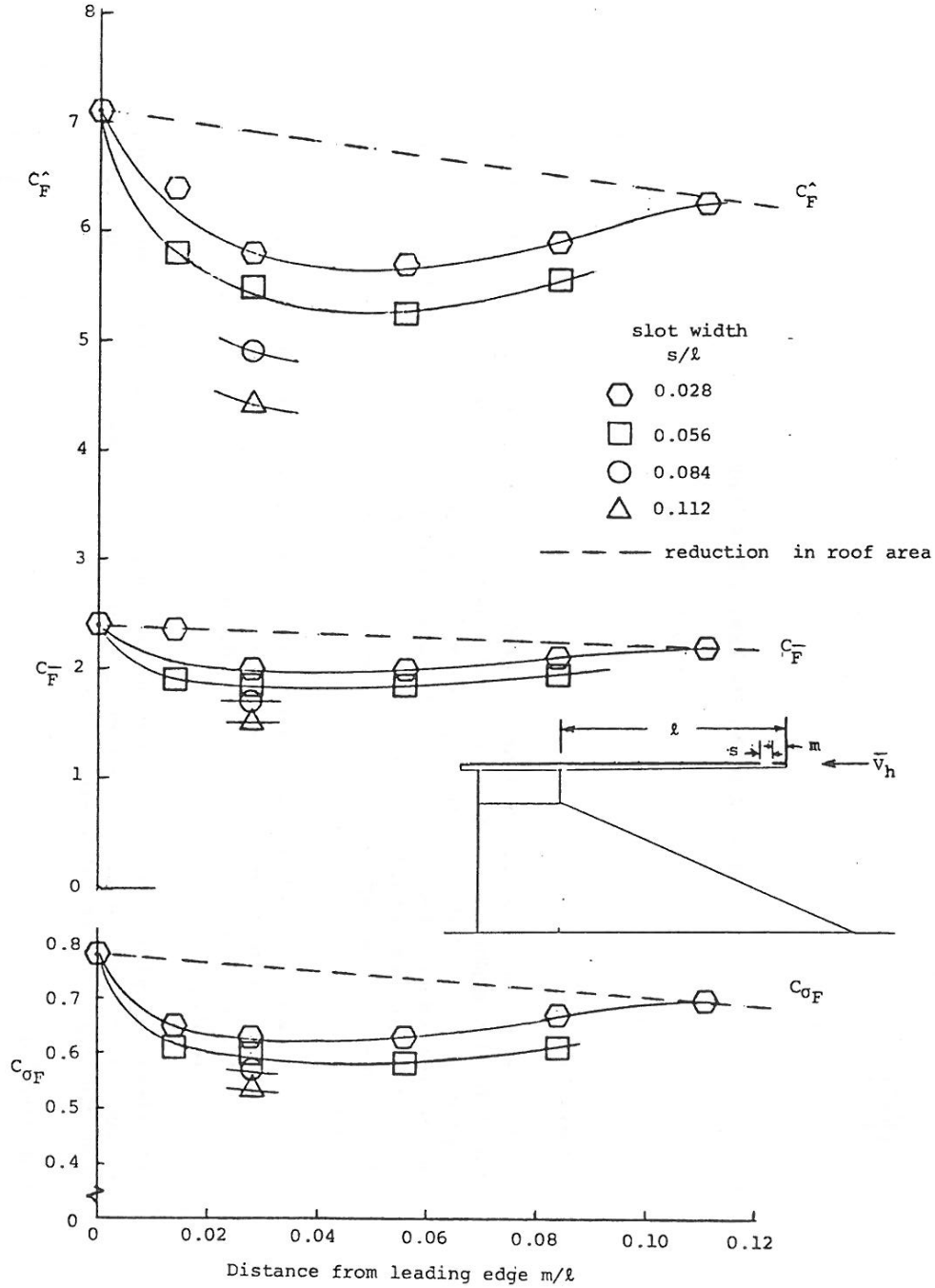

Figure 4. Effect of varying slot width and distance from the leading edge at $\bar{V}_h/n\ell = 1.2$

WIND LOADING ON TENT STRUCTURES

P S Jackson[1]

Introduction

Most studies of wind loading on membrane structures refer to problems in which the membrane is highly prestressed (as in tension and pneumatic structures), so that the loading results in small deflections about an equilibrium shape. However by far the most common membrane structure is the ordinary tent in which prestress is generally small or absent, and deflections are subsequently large. Two questions of interest in the design of such tents are as follows:

(i) To what extent is the nature of the wind loading influenced by the consequent changes in tent shape?

(ii) Are tent structures prone to dynamic amplification of wind loading?

Both these questions were addressed by the author in a study which was carried out at the University of Western Ontario (Jackson, 1982), and which forms the basis of the discussion below.

Mean Loading

One obvious effect of wind loading on a flexible tent is that the loading distorts the tent to a new shape. It is useful to know the extent to which the pressure distribution on the loaded shape resembles that on the original shape, since if the differences are insignificant the loading can be estimated from measurements on a *rigid* model of the initial, known shape.

To study this question tests were made on a series of idealised tent models. The basis model was a 1:25 scale model of a triangular tent of length 3.0m, width 2.0m and height 2.2m. Two further models were constructed with one face distorted in a manner characteristic of panels under load (as shown in Figure 1), and on a further model one face was a flexible membrane. These were tested in a flow representing flat, open terrain with a full-scale roughness length of 4mm and turbulent intensity near the ground of 10%. Because of the large model size it was not possible to scale the large eddy structure correctly - the power spectrum peaked at a length scale of around 0.6 m in the tunnel, well below the corresponding full-scale value. However since gusts of this scale were much greater than the model size it is believed that this mismatch does not have a significant effect on the comparisons between models made below.

At most of the pressure taps the mean, rms and maximum and minimum pressures were measured. In addition the pneumatic averaging technique was used to find the same statistics for the overall instantaneous load on each face, the total forces acting on the tent and the generalised forces for the first and second mode of vibration of one panel. Pressures were converted to coefficients using the free-stream static pressure and incident mean velocity at tent height as reference values. The mean

---

[1]Department of Mechanical Engineering, University of Auckland

pressure distributions on the basic model are shown in Figure 2. They do not show any surprising features, and the range of values is similar to that obtained for other highly 3-D shapes.

To determine whether the differences in C_p between models were significant it was necessary to compare them with the magnitude of error inherent in the measurements, this error being determined by repeating the entire sequence of measurements for the basic model (removing the model in between). The standard deviation of the differences between experiments was found to be 0.013 for mean values and 0.074 for peaks. Comparison with the typical values shown in Figure 2 indicates that in fact these measurements are highly repeatable. Under the hypothesis that there is no difference in point pressures between models of different shape, the ratio of the sum of squares of differences *between* models to the sum of squares of differences *within* models (between tests on the same model) has the F-distribution whose likelihood of exceeding any value is known. This test showed that the differences between models of different shape which were statistically significant were concentrated in a narrow region near the tent ridge on upwind faces. It could be concluded only that the distribution of pressure on downstream faces was insensitive to panel shape, whereas that on upstream faces may not be. The total force acting on a tent panel is arguably more useful for design, and the results obtained for this force coefficient are shown in Figure 3. It can be seen that while there *are* differences between models, they are generally small enough to be ignored. The modal forces for the first and second modes of vibration, and the X,Y,Z components of the total force on the tent were also measured, and these showed differences between model shapes which were no greater than those of Figure 3. One can conclude that area-averaged wind loads on tents can be adequately estimated from tests on rigid models. The worst loading cases are clearly obtained by assuming that the internal pressure is vented to the maximum or minimum external pressure.

Dynamic Loading

Tent structures are also unusual in that the membrane tension is determined by the wind loading itself. Since the stiffness of the structure is strongly dependent on this tension, it turns out that the stiffness, mass and damping of the tent are all of aerodynamic origin. This is illustrated by the following model for the response of tent volume to unsteady wind loads. If the volume change is V and the tent surface has area A_s, the mean speed of surface normal to itself is $\dot{V}/A_s$. A suitable equation of motion for the external flow is then -

$$M\frac{\ddot{V}}{A_s} + A_s\frac{dp}{dV}V + \rho A_s^{\,2}\,\omega^2\,C_D\,\dot{V}/c \;=\; (p_i - p_e)A_s \qquad (1)$$

where M is the tent mass plus the added mass of the (exterior) air, the third term represents damping by acoustic radiation at frequency ω and sound speed c (Ffowcs-Williams and Lovely, 1975), and $p_i - p_e$ is a weighted average over the tent area of the difference between the interior and exterior pressures. The term dp/dV can be thought of as the 'pneumatic stiffness' of the tent - the tent takes up an equilibrium mean shape under loading, and an increment dp in the internal pressure p_i then causes a corresponding change dV in tent shape. Kind (1984) shows how to estimate this stiffness for pneumatic structures, but here this stiffness depends upon the level and distribution of wind loading itself. For example if all the tent panels are highly loaded one expects this stiffness to be high.

This can be modelled by a square panel of side L, modulus E, thickness d which is loaded by pressure p_o but supported only at two ends (so it behaves as a 2-D structure). It can be shown that if the panel is initially slack with total length $L(1 + \beta)$ then -

$$\frac{dp}{dV} = \frac{p_o}{L^3} K \ , \quad K = 24\ \beta\ Ed/p_o\ L \tag{2a}$$

Typical values of K work out to be at least 100 in practice. At the other extreme if just one panel has loading which changes sign along it a small pressure rise over the entire panel can cause a large change in volume, the factor K now being found to be -

$$K = (3/2\ \beta)^{\frac{1}{2}} \tag{2b}$$

which is typically only 10 or 20.

Next consider the motion of air near a vent or leak in the tent. If the vent has area A the velocity through it is $v = -\dot{V}/A$, and the difference in pressure between the interior and the exterior pressure (p_v) at the vent is partly converted to a head loss and partly accelerates some mass of air M_i:

$$A(p_i - p_v) = M_i \dot{v} + \frac{1}{2} \rho A v |\dot{v}|$$

Combining this with our first equation gives -

$$(M + M_i\ A_s^2/A^2)\frac{\ddot{V}}{A_s} + A_s \frac{dp}{dV} V + (\rho L^2 \omega^2 C_p/c + \frac{1}{2}\rho A_s |\dot{V}|/A_s^2)\dot{V}$$

$$= (p_v - p_e)A_s \tag{3}$$

In practice M is dominated by the added mass (approximately $\rho A_s L$) so using equation (2) with $p_o = \frac{1}{2}\rho V_o^2$ leads to a natural frequency of -

$$\omega = \frac{1}{2\pi} \frac{V_o}{L} \sqrt{K/2}$$

This obviously increases with wind speed V_o and is higher for a more highly loaded tent (higher K). Note that $f = \omega L/V_o$ has a minimum value of around 0.4, whereas the energy spectrum of incident turbulence near the ground peaks at a much lower frequency. Treating the forced motion as quasi-static then leads to the tent motion -

$$V/L^3 = (C_{p_v} - C_{p_e})/K$$

with a magnitude increasing as the tent stiffness decreases. Approximating $\dot{V}$ by $\dot{V}\omega$ then leads to critical damping ratios for radiation and leakage of

$$\xi = \frac{1}{2\pi} Ma \sqrt{K/2}\ C_D/2 \ , \quad \frac{A_s^2 (C_{p_v} - C_{p_e})}{A^2\ 4\ K}$$

respectively (Ma is Mach number). Since the frequency of vibration is low the radiation damping is not significant, but the leakage ratio can easily exceed unity and therefore represents a very high level of damping. Overall it appears most unlikely that volume changing modes can be excited by turbulence.

Modes which do not cause volume changes are not damped by the leakage term, and so are much more likely to occur (as when an upwind face moves in as a downwind face moves out). Similar calculations can be carried out, giving similar estimates of natural frequency and amplitude, so that dynamic amplification again seems unlikely.

References

Jackson, P.S. (1983) *'Flexible tent structures under dynamic wind loading'*,Boundary Layer Wind Tunnel, University of Western Ontario, Rep BLWT-1-1983.

Kind, R.J. (1984) *'Pneumatic stiffness and damping in air-supported structures'*,J. Wind Eng. & Ind. Aero., 17, 295-304.

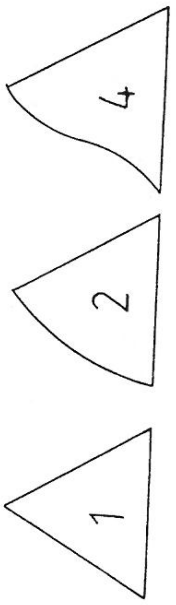

Fig. 1 : Rigid Model Shapes

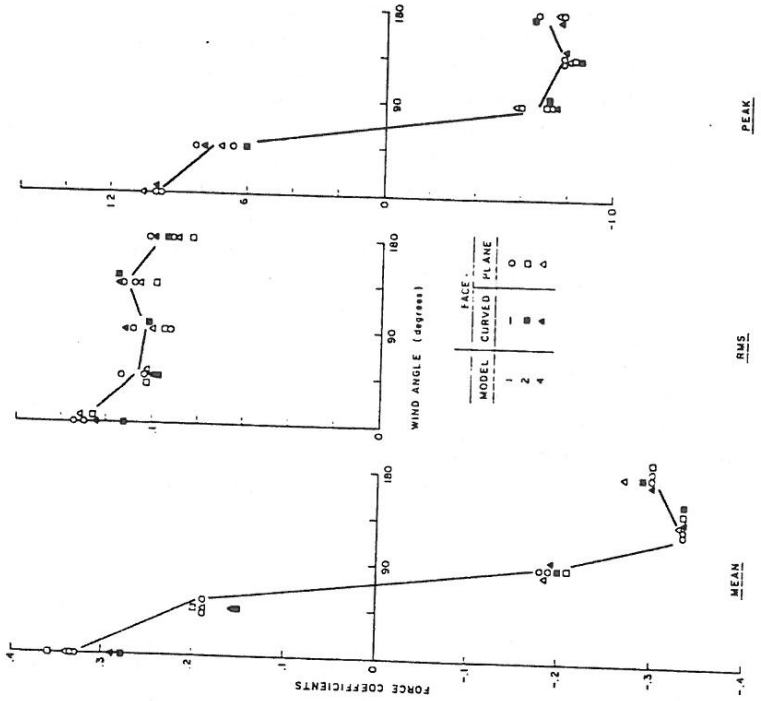

FIG. 3 FORCE COEFFICIENTS ON SLOPING FACES VS. WIND ANGLE TO FACE

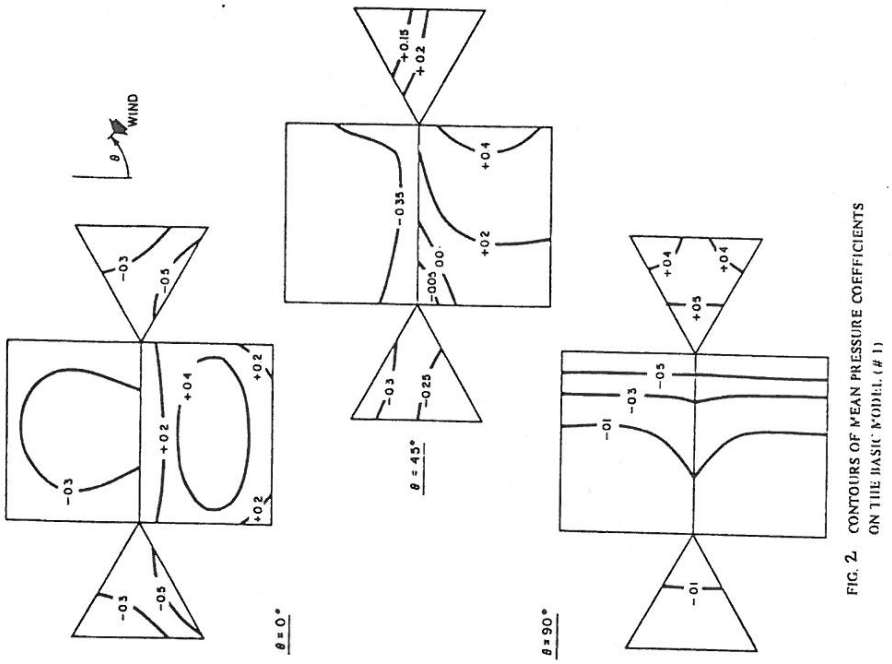

FIG. 2 CONTOURS OF MEAN PRESSURE COEFFICIENTS ON THE BASIC MODEL (# 1)

A REVIEW OF SOME PROBLEMS IN ROAD VEHICLE AERODYNAMICS

P.W. Bearman*

Introduction

Current research into road vehicle aerodynamics can be separated into three broad areas: the development of reliable wind tunnel test techniques, the physical understanding of the flow around three-dimensional bluff bodies near to a ground plane and the evolution of numerical simulation methods to predict vehicle flow fields. One feature that all road vehicles have in common is that their flow fields are extremely complicated and they are the combined result of a number of interacting flow modules. Separations on the forebody, from such features as bonnet edges and A-posts, generate vortices which trail back to influence the remainder of the flow. Flow separation at the base of the vehicle maybe predominately of the recirculating type, as with an estate car, or it may generate strong longitudinal vortices as in the case of a fast-back [1]. The underbody flow plays an important part in generating lift and drag forces as well as influencing the flow when the vehicle is yawed. Add to this the flow around the wheels, through the engine compartment and the ventilation flows and you have an extremely complex problem. Advances in understanding can only be achieved by studying flow modules separately or in simple combinations.

The present interest in vehicle aerodynamics can be attributed to the requirements to decrease the lap times of racing cars and to reduce the impact of increasing fuel prices on passenger vehicle running costs. The use of lighter construction techniques for passenger cars has brought into focus the important problem of passenger car handling in side winds.

Test Techniques

A wind tunnel cannot reproduce precisely the flow environment encountered on the road. The flow around a vehicle travelling in zero wind conditions can be simulated by using a moving ground. The moving ground can be used to drive wheels which are in contact with it. Low ground clearance racing cars are strongly influenced by the ground condition but with typical passenger cars the effects are not so clearly defined. A moving ground induces more flow under a vehicle and its use always generates a decrease in lift or an increase in downforce. Its effect on the flow field depends on the geometry of the underbody. Recently it has been shown that a moving ground changes the base flow behind a bus and alters the dust deposition patterns [2].

All the research using a moving floor that has been reported in the literature has been at model scale, full scale testing presents formidable problems. Many car manufacturers have built, or are building, fixed floor wind tunnels to test full-size cars. Scale effects on cars are largely unknown and little has been done to try and correlate the results of testing at different scales. One of the advantages of working at full scale is that the fine details of the body geometry can be reproduced precisely. Full-scale testing is not without its problems, however, and one of the most serious difficulties is coping with the effects of wind tunnel blockage. Cost is a strong factor in limiting the size of a wind tunnel and the final design is often dictated by the value of the highest blockage that can be tolerated. Considerable research has gone into devising reliable correction methods for typical car shapes. An alternative approach has been to develop wind tunnels with slotted-wall test

---

* Department of Aeronautics, Imperial College, London, SW7 2BY, U.K.

sections to minimize the effects of blockage. It is claimed that geometric blockage can be increased to up to around 15 percent without the need for any correction to measured coefficients [3]. The use of this type of facility in other application areas should be studied.

Little is available on the influence of the natural wind on the aerodynamics of road vehicles. In a tunnel the effect of the wind is usually simulated by placing the vehicle at a fixed yaw angle to the uniform tunnel flow. On the road the approaching wind is sheared and turbulent and the relative conditions experienced by the vehicle are dependent on its own speed. The influence of the wind on vehicle flows is an area requiring much greater attention.

Flow Field Studies

Three-dimensional bluff body flows depend very strongly on the details of the geometry. In two-dimensions a few simple bluff body shapes have been extensively researched by a large number of authors. There are no corresponding standard shapes that have been used widely for 3D bluff bodies near the ground. In order to introduce a relatively simple family of shapes Davis [4] devised a form with a smooth forebody and a flat under surface that generated no separations at zero yaw. To this could be added different base geometries ranging from a flat base to a continuously sloping fast back. He investigated the time-mean wake structure at various downstream positions using a multi-tube, self-aligning pressure probe. The pressure data can be processed to give mean velocity and vorticity profiles. Typical cross flow velocity plots together with longitudinal vorticity contours are shown in figure 1. Using a method due to Maskell [5], the wake data can be suitably integrated to determine drag and side force. The calculated values agree well with balance measurements [6]. Further information is being gathered on the turbulence characteristics of vehicle wakes. An outstanding question is what proportion of the unsteadiness in the wake is associated with turbulence and how much is due to the movement of coherent vortex structures?

Numerical Simulation

From the previous discussion it will be realized that it is extremely difficult to predict vehicle flows accurately. The first techniques employed used panel methods and assumed attached flow. More recently, attempts have been made to incorporate boundary layer development and to use a simple wake model. At best success has been very limited. Current developments with panel methods include the representation of the wake using a time development of discrete line vortex elements. This approach is promising but it still leaves the difficult problem of predicting flow separation position.

Most effort at present is being directed towards using Navier-Stokes codes with a time-averaged Reynolds formulation and a simple turbulence model. Some of the shapes examined experimentally by Davis [4] are being used as computational test cases. In some recent impressive calculations by Coeffe and Darras [7] the flat back model of Davis was calculated using a finite element code and the k-e turbulence model. The general features of the flow were reproduced but the drag coefficient was in error by 20 percent. It should be borne in mind that manufacturers are often interested in drag coefficients to better than 1 percent. Although numerical methods require considerably more development they may one day be able to reduce expensive tunnel testing time.

References

1. T.Morel, 'The Effect of Base Slant on the Flow Pattern and Drag of Three-Dimensional Bodies with Blunt Ends'. Aerodynamic Drag Mechanisms of Bluff Bodies and Road Vehicles. New York. Plenum Press, 1978.

2. T.Lajos, L.Preszler and L. Finta, 'Effects of Moving Ground Simulation on the Flow past Bus Models', 6th Colloquium on Industrial Aerodynamics, Aachen 1985.

3. S.Raimondo and P.J.F.Clark, 'Slotted Wall Test Section for Automotive Aerodynamic Test Facilities', AIAA 12th Aerodynamic Testing Conference. Williamsburg, Virginia, March 22-24, 1982.

4. J.P.Davis, 'Wind Tunnel Investigation of Road Vehicle Wakes', PhD Dissertation, University of London, 1982.

5. E.C. Maskell, 'Progress towards a Method for the Measurement of the Components of the Drag of a Wing of Finite Span', Royal Aircraft Establishment Report 72232, January 1973.

6. P.W. Bearman,'Some Observations on Road Vehicle Wakes', Society of Automobile Engineers, Paper 840301, 1984.

7. Y. Coeffe and M.Darras, 'Modelisation of Navier Stokes Equations: Some Methods and Results', Symposium 'Separated Flow around Marine Structures', Trondheim, Norway, June 1985.

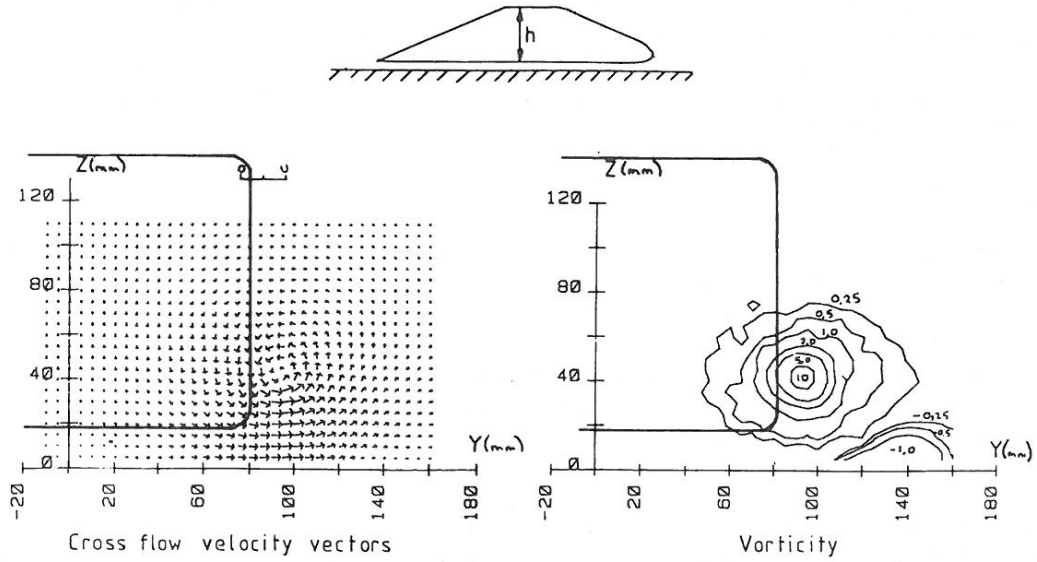

Figure 1. Wake survey behind 25 deg slanting base at x/h = 6.5, ground clearance = 0.15h.

CORRELATION BETWEEN SCALE MODEL WIND TUNNEL TESTS AND FULL SCALE FUEL CONSUMPTION

T.G. Hird[1] and S. Watkins[1]

Abstract This paper reports the methods used, and results obtained, in two separate investigations carried out in the RMIT Industrial Wind Tunnel and duplicated on the road.

The results show that model-scale tests in a wind tunnel can be used as predictors for the likely fuel consumption changes effected by external geometry modifications to road vehicles.

Since on-road tests are time-consuming and costly, only devices that show promise in the wind tunnel need be studied in full scale, provided certain restrictions are realised.

Introduction During 1984 two separate investigations were carried out by staff and students of RMIT. The first was a study of the effects of geometry changes to passenger car drag, Gregory (1), the results of which were compared with actual fuel consumption changes measured on the road, Hird and Gregory (2). The car was a highway chase car used by the Victoria Police.

The second investigation centred on the possible fuel savings obtained by aerodynamic modifications to tri-axle tipper trucks. The work was commissioned by the New South Wales Energy Authority, Watkins et al (3). Both model tests were carried out in the 3 m x 2 m Industrial Wind Tunnel at RMIT, Hird (4).

Victoria Police Car Tests In answer to a request from the Victoria Police, model tests were performed on a 1/4 scale sedan car model to ascertain the drag increases (and other aerodynamic property changes) likely to occur by the addition of roof-mounted warning gear (lights and horns). Three configurations were tested as used by the police. While the model was available, further tests were performed namely ; attaching a streamline fairing to the span-light police configuration, attaching taxi hiring and advertising signs as commonly seen on city and suburban taxis in Melbourne, and attaching bull bars.

CONFIGURATION	$\Delta(C_D.A)$%	Δ(FC)%	DECREASE IN TOP SPEED (km/h)
Baseline	0	0	0
Spanlight	58.2	13.9	9.4
Spanlight + Fairing	21.5	5.6	3.4
Horns 1	17.3	4.6	3.2
Horns 2	30.8	8.6	5.5
Taxi Dome	14.1	-	-
Taxi Advert	10.1	-	-
Taxi Dome + Advert	14.1	-	-
Bull Bar	3.8	-	-

TABLE 1 INCREMENTAL DRAG AND FUEL - CAR TESTS

The increases in zero-yaw drag force obtained over the baseline model are given in Table 1 as a listing of $\Delta(C_d.A)$ % All tunnel tests were carried out at a Reynolds number of 1.2×10^6 per metre, and a longitudinal rms turbulence level of 1.5 % The fuel consumption figures are also given as a percentage over baseline.

[1] Department of Mechanical and Production Engineering, RMIT.

Upon request, the Victoria Police made available a road car and roof-mounted gear. The vehicle was fitted with a digital fuel meter and, for each configuration, two return runs of 117.5 km were made along a section of the Hume Highway. All runs were planned at 97.5 km/h, the average of all runs being 97.54 km/h with a standard deviation of 0.5 km/h. The total fuel usage was recorded. The vehicle mass was identical at the start of each run. The road was dry throughout the duration of the tests and days were selected for testing such that there was negligible wind. Thus the only flow difference between each run was that of other vehicle wakes.

A mock-up foam fairing was used on the span light to model the previous wind-tunnel tests.

A further test was carried out at a proving ground to determine the degradation in top speed due to the roof-mounted devices.

Interpretation of Sedan Car Tests Figure 1 shows a plot of incremental fuel consumption against incremental model drag, all essentially at zero yaw angle. Since no similar data could be found in the literature, data from Rose (5) on truck drag reductions are also presented. Further, a prediction of likely fuel savings from reduction of fuel consumption with reducing drag coefficients on European sedan cars, Hucho (6) has been re-interpreted to compare with this study and is also incorporated in Figure 1.

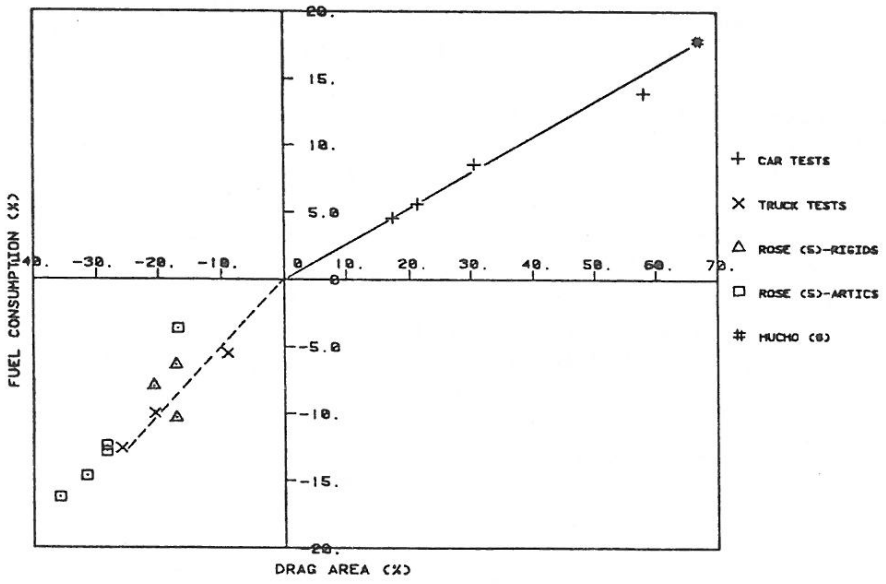

FIGURE 1 CORRELATION BETWEEN ON-ROAD FUEL CONSUMPTION AND WIND-TUNNEL DRAG

It can be seen that a strong correlation exists between full-scale fuel use and model-scale drag. It is sufficiently strong to be able to advise taxi fleet operators that the use of the dome sign and advertising hoarding could result in nearly 6% increase in fuel usage on suburban freeways at speeds approaching 100 km/h.

New South Wales Energy Authority Tests Following discussions between the New South Wales Energy Authority, Aztec Transport Services and RMIT, a study was undertaken on aerodynamic drag-reducing devices for articulated tipper trucks. The initial phase of the work was a series of tunnel tests on a 1/10 scale MACK R686 bonneted prime mover, coupled to an ALCAN tri-axle tipper trailer. Aerodynamic add-on devices were tried individually, and in various combinations and are described in Table 2. If the wind-tunnel results were sufficiently encouraging, it

was proposed that the most promising practical combinations were then manufactured in full scale for road testing.

Unlike many production cars, the majority of articulated trucks exhibit large increases in aerodynamic drag with quite small increases in yaw angle. In addition to generating a non-zero yaw angle, ambient winds change the relative airspeed experienced by the moving vehicle. A process of wind-averaging the wind-tunnel drag coefficient has been developed by Buckley et al (7) to cope with the primary effects of winds. The procedure simulates the long-term steady wind environment and provides a single drag coefficient which is more representative than any drag coefficient obtained at a single yaw angle. It is a particularly useful technique for ranking drag-reducing devices whose performance is a function of yaw angle. This procedure has been applied (for average Australian conditions) to the results presented in Figure 1 and Table 2, denoted by $\bar{C}_D$.

CONFIGURATION	$\Delta(\bar{C}_D.A)$%	Δ(FC)%
Baseline	0	0
Tarpaulin	-20.5	-10.0
Tarpaulin + Fairing	-25.5	-12.6
Tarpaulin + Fairing + Skirts	-31.5	-
Fairing + Gate Fairing	-9.0	-5.5

TABLE 2 INCREMENTAL DRAG AND FUEL TIPPER TRUCK TESTS

Previous work at RMIT (8) indicated that the results for the best of the devices tested in the tunnel should translate to about 10 % fuel savings on the road, under realistic road conditions. It was thus decided to proceed with the second stage of the work; to manufacture full-size devices and verify their performance by on-road testing.

The harsh work environment of tipper trucks precluded the use of the trailer skirts on the road.

Tipper Trucks - Road Tests Two unladen, geometrically-similar, vehicles were supplied by Aztec Transport Services and were instrumented with in-line fuel monitoring systems and stop-watches. To monitor the wind conditions an instrumented car was used.

The test route ran south from Sydney on the Hume Highway, from the 50 km to the 90 km marker. All tests were run at 100 km/h, and road conditions were dry with only light traffic. The two trucks completed several runs with no aerodynamic devices fitted during testing, to establish a calibration factor.

A total of 600 km were accumulated during the calibration runs, and an average of 500 km were travelled for each test with devices fitted. Providentially, each test encountered a range of yaw angles from zero to nine degrees and the average windspeed was very close to that used in the tunnel wind-averaged drag calculations. The ambient windspeed measured at a height of 3 m averaged 11.5 km/h for the tests with devices. The percentage fuel savings for the devices tried are shown in Table 2 and the results of the tunnel and road studies can be seen plotted with the car data on Figure 1.

Interpretation of Truck Data The data from Rose (5) was obtained at zero yaw angle in the tunnel, and in on-road situations where the wind was 16 km/h or less. For the road conditions, yaw angles of up to 11.5 degrees could be generated but this was not reproduced in the tunnel. This is thought to be the major

cause of scatter. The present study wind-averaged the data from the tunnel, and the road tests covered a range of yaw angles and relative windspeeds. It was found that this contributed to improving the correlation between road and model scale, Watkins et al (3), although some scatter was still evident, which was thought to be due to an inability to reach full-scale Reynolds number and a lack of turbulence simulation in the tunnel tests.

Overall Conclusions As a strong correlation exists between tunnel and road tests for vehicles of the same type and weight, when travelling at the same speed, it is concluded that;

1) close predictions can be made for fuel changes resulting from the external geometry changes ;
2) the tunnel is a good tool for design and diagnosis and can determine if devices are worthy of full-scale evaluation.

It is further concluded that a relatively cheap wind-tunnel investigation can have substantial beneficial effects on the time and cost of full-scale vehicle aerodynamic studies. However, if the vehicles or devices are sensitive to yaw angle, or to other effects of ambient winds, it is recommended that the procedure of wind-averaged drag be considered.

References

1. Gregory R. — Aerodynamic Effects of External Body Changes to Sedan Cars. Final Year Thesis, RMIT, December 1984.

2. Hird T.G., Gregory R. — Fuel Usage Tests on Victoria Police Highway Patrol Cars, WTP 1025, RMIT, June 1984.

3. Watkins S., Gibson K.A., Saunders J.W. — Wind-Tunnel Tests on a One-Tenth Scale Tipper Truck. Study for the Energy Authority of New South Wales, WTP 1034, RMIT, Sept. 1984.

4. Hird T.G. — The Design and Construction of an Industrial Wind Tunnel, WTP 1001, RMIT, 1979.

5. Rose M.J. — Commercial Vehicle Fuel Economy - The Correlation Between Aerodynamic Drag and Fuel Consumption on a Typical Truck. Journal of Wind Engineering and Industrial Aerodynamics, Vol 9, 1981.

6. Hucho W-H. — The Aerodynamic Drag of Cars : Current Understanding, Unresolved Problems and Future Prospects. Proceeding of 1976 General Motors Research Symposium, Plenum Press 1978.

7. Buckley F.T., Marks C.H., Walston W.H. — A Study of Methods for Improving Truck Fuel Economy. Prepared for the National Science Foundation. University of Maryland, USA, 1978.

8. Saunders J.W., Watkins S, Hoffmann P.H., Buckley F.T. — Comparison of On-Road and Wind-Tunnel Tests for Tractor-Trailer Aerodynamic Devices, and Fuel Saving Predictions. SAE (US) 850286 Presented at the SAE Congress, Detroit 1985.

AN ON-ROAD TESTING PROCEDURE FOR DETERMINING UNDERBODY PRESSURE DISTRIBUTIONS ON VEHICLES

P.D. Cenek* and J.W. Docherty*

Introduction

The flow underneath a vehicle occurs in a complex region defined by the rough underside of the vehicle and the road surface. This underbody flow field interacts with and influences the external flow field. It is in turn influenced by the pressure distributions established by the forebody and afterbody flow fields. Accordingly the management of the underbody flow and its effect on the overall aerodynamic loading of a road vehicle is now being investigated.

This paper presents the findings of experiments which were undertaken to determine if modifications to a vehicle's underbody area could be assessed by analysing the static pressure history recorded as a vehicle approaches and passes a measurement point located on the road surface. Full-scale on-road testing is preferred to wind tunnel testing in the investigation of underbody flow fields because it eradicates errors caused by imperfect modelling of road boundary effects and wheel rotation.

Description of Test Technique

A literature review indicated that the underbody flow field effects produced by various treatments, such as altering ride height or the addition of airdams, could be determined by carrying out underbody pressure measurements. Most of the published data referred to wind tunnel tests of models using a series of pressure tappings on the underbody to determine the pressure distribution on the underside of the vehicle. In addition, there were some reports of using the 'ground plane' (i.e. road level) pressures as a measure of an airdam's performance [1], although no full-scale test results were found.

As a relatively simple test method was required, it was decided to experiment with the use of a pressure transducer, located so that it measured the static pressure of the road as a vehicle was driven over it. This method, first suggested by Buckley [2], was found to work well, the effect of minor modifications such as a 10 millimetre change in front axle ride height being detected. In addition, it was found that the pressure distributions were repeatable, with good agreement obtained for the pressure magnitudes over the front third of the underbody.

Prevailing wind appeared to have little effect on the underbody pressure distributions and was thus not considered to be a factor which affected the repeatability of the results.

In order to automate the testing process a computer was used to sample the output from the pressure transducer at high speed, sampling being initiated automatically by a vehicle detector located some 15 metres in front of the measurement point. A second vehicle detector, in-line with the transducer, was used to indicate when the car passed over the transducer. The computerised sampling system allowed testing to be carried out at speeds between 50 and 150 km/h with adequate resolution.

Software was developed to allow the data obtained from these runs to be analysed quickly as the testing proceeded. This system allowed the pressures to

---

* Central Laboratories, MWD, P.O. Box 30-845, Lower Hutt, NZ

be normalised by the vehicle speed (determined by the time the car took to pass the vehicle detector), resulting in direct calculation of both the underbody pressure coefficient profile along a longitudinal section of the vehicle and the lift force acting on the section. By analysing the data in this manner, results from runs at various speeds could be easily compared.

Equipment

The transducers used for the measurement of underbody pressures were Setra 0.1 psi differential pressure transducers. These have a high frequency response (in excess of 1000 Hz) and provide good resolution over the range of pressures encountered during this type of testing.

The system used to detect the presence of a vehicle consisted simply of a photo-electric cell driving a switching circuit, and a high powered lantern. This system was arranged to give a nominal output of zero volts with no interruption to the light source, and 5.0 volts when the light beam was interrupted.

The computerised sampling system consisted of a Digital Equipment Corporation PDP 11/23 Plus computer running under the RSX-11M operating system. Data acquisition was by way of a 12 bit analogue-to-digital converter.

Software was developed specifically to allow the inputs from the pressure transducer and vehicle detectors to be monitored or recorded as required. In the monitor mode 500 samples were taken from each channel at a rate of 500 Hz and the data then analysed to give the mean, minimum and maximum values for each of the three channels. As soon as the information was displayed on the VDU the process was repeated. In the recording mode the system monitored the input from the first vehicle detector continuously. As soon as the presence of the vehicle was indicated the system then began recording the output from the pressure transducer and the second vehicle detector at a rate of approximately 1400 Hz, taking 1000 samples for each channel. This data was then written to disk for later analysis.

Results

(1) Comparison with Published Data

Although there is relatively little published data available on full-scale measurements of underbody pressure, one paper by Carr [3] was found which included both road and wind tunnel pressure measurements. As results from tests on a 1967 VW Fastback were included in this paper, and a similar vehicle was available for testing at Central Laboratories, a comparison was carried out of the two underbody pressure profiles.

The method used by Carr to measure the underbody pressure was different from that used at Central Laboratories. In his tests Carr used a total of nine pressure tappings on the underbody of the car, the pressures being measured by an inclined manometer, which was clamped to record the reading after the test speed had been maintained for some 30 seconds.

In spite of the difference in the measuring techniques, the agreement between the two sets of results is relatively good (see Figure 1). In particular, the point at which the minimum pressure occurs is the same in both cases and the initial rate at which the pressure decreases is almost identical. The large high frequency fluctuations in pressure occurring in the data obtained at Central Laboratories were caused by a faulty exhaust, the resultant noise being recorded by the transducer.

(2) Flow Field Effects Produced by an Airdam

Ground plane centreline pressures for a 1985 Toyota Corolla hatchback, with and without a 45 mm deep airdam fitted, are given in Figure 2. These results, which represent approximately a one second history of the ground plane pressures, enable the effect of the airdam on the approach, underbody, and wake flow fields to be examined.

Referring to Figure 2, the ground pressures ahead of the vehicle are positive due to the vehicle's decelerating effect on the approach flow as it has to change direction to pass over, around and under the vehicle. The addition of the airdam in this case does not appear to raise the upstream pressure levels.

Investigation of the pressures in the vehicles underbody region indicates that the airdam also causes the flow to converge under the airdam, the resulting flow acceleration reducing the static pressures forward of the front axle. This has the desirable effect of decreasing the front axle lift and the vehicle pitching moment. However, the pressure reduction at the nose of the vehicle is partially offset by the increase in pressure on the floor pan and so only a small change in the overall lift force acting on the underbody results.

Ideally, if the base pressure of the wake is increased, the net drag on the car will be reduced. From the pressure data given in Figure 2, it can be seen that the base pressures are relatively unaffected by the addition of the airdam, although the extent of the far wake appears to have increased. This may be due to an increase in the intensity of the trailing vortices brought about by the airdam deflecting more air along the sides of the vehicle.

In general, the results of these on-road measurements are in close agreement with the wind tunnel findings presented in [1].

Conclusion

This study has verified the feasibility of using ground surface pressure measurements to investigate the airflow beneath a road vehicle and its interaction with the external flow field. The resulting on-road procedure developed for obtaining the required aerodynamic data has the following advantages when compared with other test methods:

(1) no vehicle modifications are required;
(2) since all measurements are taken from the road surface, not from the vehicle, instrumentation noise problems normally associated with full-scale testing have virtually been eliminated;
(3) calm wind conditions, although desirable, are not necessary to obtain useful results; and
(4) being computer based, preliminary analysis of the data can be carried out while the tests are in progress so configuration changes can be rapidly assessed.

The procedure is therefore particularly applicable to the investigation of various methods used for reducing underbody drag and for improving handling through 'ground effects'.

Acknowledgments

The authors wish to thank Toyota NZ Ltd and Ministry of Works and Development for the permission to present this paper. The assistance of Messrs D. Brown (Central Laboratories) and A. Rowe (Toyota NZ) in performing these tests is gratefully acknowledged.

References

1. F.K. Schenkel, 'The Origins of Drag and Lift Reductions on Automobiles with Front and Rear Spoilers', SAE Paper 770389, 1977.

2. B.S. Buckley, 'Road Test Aerodynamic Instrumentation', SAE Paper 741030, 1974.

3. G.W. Carr, 'Correlation of Pressure Measurements in Model and Full-Scale Wind Tunnels and on the Road', SAE Paper 750065, 1975.

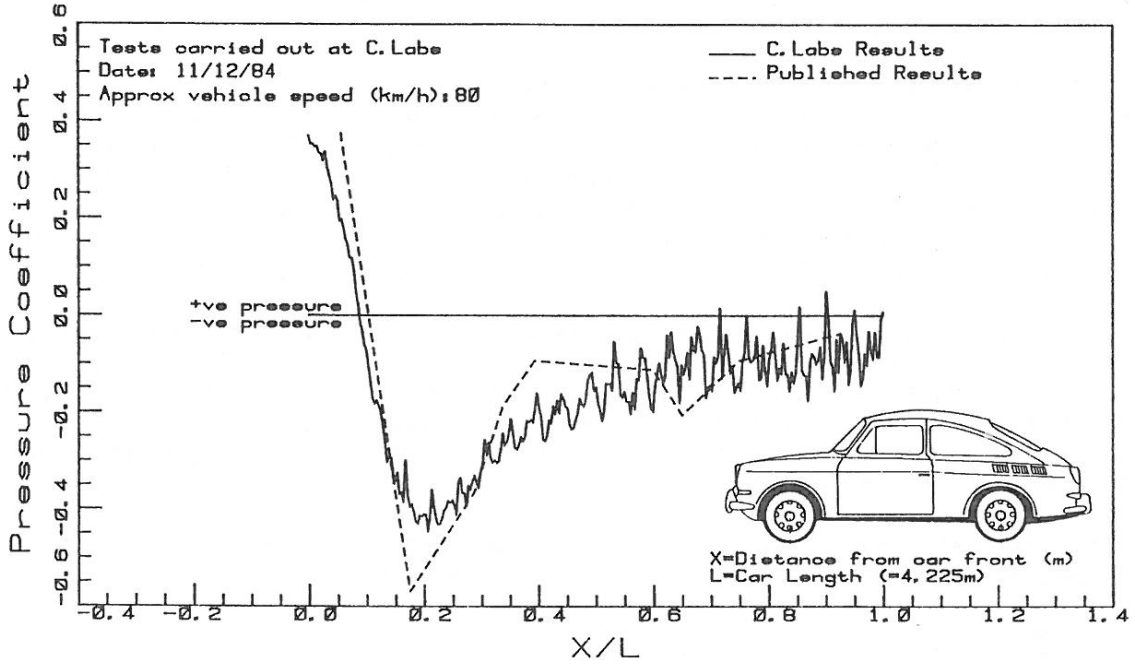

Figure 1: 1967 VW FASTBACK underbody pressure comparison

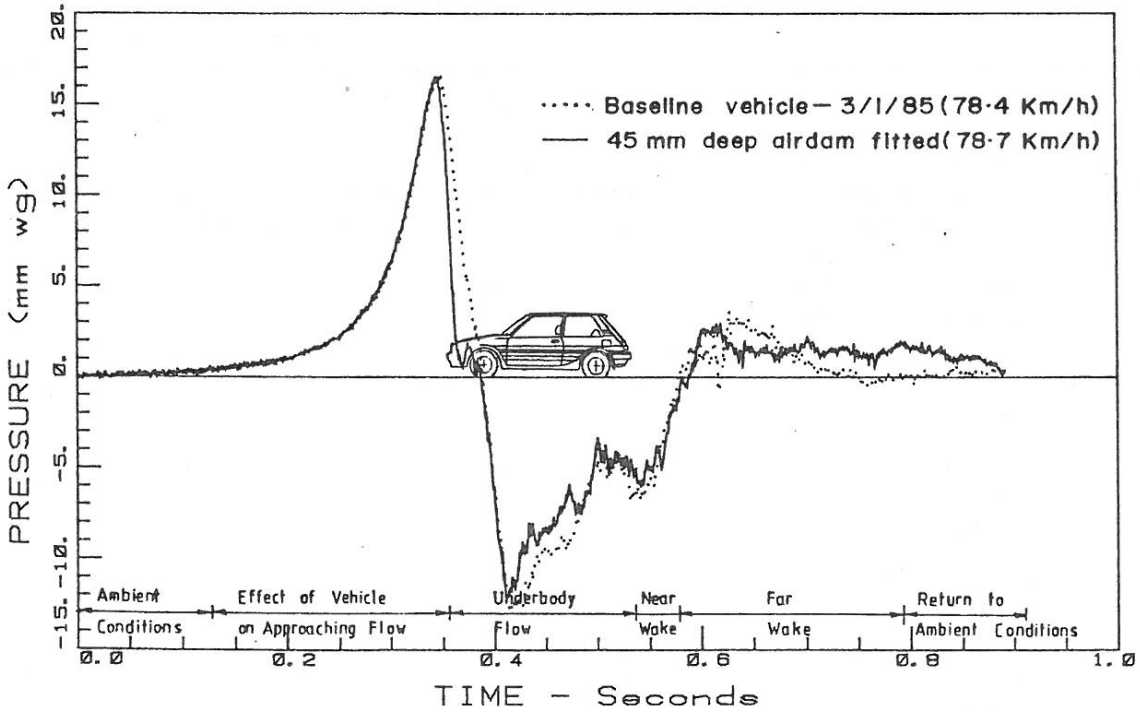

Figure 2: Centreline ground pressure changes produced by an airdam

THE WIND ENVIRONMENT EXPERIENCED BY MOVING VEHICLES

S. Watkins*

Introduction The relative wind velocity, V_r experienced by surface vehicles is the vector sum of the vehicle velocity relative to the ground, V_t and the velocity of the natural wind relative to the ground, V_w. Additionally a yaw angle ψ is generated when the direction of the natural wind is inclined at an angle Φ to the direction of motion of the vehicle, as shown below in Figure 1.

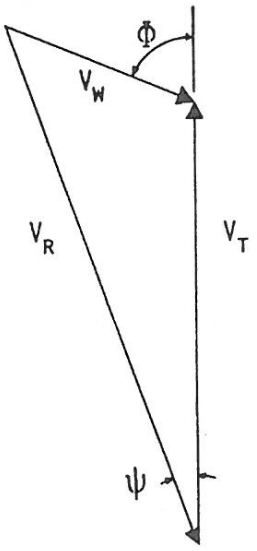

The first effect of a crosswind is commonly simulated in a wind tunnel by yawing the model at various angles ψ to the oncoming flow and measuring forces which are reduced to coefficient form using the vehicle velocity V_t. Frequently the change in relative velocity which can occur in full-size (due to ambient winds) is ignored when interpreting tunnel results.

To take into account both effects when calculating a long-term drag coefficient, Buckley et al (1) suggested a process of wind-averaging tunnel drag coefficients. This is a simple, but useful model for analysing the average primary effects of steady winds on a vehicle's aerodynamic performance and involves weighting the drag coefficient at various yaw angles to account for the change in relative velocity. It is becoming widely used for interpreting tunnel data from commercial vehicle tests.

It has been shown that for the UK, (2) it is reasonable to assume that the natural wind can approach a vehicle's direction of motion from any angle Φ, ie there needs to be no weighting for wind and route directions. Thus the angle Φ has equal probability of lying in the range 0 to 360 degrees.

	NATURAL WIND V_w	WIND DUE TO VEHICLE MOTION V_t
STEADY EFFECTS	$\overline{V_r} = \overline{V_t} + \overline{V_w}$ ($\overline{V_r}$ varies with height) Generates a yaw angle ψ (ψ changes with height)	Steady component due to vehicle motion $\overline{V_t}$
UNSTEADY EFFECTS	Natural Wind Turbulence Wakes of Stationary Objects	Changes in Speed Changes in Direction Wakes of other moving vehicles
Note : There are sub-sets of the above but their influence is considered minimal		

However, the natural wind is far from steady. It is turbulent, with continuous fluctuations in speed, and the amplitude and frequency vary in a random manner. There is also a mean variation with height. This paper attempts to document these effects, and to aid this, components of the relative wind sensed by a moving vehicle are separated and presented in Table 1 on the left.

Steady Wind Effects It is commonly known that the natural wind has a mean variation with height. From theoretical

* Department of Mechanical and Production Engineering, RMIT.

considerations, the profile can be shown to be a logarithmic function although it is sometimes convenient to fit a power function. This effect has been considered by Buckley (1) and Cooper (3) and shown to produce small changes in yaw angle and relative velocity compared to the magnitiude of the total changes.

Unfortunately there appears to be little data to verify that the velocity profile is close to a log or power fit for the type of terrain and the heights relevant to vehicles. Panofsky (4), and Bradley (5) have studied some of the properties of the wind at heights under 4.3 m (the maximum road-legal height for Victoria), but both studies were over flat landscapes (plains) which had very low associated roughness heights. Most work in this area has been for agricultural purposes. Recent work by Flay (6), has substantially increased the data base on wind effects close to the ground, although problems were experienced from the lowest anemometer (3.2 m) due to flow non-stationarities. It seems likely that for many roads the scale of local roughness (trees, bridges, cuttings etc.) is such that a well-defined velocity profile could be lost, and the unsteady wind effects exert greater influence. Lawson (7) warns against using the power law at the extremities of its fitted range, particularly when the zero plane displacement is large. Considerably more work appears necessary in this area.

Unsteady Effects Rapid vehicle accelerations and changes of direction can change the wind conditions sufficiently rapidly to be viewed as unsteady effects, however this paper is mainly concerned with wind effects that occur on vehicles travelling at highway speeds where these effects are minimal, or may be regarded as quasi-static. For this paper they will be ignored.

Some theoretical work has been done on the effects of natural wind turbulence for vehicle stability studies, Balzer (8) and also Cooper (9) who used data compiled from a variety of sources by ESDU (10). Again there is little experimental work to verify the low-level unsteady effects. There has been some experimental work in the UK by Smith (11) who found that majority of "gusts" measured by a moving car were caused by identifiable local effects. There has also been some work in Japan and France.

Work at RMIT To investigate unsteady wind effects, a car instrumented with a GILL propeller-vane anemometer and a TSI hot film anemometer, recorded data along the Geelong Road. A typical trace is shown below. The wind relative to the ground (at a height of 3.3 m) averaged 2.2 m/s and this data was recorded near the 40 km marker (from GPO Melbourne). This windspeed appears close to the average Australian daily windspeed, Giang (12).

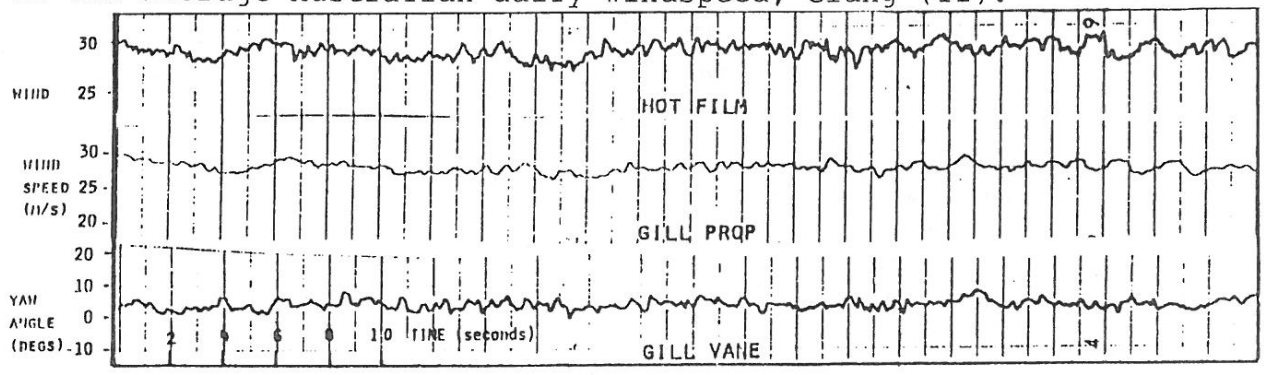

Figure 3 below, was obtained from the same vehicle, but the measurements were made along the Hume Highway approximately 60 km south of Sydney. The data was filtered at 1 Hz and sampled every 8 s. Roadside obstructions differ markedly from the Geelong Road as the tree cover is far more dense and there are many more cuttings and forested areas close to the highway.

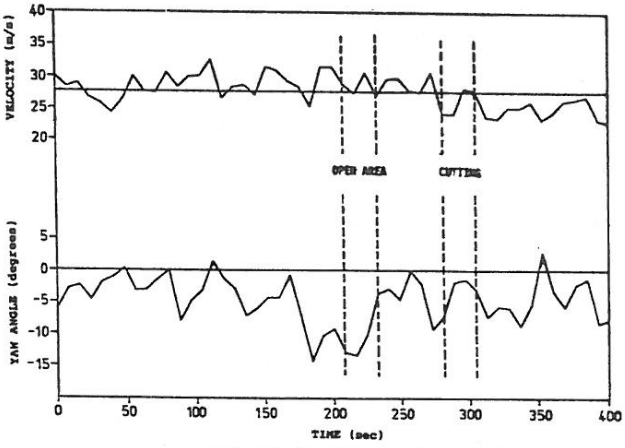

FIGURE 3 WIND DATA-N.S.W.

For all runs the car speed was held constant at 100 km/h (27.8 m/s) to within + 1 km/h. The mean windspeed relative to the ground was 3.1 m/s and it was orientated at a mean angle Φ of 30 degrees to the direction of motion. 10 degree variations of yaw angle within a period of 20 seconds were frequently encountered, accompanied by changes in relative wind velocity of the order of 5 m/s. This is thought to be typical of roads which have intermittent roadside tree cover.

Further work has been undertaken on the Geelong Road test route and a summary of some of the parameters is shown below. Data were recorded at sites along the roadside and the car was positioned upwind of the road to ensure that the effects of moving vehicle wakes were not recorded. Data was also recorded with the vehicle moving (denoted by asterisk) at 100 km/h and all runs were made immediately after the preceding stationary run. To calculate the turbulence intensity for the moving vehicle, it was desired to remove the effects of slow changes in vehicle speed. This was done by high-pass filtering all the data at 0.1 Hz, which corresponds to a road distance of 280 m or approximately 17 articulated vehicle lengths. All data were recorded on analogue tape. The output from the GILL propellor was low-pass filtered to remove only discrete fluctuations from the tach-generator output, hence the maximum frequency response was dictated by the inertia of the instrument. The output from the hot film was low-pass filtered at 50 Hz. Measured intensities for the moving vehicle range

RUN NO	LOCATION	SAMPLE (mins)	WIND SPEED (m/s)	WIND D'ION	TURBULENCE INTENSITY GILL	TURBULENCE INTENSITY HFA	COMMENTS ON TERRAIN
1	30 km	12	1.9	SW	26.4	34.5	In tree wake
2	50 km	12	2.5	SSW	9.1	13.4	Short bushes
3	70 km	12	4.6	SSW	8.2	12.2	Short grass
4	90 km	12	8.3	SSW	8.4	12.4	Short grass
5	50 km	12	6.5	S	11.5	16.4	
6*	50-40 km	6	29.1	S	3.0	4.0	Passed one truck
7	30 km	12	5.8	S	11.6	20.2	
8*	30-50 km	12	33.1	S	2.8	3.0	Light traffic
9	70 km	12	6.8	S	7.8	11.8	
10*	70-90 km	12	27.4	S	2.8	2.9	Light traffic
11	90 km	12	4.5	S	12.7	15.7	Fine rain
12	70 km	12	6.5	S	9.6	15.1	
13*	70-90 km	12	25.6	S	2.4	2.6	Light traffic
14	90 km	12	5.5	S	9.6	15.0	
15	30 km	8	1.2	SE	13.9	-	
16*	30-50 km	12	30.2	SE	1.5	1.7	Light traffic
17	50 km	10	2.2	SE	13.8	34.6	
18*	50-30 km	12	27.7	S	1.9	2.5	Light to medium traffic
19	30 km	12	2.7	S	12.7	28.9	
20	70 km	5	2.6	S	11.3	20.6	
21*	70-90 km	12	25.0	S	2.4	2.4	Light traffic
22	90 km	3.5	2.6	S	13.5	21.5	
23*	90-70 km	12	27.1	S	2.0	2.1	Light traffic
24	70 km	2	1.4	S	16.2	38.0	Short run (tape ran out)

Table 2 Stationary and Moving Wind Data - Victoria Test Route

from the lowest value of 1.5 % rms from the GILL to a maximum of 4.0 % rms for the hot film, with windspeeds varying from 1.2 to 6.8 m/s. Other work undertaken during periods of stronger winds (≈10 m/s) resulted in turbulence intensities of up to 6 %.

To investigate the frequency distribution, power spectral density functions are currently being calculated.

Concluding Remarks Currently major vehicle tunnels have turbulence levels of less than 1 % and none have the ability to investigate possible velocity profile effects. With increasing pressure being put on vehicle manufacturers to reduce drag coefficients, it may become necessary to improve the wind tunnel's simulation of the on-road flow conditions. For this to occur further knowledge of the wind environment of the moving vehicle is necessary.

References

1. Buckley F.T., Marks C.H., Walston W.H. — A Study of Methods for Improving Truck Fuel Economy. Prepared for the National Science Foundation, University of Maryland, USA, 1978.

2. Ingram K.C. — The Wind-Averaged Drag Coefficient Applied to Heavy Goods Vehicles. TRRL (UK) Supplementary Report 392, 1978.

3. Cooper K.R., Campbell W.F. — An Examination of the Effects of Wind Turbulence on the Aerodyanamic Drag of Vehicles. J. Wind Eng. & Ind. Aero. 9, (1978), 167-180.

4. Panofsky H.A. — Scale Anaylsis of Atmospheric Turbulence at 2 m. Qt. Jl. Royal Met. Soc. 88, 1962.

5. Bradley E.F. — Private Communication. CSIRO., July, 1984.

6. Flay R.G.J. — Structure of a Rural Atmospheric Boundary Layer Near the Ground. PhD. Thesis, University of Canterbury, New Zealand, 1978.

7. Lawson T.V. — Wind Effects on Buildings, Vol 2. Applied Science Publishers Ltd., 1980.

8. Balzer L.A. — Atmospheric Turbulence Encountered by High-Speed Ground Transport Vehicles. Jl. Mech. Eng. Sci. Vol 19, No 5, 1977.

9. Cooper R.K. (sic) — Atmospheric Turbulence with Respect to Moving Ground Vehicles. J. Wind Eng. & Ind. Aero., 17 (1984).

10 ESDU — Engineering Science Data Unit. Data Sheets 74030, 74031 and 75001.

11 Smith N.P. — Wind Gusts Measured on High-Speed Roads. Motor Industry Research Association (UK), Report 1972/7.

12 Giang N. — Computer Simulation of the Effect of Climatic Winds on the Performance of Trucks in Australia. Final Year Thesis, Department of Mechanical and Production Engineering, RMIT, Dec 1984.

AUTOMOTIVE ENGINE COOLING SYSTEM DESIGN WITH PARTICULAR REFERENCE TO AIR CIRCUIT COMPONENTS

C.Y.L. Chan* and P.I. Cooper*

Introduction

Many vehicles with water cooled engines are now fitted with thermostatically-controlled electric cooling fans. The optimum design of an engine cooling system requires a knowledge of the performance characteristics of the radiator core, the cooling fan, the fan shroud and their interaction because the airside capacity is the controlling factor in heat dissipation.

The present paper describes briefly the results of two research projects recently sponsored by Davies Craig Pty Ltd and Natra Pty Ltd on automotive cooling systems. The first project was to design a high efficiency engine cooling fan driven by an electric motor, and to establish fan design techniques for future applications. The second project was to examine the various factors affecting the airside performance of an automotive engine cooling system.

Fan Design Considerations

To minimise power consumption of the fan/motor assembly, it is important to match the fan and fan motor. Figure 1 illustrates this principle. Curve 1 in Fig. 1(a) shows the fan static pressure and air flow rate relationship, where point A is the design point for the fan. For example, a typical design point could be 600 litres/s of air at 100 Pa static pressure. Curve 2 is the fan total efficiency curve, where peak fan efficiency occurs at B. If a fan is properly designed, fan design point A should be near the peak (point B) of the fan efficiency curve. Curve 3 is a plot of fan torque versus air flow rate; point C thus indicates the torque required to drive the fan motor.

Fig. 1(b) shows the method used to optimise fan and motor performance. The volume flow rate versus torque curve (curve 3) is as in Fig. 1(a), except that it has been placed with the origin of its co-ordinates in the top left hand corner. Motor efficiency is shown by curve 4 and the intercept between curves 3 and 4 is the operating point for the particular fan and motor assembly. This point should coincide with the peak efficiencies for both the fan and the motor for proper matching.

Figure 2 shows the typical non-dimensional characteristics K and Λ of a six-bladed fan of arbitrary vortex design, developed during the project for four different blade setting angles. K is defined as the ratio between the total pressure rise through the fan (P_T) and the dynamic pressure in the fan annulus ($0.5\ \rho U_A^2$), while Λ is defined as the ratio between the mean axial velocity in the fan annulus (U_A) and the circumferential tip speed of the rotor (ΩR), i.e.

$$K = \frac{P_T}{0.5\ \rho U_A^2} \quad ; \qquad \Lambda = \frac{U_A}{\Omega R}$$

* CSIRO Division of Energy Technology, Melbourne, Australia.

The performance of a fan for a given geometry is then given by one curve of K versus Λ and this curve applies for all rotational speeds of the fan. Apart from the advantages of condensing the data presentation for a particular fan, fans of different sizes can then be designed from this data to meet different pressure duties.

Fan Shroud/Radiator Performance under Ram Air Conditions

Ram air is that quantity of air that passes through the radiator due to the forward motion of the car and if sufficient ram air is available for engine cooling, operation of a fan is not required. An unshrouded fan would give essentially unimpeded air flow performance under high vehicle speed conditions, but it may be inadequate at low vehicle speed. Therefore, a fan shroud if used, should give minimum resistance to ram air and maximum air flow under fan-induced conditions.

There is a lack of information on shroud design in the literature, but Ref [1] gives some guidelines on shroud configurations for on-highway vehicles. Several experimental shrouds were constructed: a ring type shroud with bellmouth entry, a ring type with venturi duct, and a box type shroud with straight duct or venturi duct. The aerodynamic resistance of each of the radiator/shroud assemblies was measured in the wind tunnel, and used to estimate the effectiveness of the various shrouds under ram air conditions.

Air resistance in the cooling system is due to the front grille, the radiator and fan/shroud assembly and restrictions in the engine compartment behind the radiator and the amount of air that passes through the radiator-shroud assembly will be less than that calculated directly from the vehicle's motion. Costelli et al [2] indicate that the radiator/shroud assembly contributes about 50% of the total system resistance. Paish and Stapleford [3] have provided a simple relationship for the ratio R_v (V/V_o) between the free stream velocity V_o and radiator face velocity V in terms of the radiator/shroud pressure drop coefficient, K_p, i.e;

$$R_v = \frac{1}{1 + \frac{K_p}{4}}$$

If K_p and V_o are known, then the velocity ratio and the radiator face velocity may be calculated. It is assumed for the purposes of this report that the measured K_p values for various radiator/fan/shroud assemblies represent the total system resistances. It has also been necessary to estimate values of K_p at high velocities. Figure 3 shows the calculated air flow performance of various shrouds, under ram air conditions, with the radiator fan not operating. As expected, at a vehicle speed of 100 km/h, the full "box" shroud (S4) has an estimated air flow rate which is considerably less than the S1 bellmouth "ring" shroud.

Radiator Thermal Performance

A convenient indication of the temperature driving potential of the radiator is the "mean temperature difference (MTD)" [4]. It is defined as the difference between the average inlet and outlet water temperatures (T_{WI} and T_{WO}) and the inlet air temperature (T_{AI}), i.e.:

$$MTD = \frac{T_{WI} + T_{WO}}{2} - T_{AI}$$

Specific heat dissipation (SHD) is used to express the specific heat transfer capability of the heat exchanger. It is defined as the amount of heat dissipated by the radiator q divided by the face area of the radiator A and MTD, such that:

$$SHD = \frac{q}{A.MTD}$$

The specific heat dissipation of the test radiator (2 rows, 11 fpi, 0.24 m^2 face area) was measured with water flow rates from 0.3 to 1.2 kg/s, and radiator face velocities between 1 and 10 m/s. The results are shown in Figure 4, which shows that the specific heat dissipation is a strong function of radiator face velocity, but is relatively insensitive to water flow rate.

It has been found in this project that when air flow is induced through the radiator core by an attached fan/shroud assembly, considerable design freedom exists in placement of the fan on the core and the shape of the fan ventilated area. From a thermal point of view, there is no preferred position or shape. For a given air volume flow rate, it is also desirable to ventilate the maximum area possible with the further benefit that the lower core velocities will result in a lower core pressure drop and less fan power. A practical consideration is that the largest fan diameter is normally restricted to the minimum dimension of a rectangular radiator and to utilise more core area for fan cooling, a shroud with a rectangular to circular transition is necessary. For ram air cooling alone at high speed, it is preferable to have a fan/shroud assembly which presents the lowest pressure drop so that for a given vehicle speed, the core velocity is maximised.

The experimental work done in this project has shown that the fan design principles established previously result in a rotor design which presents a small aerodynamic resistance to ram air (as well as optimum efficiency when being driven). The resistance of the shroud (which ensures efficient fan operation) is minimised using a simple bellmouth ring shroud. Contrary to published information, venturi style shrouds did not perform as well and are necessarily more complex. It is apparent that there is insufficient knowledge of the fundamentals of shroud design, particularly those with a limited axial dimension and considerable scope exists for putting shroud design on a rational basis.

References

1. Cooling of Detroit Diesel On-Highway Vehicle Engines. Detroit Diesel Engineering Bulletin No.41, 1982.

2. A. Costelli, D. Gabriele, and D. Giordanengo - Experimental analysis of the air circuit for engine cooling systems. SAE Paper 800033, 1980.

3. M.G. Paish. and W.R. Stapleford - A rational approach to the aerodynamics of engine cooling system design. Proc.Inst.Mech.Engrs. 1968-69, Vol.183, Pt.2A, No.3.

4. W.R. Stapleford - Factors affecting the selection of fans for automotive engine cooling applications. Int.Conf. on Fan Design and Applications, Guildford, England, September 1982.

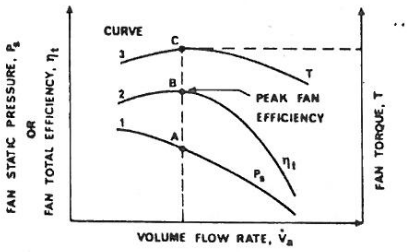

(a) TYPICAL FAN PERFORMANCE CURVES

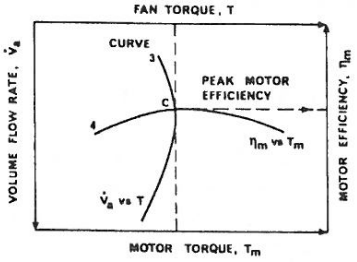

(b) IDEALISED MATCHING OF FAN AND FAN MOTOR

Fig. 1 Matching of fan and fan motor for optimum performance.

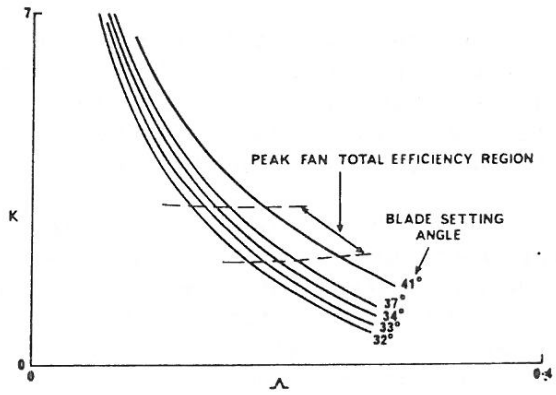

FIG. 2 TYPICAL NON-DIMENSIONAL CHARACTERISTICS OF AN ARBITRARY VORTEX FAN

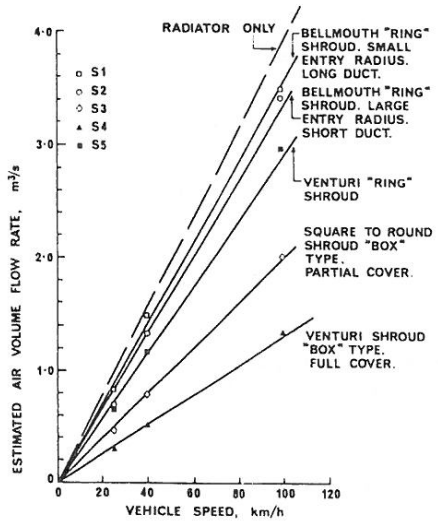

FIG 3. COMPARISON OF ESTIMATED AIR FLOW PERFORMANCE BETWEEN VARIOUS SHROUDS, UNDER RAM AIR CONDITIONS. (FAN NOT OPERATING.)

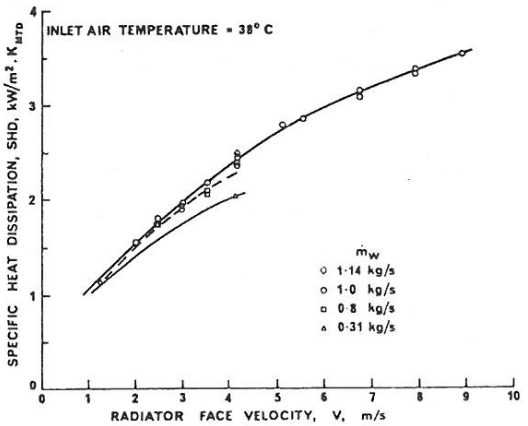

FIG. 4 SPECIFIC HEAT DISSIPATION VERSUS RADIATOR FACE VELOCITY FOR VARIOUS RADIATOR WATER FLOW RATES.

EFFECT OF RAM AIR AND FAN AIR ON AUTOMOTIVE HEAT EXCHANGER PERFORMANCE

by P.I. Cooper and C.Y.L. Chan*

Introduction

An experimental investigation with a test radiator from a popular passenger vehicle was undertaken to examine the effect of a range of design variables on its thermal performance. The work reported here is part of a wider study conducted for NATRA Pty. Ltd. and Davies, Craig Pty. Ltd. by the CSIRO Division of Energy Technology on the design of optimum automotive cooling systems.

The experimental work was carried out with a NATRA radiator type 92000114 of standard copper/brass construction with a 2 row/11 f.p.i. core. A closed circuit controlled temperature wind tunnel capable of air flows up to 1000 L s^{-1} was constructed for the project. Controlled temperature hot water was supplied to the test radiator from a 37 kW electric heater. The primary measurements from which the heat transfer rate was derived were the radiator water flow rate (measured to $\pm$ 1% of rate) and radiator inlet and outlet water temperatures (measured to $\pm$ 0.2 k). The closed circuit wind tunnel incorporated an air flow measuring device with an accuracy of $\pm$ 2%.

This paper presents some of the results from experimentally determining the radiator's heat transfer capability as a function of total air flow rates and different velocity distributions across the radiator face. Ram air refers to air flow through the radiator due to the vehicle motion while fan air is the air flow due to the operation of a cooling fan. Ram air flow can occur through the fan air section but no fan induced flow occurs through the ram air section.

Measurement of radiator heat dissipation

Specific heat dissipation

The specific heat dissipation is defined as the heat dissipation rate of the radiator per unit ventilated area per degree mean temperature difference, i.e.

SHD = q/(A x MTD) where q is the heat transfer rate in kW, A is the ventilated area in m^2 and $MTD = \left[\left(\frac{T_{wo} + T_{wi}}{2}\right) - T_{ai}\right]$.

T_{wo}, T_{wi} and T_{ai} are the water outlet and inlet temperatures and air inlet temperature respectively.

A series of tests were performed in which the air velocity, water flow rate and ventilated area size, position and shape were varied [1]. The conclusions were:-

---

* CSIRO Division of Energy Technology, Melbourne, Australia

(i) For a given radiator core the SHD is primarily determined by the ventilated area velocity.

(ii) The SHD is only slightly dependent on the water flow rate and is insensitive to the ventilated area size, position and shape.

The data from many tests for a typical water flow rate of 1 kg s^{-1} resulted in an equation of the form;

$$SHD = 1.052\ V^{0.57}$$

where V is the average velocity of the air onto the radiator face. The 0.57 exponent is close to the typical value of 0.6 for louvred fin radiator cores [2]. This supports the assumption that the radiator under test was typical of the type normally used in automobiles.

In all tests, the shape, size and position of the ventilated area were varied using blanking pieces which only allowed air to pass through the area under consideration; everywhere else over the radiator face it was essentially zero. In a practical vehicle situation, the presence of a ventilating fan/shroud assembly with an associated thermostatically controlled electric motor will only partially restrict the ram air flow through the fan region. In this case, because of the non-linear dependence of the SHD on the average velocity, it could be expected that the overall heat transfer capability of a radiator will be determined to some extent by the relative aerodynamic resistances and areas of the fan and ram air sections. The results from examining this are given in the following section.

Effect of ram air/fan air veocity ratio

For experiment and analysis, the real situation was simulated by partly blanking different areas of the test radiator with grids whose measured dimensionless pressure drops $K = 0.5\ \rho\ V^2$ were similar to the K values to be expected for typical fan/shroud combinations. The results of some of the tests are shown in Table 1. It can be seen that over the range of K's considered and the resulting velocity ratios, there is no significant effect of velocity ratio on the overall heat transfer. Measurement of the velocity distribution over the radiator was not possible for this project, so the velocity ratios shown were calculated from the following simple analysis.

Referring to Fig. 1 it can be shown that;

$$V_1 = \left(\frac{V^2}{1 + K_1}\right)^{1/2}; \qquad V_2 = \left(\frac{V^2}{1 + K_2}\right)^{1/2}; \qquad V_1/V_2 = \left(\frac{1 + K_2}{1 + K_1}\right)^{1/2} = \left(\frac{R_2}{R_1}\right).$$

With the assumption that the MTD is the same for regions 1 and 2, the total heat transferred, Q_T, is;

$$Q_T = CV^n \left(\frac{A_1}{R_1^n} + \frac{A_2}{R_2^n}\right) MTD\ , \qquad \text{where } SHD = CV^n$$

For a given radiator with fixed R_2, maximum cooling is obtained when $R_1 = R_2$ i.e. when the fan/shroud assembly presents no additional resistance and therefore V_1 and V_2 are a maximum for a given vehicle forward speed V. As R_2 and R_1 increase more air is "spilled" around the radiator and the mass flow rate through and heat transfer from the radiator decreases. For the in-duct case, the situation that applied in the laboratory, it can be shown that the velocity ratio is as above, but because the mass flow rate through the radiator for a constant average upstream velocity is independent of the resistance, the relationship between V_1 and V_2 is different. In this case, it can be shown that:

$$\frac{V_1}{V} = \frac{A\frac{R_2}{R_1}}{(A_1\frac{R_2}{R_1} + A_2)} \quad ; \quad \frac{V_2}{V} = \frac{A}{(A_1\frac{R_2}{R_1} + A_2)} \; .$$

If Q is the total heat dissipation rate from the radiator for the same total air flow with no velocity variation over the radiator face, than it can be shown that:

$$\frac{Q}{Q_T} = \frac{(f + a)^{1-n}}{f} \; r^n \; \left[\frac{(\frac{f}{r} + 1)^n}{(1 + \frac{r^n}{f})}\right]$$

where Q_T is the total heat transferred due to V_1 and V_2 through areas A_1 and A_2; $f = \frac{A_1}{A_2}$ and $r = \frac{R_1}{R_2}$.

This heat tranfer ratio as a function of r for various values of f is shown in Fig. 2. $\frac{Q}{Q_T}$ increases for increasing r and f but for values of r less than about 2, there is little effect of velocity distribution on the overall heat dissipation rate for the same total airflow.

For the 92000114 radiator used in this investigation, the measured K_2 (radiator core only) is about 4.2 at 4 ms^{-1} velocity. For a value of r of 2, K_1 would then be about 21. Estimated values of K_1 for the radiator together with a full rectangular-to-round shroud and installed fan (a high K combination) is about 10.6, corresponding to a value of r of only 1.5. It is apparent that in most circumstances the distribution of air flow will have little effect on the heat transferred, a conclusion that applies in either the in-duct or in-car situation. In the latter case, altering the aerodynamic resistance of the radiator assembly will change the total heat transfer rate only if the average velocity changes.

The insensitivity of the system to air flow distribution (for practical values of K) is supported by the tests in which the use of grids of different K at the same total air flow rate had no discernible effect on the heat transfer rate. Unfortunately, there are no results available to test the validity of the conclusions in a realistic situation. This is planned for the future.

One of the interesting aspects of this work is the possibility of utilising in-situ water side measurements of radiator performance in a vehicle as a way of determining the total air flow rate through the radiator, an important consideration in analysing the effect of body style changes on the under bonnet aerodynamics and hence radiator performance. All that is required is a knowledge of the SHD of the case as a function of velocity for a given water flow rate, which can be readily determined in equipment such as the closed circuit wind tunnel facility at the Division of Energy Technology.

References

1. CHAN, C.Y.L. and COOPER, P.I. - Automotive engine cooling system design with particular reference to air circuit components. Second Workshop on Wind Engineering and Industrial Aerodynamics. CSIRO Division of Energy Technology, 28-30 August, 1985.

2. STAPLEFORD, W.R. -Factors affecting the selection of fans for automotive engine cooling applications. Int. Conf. on Fan Design and Applications, Guildford, England, September 1982.

TABLE 1. Results of Thermal Tests on Test Radiator with Various Ram/Fan Air Velocity Ratios

Test No.	Air Flow Rate $L.s^{-1}$	Ram/Fan Area Ratio $\frac{A_2}{A_1}$	Estimated Ram Area Resistance K_2	Estimated Fan Area Resistance K_1	Calculated Velocity Ratio $\frac{V_2}{V_1}$	Ave Face Velocity V	Specific Heat Dissipation SHD $kW.m^{-2}.K^{-1}$	
							MEASURED*	$1.05\ V^{0.57}$
110A	850	1.0	4.6	11.7	1.51	3.54	2.13	2.16
111A	850	1.0	4.6	9.2	1.35	3.54	2.20	2.16
104A	850	0.25	4.6	11.7	1.51	3.54	2.17	2.16
105A	850	0.25	4.6	9.2	1.35	3.54	2.19	2.16
110B	720	1.0	4.9	12.2	1.50	3.02	1.97	1.97
111B	720	1.0	4.9	9.7	1.35	3.02	1.97	1.97
104B	720	0.25	4.9	12.2	1.50	3.02	1.99	1.97
105B	720	0.25	4.9	9.7	1.35	3.02	1.99	1.97

*At test conditions: P_{IN} = 20.5 kW, $\dot{m}_w$ = 1.0 kg/s, T_{AI} = 38.0°C

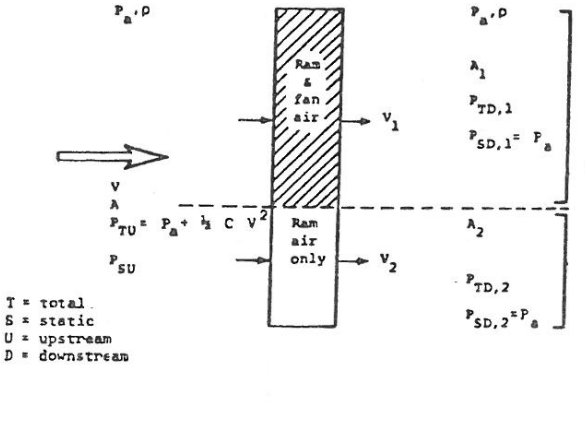

Fig. 1.

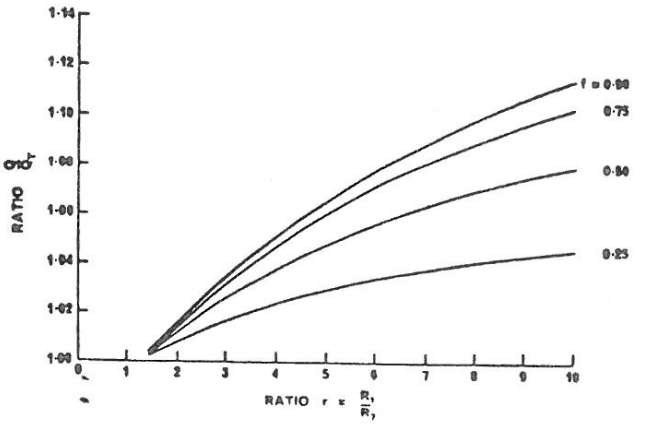

Fig. 2.

ACOUSTIC PROPERTIES OF PLATES IN TANDEM

S.A.T. Stoneman,* M.C. Welsh** and R. Parker*

Introduction

Acoustic resonances in turbomachinery have been known for a number of years [1]. Latterly, in collaboration with Rolls-Royce, Parker and Stoneman have been investigating the nature of acoustic resonances in a single stage, axial flow compressor test rig to identify the parameters which are a major influence on the generation of circumferentially propagating acoustic waves. The collaboration arose from the identification by Rolls-Royce of unacceptably high rotor blade stresses in a research compressor for the RB-211 aero-engine.

This paper briefly restates the main conclusions of the above work [2 to 5] and reports the results of wind tunnel experiments conducted at the Division of Energy Technology, CSIRO Melbourne to investigate the acoustic properties of tandem plate configurations, of varying axial spacing, which was intended to model the Inlet Guide Vane and rotor blade geometry of the turbomachine.

Turbomachinery Test Rig and Results, University College of Swansea

Figure 1 is a half sectional elevation of the single stage axial flow compressor test rig at the Dept. of Mechanical Engineering, University College Swansea. Figure 2 is a partially assembled view of the test rig showing the major components.

Figure 3 shows the blade geometries for the two main phases of the work, i.e. vortex shedding from (a) 33 zero stagger, slab sided, rounded trailing edged IGV's and (b) 33 and 66 zero stagger, airfoil sectioned IGV's subjected to incident flow produced by an upstream row of pre-swirl vanes. The results from the slab sided test are representative of all the results obtained and the following is therefore limited to this geometry.

Figure 4 shows the frequency/flow velocity relationship for a stationary microphone upstream of and between two IGV's. These results are for an IGV/rotor axial spacing of 33 mm which, non-dimensionalised in terms of the thickness of the vortex shedding IGV's (5 mm), is a space to thickness ratio of 6.6 . It can be seen that the resonances manifest themselves as a series of locally approximately constant frequency lines over small ranges of velocity, with the mode number varying from 7 to 16, propagating sometimes with and sometimes against the rotor direction of rotation. The range of Strouhal numbers over which resonances are generated being 0.229 to 0.292.

Figure 5 shows the relationship for a space to thickness ratio of 1.04 where the long series of resonances has been replaced by just two resonances, modes 16 and 15 which are frequency locked over a very large velocity range, corresponding to a range of Strouhal numbers from 0.252 to 0.335.

When the space to thickness ratio was an intermediate value of 2.68 (Figure 6) two series of resonances were generated. As the flow velocity was decreased the modes changed in a series of steps from 16 to 12 whereupon the mode number jumped to 16 again, decreasing to mode 8 with decreasing velocity. The Strouhal number ranges corresponding to these series of resonances were

* University College of Swansea, Wales, UK
** CSIRO Division of Energy Technology, Melbourne, Australia

0.212 to 0.260 for the high velocity series and 0.316 to 0.363 for the low velocity series. It was to provide an explanantion of the means by which two very different resonances can be excited at similar flow velocities as a result of changing the axial blade spacing that an experimental programme was undertaken in collaboration with CSIRO.

Tandem Plates in a Wind Tunnel, CSIRO

To simulate the geometry of a vortex shedding IGV positioned upstream of a rotor row, two plates were mounted on the axial centreline of a wind tunnel in a tandem configuration (Figure 7) such that the axial spacing between the two plates could be varied from zero to 200 mm (space to thickness ratios of 0 to 25). The vortex shedding and the acoustic field were monitored by a probe microphone located in the wake region of the upstream plate and a 3582A Hewlett Packard spectrum analyser.

Figure 8 shows the now familiar result for a single plate in a wind tunnel where over a limited speed range, the vortex shedding excites a duct acoustic resonance which in turn becomes locked to the acoustic resonant frequency. Figure 9 shows the results obtained with a second plate installed 30 mm downstream of the first plate (space to thickness ratio of 3.75) where it can be seen that when the vortex shedding frequency is near to the acoustic resonant frequency the vortex shedding is locked to it, as with a single plate. Over and above this, there were a number of other flow velocities at which a resonance was excited which were found to occur when the vortex shedding frequency was an integer sub-multiple of the acoustic resonant frequency, e.g. 8:9, 7:5, 5:2 and 2:1. The particular value of the integer sub-multiple was a function of the axial spacing between the plates. Work is in hand at CSIRO to mathematically model the transfer of energy from integer sub-multiple vortex shedding to an acoustic field and initial results indicate that the essential character of the phenomenon can be predicted.

When the flow velocity was set at a constant 22 m/s (such that in the absence of the second plate a strong acoustic resonance would have been generated) then varying the plate spacing from zero to 200 mm caused the peak sound pressure level to vary as shown in Figure 11. The peak sound pressure levels obtained corresponded approximately to those found in the absence of a second plate. However, at the intermediate positions the acoustic resonances were effectively destroyed being some 30 to 50 dB lower than the peaks.

Discussion

It is not known at this time whether the low velocity series of resonances in the compressor (Figure 6) is integer sub-multiple vortex shedding. The frequency step from mode 12 to mode 16 is an integer ratio of 5:6 but no evidence has yet been found to indicate that the IGV vortex shedding is not locked to the acoustic field. This may not be necessary since in the turbomachine the SPL's are much higher and may lock the shedding once the resonance is established.

An explanation of the variation of SPL with plate spacing is that energy can be transferred from the flow to the acoustic field when there is a net positive imbalance in the summation of the individual values of the vector triple product of the Howe formula associated with each vortex as it traverses the acoustic field [6,7]. The position of the second plate inlfuences the total number of generating vortices in relation to the total number of

absorbing vortices since when a vortex traverses the second plate its net effect on the acoustic field must be zero since the convection and acoustic velocities (as terms in the vector triple product) are parallel.

The IGV/rotor spacings at which the turbomachinery results were obtained are indicated in Figure 11 and it is significant that the spacing at which the double series of resonances was obtained (Figure 6) corresponds to one of the spacings at which the tandem plate resonance was effectively destroyed. This may indicate that the phase relationship of the vortex arrival at the rotor favoured the excitation of the sub-multiple resonances at the low flow velocities over those at the higher flow velocities.

Conclusions

1. The results of turbomachinery experiments and those from tandem plates in a wind tunnel show encouraging similarities suggesting that modelling the acoustic properties of turbomachines with stationary plates in a wind tunnel has a contribution to make in expediting investigations.

2. Two plates in tandem in a wind tunnel can excite the an acoustic resonance when vortex shedding frequency is an integer sub-multiple of the acoustic resonant frequency.

3. The presence of a second plate in tandem with a vortex shedding plate in a wind tunnel can destroy the presence of the acoustic resonance normally associated with vortex shedding at the acoustic resonant frequency.

References

1. R. Parker, 1967 J.S.Vib. 6(3),302-309. Resonance effects in wake shedding from compressor blading.

2. R. Parker, and S.A.T. Stoneman, 1984 J.S.Vib. 97(3). An experimental investigation of the generation and consequences of acoustic waves in an axial flow compressor: large axial spacings between blade rows.

3. R. Parker, and S.A.T. Stoneman, I.Mech.E. (UK) Third International Conference on Vibrations in Rotating Machinery, York, September, 1984. Acoustically excited vibration of compressor blades.

4. R. Parker, S.A.T. Stoneman, and M.C. Carr, 1984 Unsteady Aerodynamics of Turbomachines and Propellers, Jesus College Cambridge. Excitation of blade vibration by flow induced acoustic resonances in axial flow compressors.

5. S.A.T. Stoneman, Ph.D. Thesis, 1984 University College Of Swansea. An experimental investigation of flow excited acoustic fields in an axial flow compressor.

6. M.C. Welsh, A.N. Stokes and R. Parker, 1984 J.S.Vib. 95(3),305-323. Flow resonant sound interaction in a duct containing a plate, Part I: semicircular leading edge.

7. A.N. Stokes and M.C. Welsh, 1985 J.S.Vib. In Press. Flow resonant sound interaction in a duct containing a plate, Part II: square leading edge.

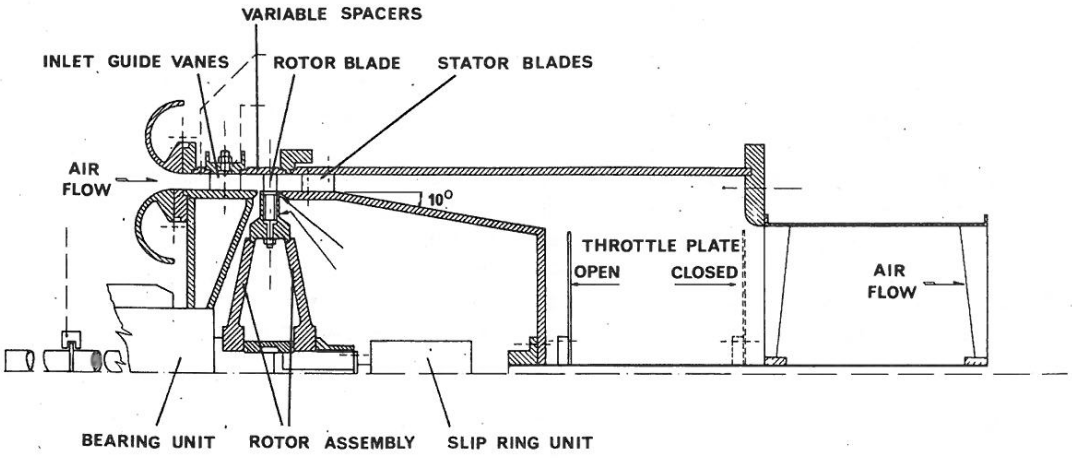

Fig. 1 Half sectional elevation of axial flow compressor test rig.

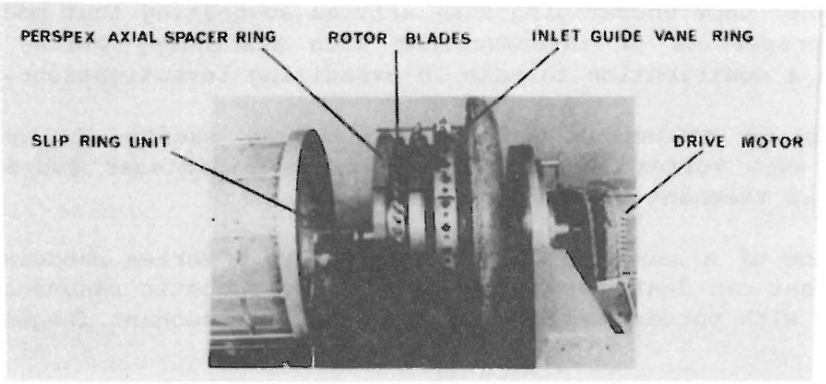

Fig. 2 Partially assembled view of test rig.

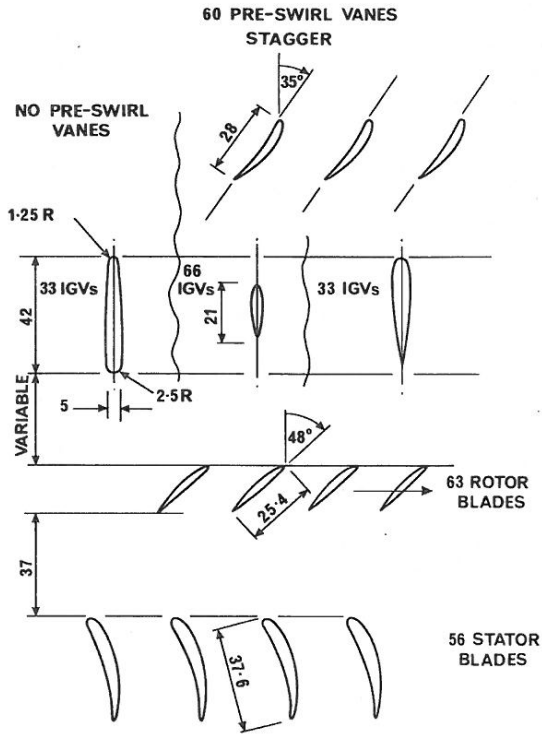

Fig. 3 Compressor blade geometries.

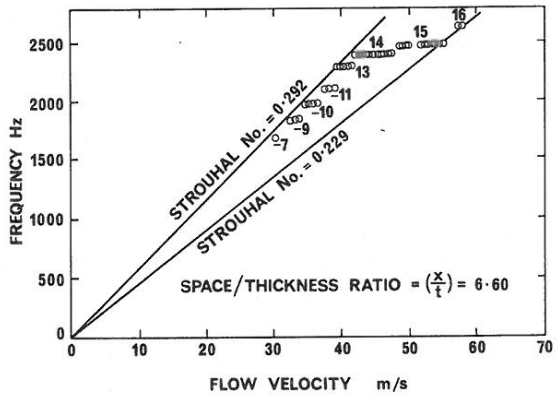

Fig. 4 Frequency/velocity relationship x/t = 6.6

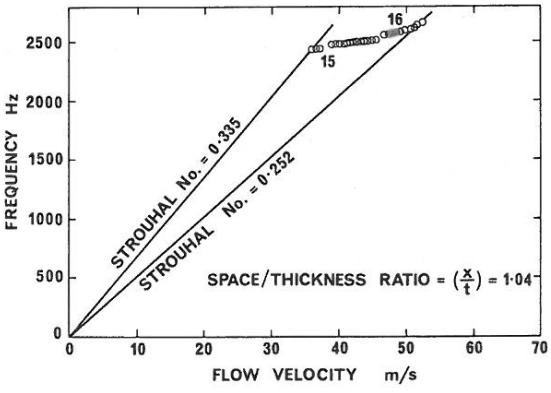

Fig. 5 Frequency/velocity relationship x/t = 1.04

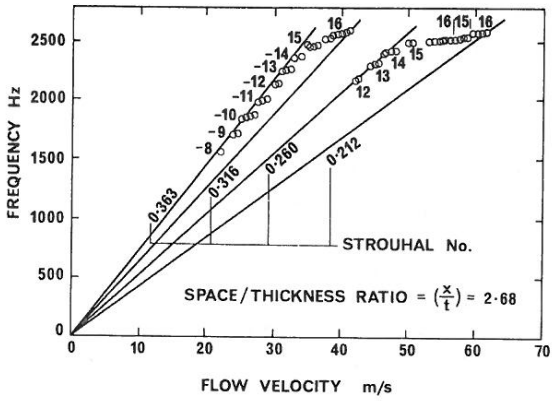

Fig. 6 Frequency/velocity relationship x/t = 2.68

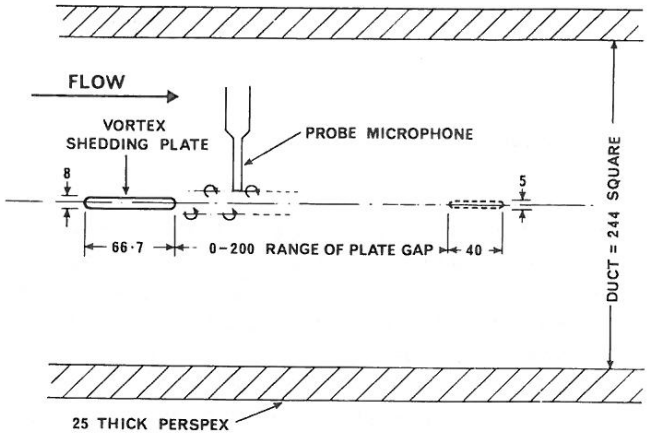

Fig. 7 Variable spacing tandem plates in wind tunnel.

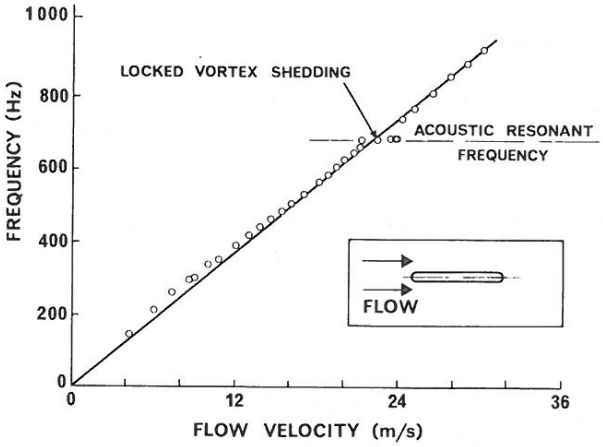

Fig. 8 Frequency/velocity relationship - single plate.

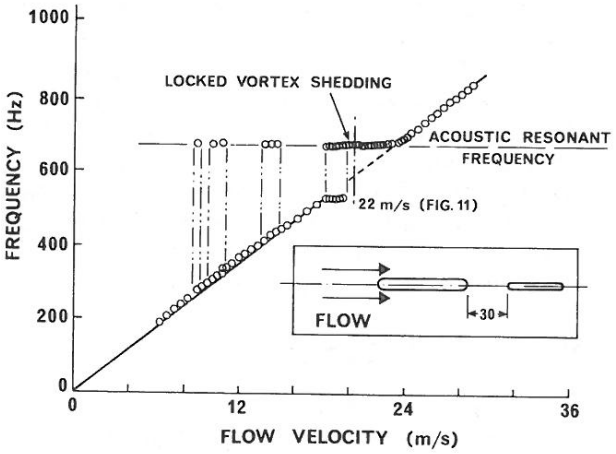

Fig. 9 Frequency/velocity relationship - single plate.

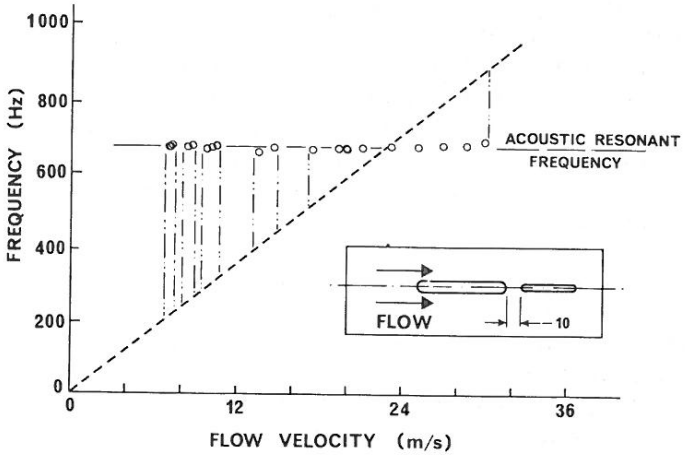

Fig. 10 Frequency/velocity relationship - single plate.

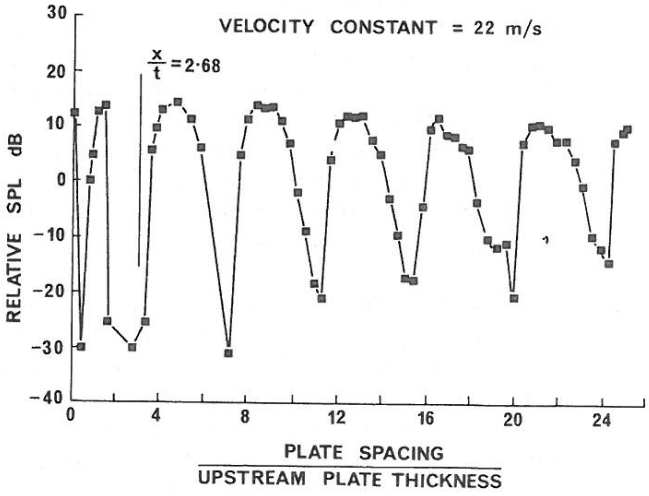

Fig. 11 Variation of peak SPL with plate axial spacing at constant flow velocity.

DUCT RESONANCE IN HIGH PRESSURE RATIO THRUST AUGMENTING EJECTORS

A.M. Abdel-Fattah*

Introduction

Unsteady effects in various forms, when imposed on the mixing process between the two streams in an ejector duct such as that shown in figure 1, can greatly enhance the levels of entrainment and thrust augmentation. As part of a broader investigation of the use of ejectors for improving the static thrust of rocket motors, the effect of natural duct resonance on the performance of ejectors with very high pressure ratio primary jets of unheated air were investigated experimentally. A family of five convergent-divergent nozzles of different sizes but with the same exit to throat area ratio of 4.03 was tested with three constant cross sectional area ducts of different diameters, such that the duct to nozzle throat area ratio varied between 36 and 450. The primary jet stagnation pressures were up to 50 atm, covering such a range that the jet at the nozzle exit varied from highly overexpanded to underexpanded.

The thrust variations obtained experimentally with changing blowing pressure for a given ejector configuration showed irregularities which are not predicted or explained by the idealised ejector theory. These irregularities were found to be associated with discrete tones of acoustic radiation called screech. Similar phenomena were noticed by Quin, 1975, 1977. All of his experiments were performed with one underexpanded convergent nozzle blowing relatively low stagnation pressure unheated air jets at up to 6 atm at the inlet of a family of constant area ducts of one diameter (duct to nozzle area ratio 25) but with different lengths. He found that the discrete tone of acoustic radiation corresponded to the resonant mode of the mixing duct. With much higher pressures and area ratios, similar to those used in the present experiments, Fisher (1980) also observed thrust irregularities in a range of ejector geometries which were somewhat more pronounced than those reported by Quin.

Results and Discussion

Experimental results for a typical family of ejectors are shown in figure 2, in the form of duct thrust F versus the jet stagnation pressure P_o. Results shown in this figure are for different values of duct to nozzle exit area ratio A_D/A_n but for one ejector duct of fixed diameter and length. These were obtained by an X-Y Plotter, continuously activated by the output of a pressure transducer connected to the jet blowing pressure supply and a force cell connected to the ejector duct.

Spectral analysis of the noise radiated by each ejector at various points on the thrust/pressure characteristic was used to identify the fundamental frequency and harmonics of the discrete tone oscillations whenever they could be detected. A plot of the discrete tone fundamental frequency versus blowing pressure ratio P_o/P_1 for all ejector configurations of duct length to diameter ratio $L/D = 4$ is shown in figure 3. P_1 is the static pressure in the duct at the nozzle exit. From this figure it is obvious that the frequency was not a continuous function of blowing pressure, but that clear discontinuities occurred at certain pressures. Depending on the ejector configuration and range of pressure, more than one discontinuity can be identified.

For each family of ejectors having different nozzle sizes but the same duct diameter D_1 and length L_1, the tonal frequencies which defined the limits of different discontinuity ranges were nearly the same for each member of the family. However the levels of nozzle pressure ratio at which certain tones were generated, and at which the discontinuous frequency changes occurred, varied with nozzle size. For a new family of ejectors of duct diameter D_2, but with $L_2/D_2 = L_1/D_1$, the tonal frequencies changed by a factor equal to the ratio of duct diameters D_2/D_1.

*ARL, Aero Propulsion Division, Melbourne, Australia

The theoretical transverse natural resonant modes for a long circular duct of constant cross sectional area are given by (Rschevkin, 1963):

$$f_{p,n} = \frac{c}{\pi D}\nu_{pn}$$

where c - Speed of sound in the duct medium
ν_{pn} - Roots of derivatives of Bessel function
P - Number of modal diameters
n - Number of modal circles.

The calculated resonant modes for the ducts used in our experiments are given in table 1. When compared with the experimental results in figure 3, these theoretical frequencies (with the notable exception of f_{11}) do not always coincide with the measured frequencies of apparent resonances. Indeed, it could be argued that there is a more consistent correlation of the theoretical frequencies with the frequency bands spanned by discontinuities between different resonant modes. This may not be surprising, in view of the fact that the theoretical modal frequencies were calculated for the ideal case of a duct with no flow and uniform pressure, and did not take into account the nonuniform flow structures through the duct. These nonuniformities, which are primary jet pressure ratio dependent, include coflowing streams and shock cell formations associated with over-or-underexpansion of the supersonic jet.

The limits of each frequency discontinuity in figure 3 are replotted as duct to nozzle exit area ratio A_D/A_n versus blowing pressure ratio P_o/P_1 in figure 4. The discontinuities can be grouped into bands, each of which assumes a linear relationship between A_D/A_n and P_o/P_1; and each of which can be ascribed a given value of the non-dimensional frequency parameter fD/c.

The jet stagnation pressures which correspond to the maxima and minima on the thrust/jet pressure ratio characteristics for different ejector configurations are compared with those corresponding to the frequency discontinuities in figure 4. The maxima or minima are also shown to assume linear relationships between A_D/A_n and P_o/P_1. The pressures for the minimum duct thrusts coincided with those for the lower limits of frequency discontinuities.

Conclusions

The resonant modes of the mixing ducts of thrust augmenting ejectors can be correlated with gross changes observed in ejector performance. This provides a clue as to why these changes occur, but it does not explain how the performance is affected. The mixing between the primary jet and the entrained secondary stream is evidently enhanced by the duct resonance, but the flow mechanism which results in increased mixing is still to be described. Investigation of this aspect of the phenomena continues, using pressure probing and flow visualisation with single, two plane, and stroboscopic schlieren photography.

References

1. Quin, B, "Effects of Aeroacoustic Interaction on Ejector Performance",J.Aircraft, Vol.12, Nov 1975.

2. Quin, B, "Interactions Between Screech Tones and Ejector Performance",J.Aircraft, May 1977.

3. Fisher, S.A, "Thrust Augmenting Ejectors for High Pressure Ratio Propulsive Jets", 7th Australasian Hydraulics and Fluid Mechanics Conference, Brisbane, Aug. 1980.

4. Rschevkin, S.N, "A course of lectures on The Theory of Sound", Pergamon Press, 1963.

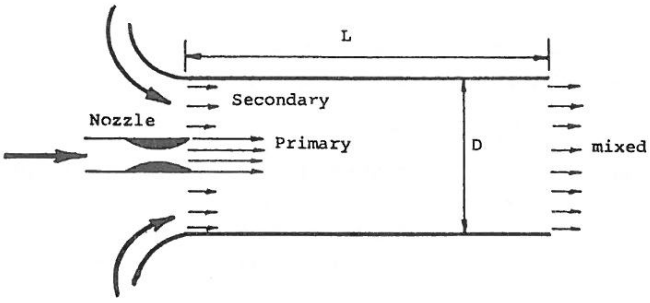

Figure 1: Schematic diagram for a thrust augmenting ejector.

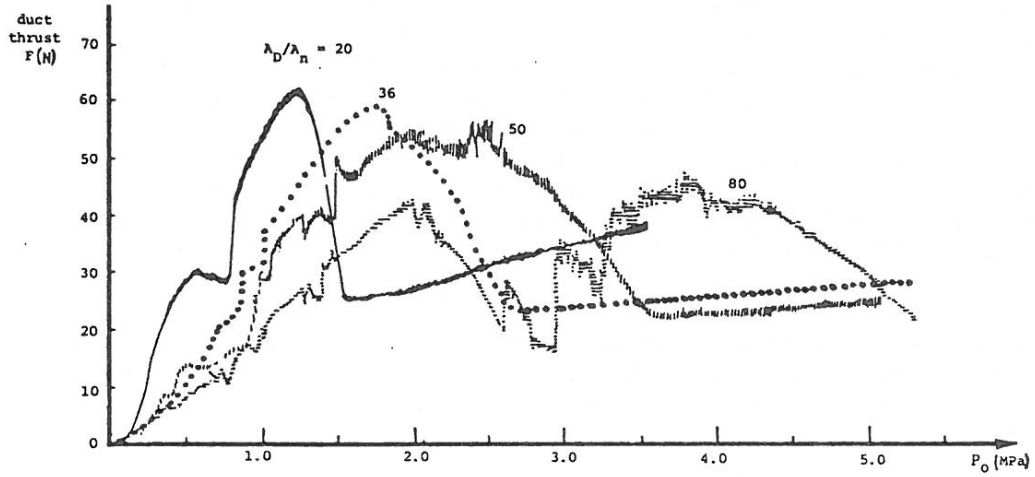

Figure 2: Ejector duct thrust for a family of ejectors of different nozzle sizes but with the same duct diameter and length.

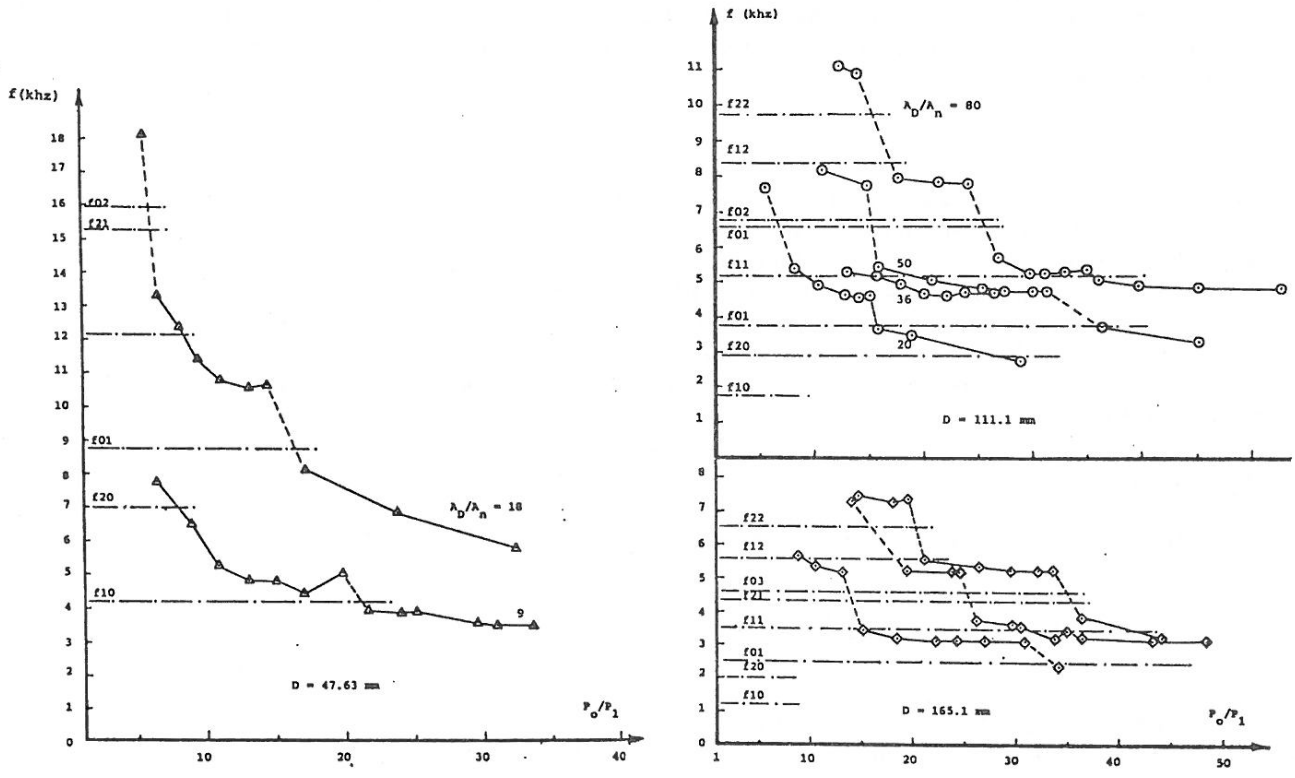

Figure 3: Discrete tone fundamental frequencies obtained for different ejector configurations.

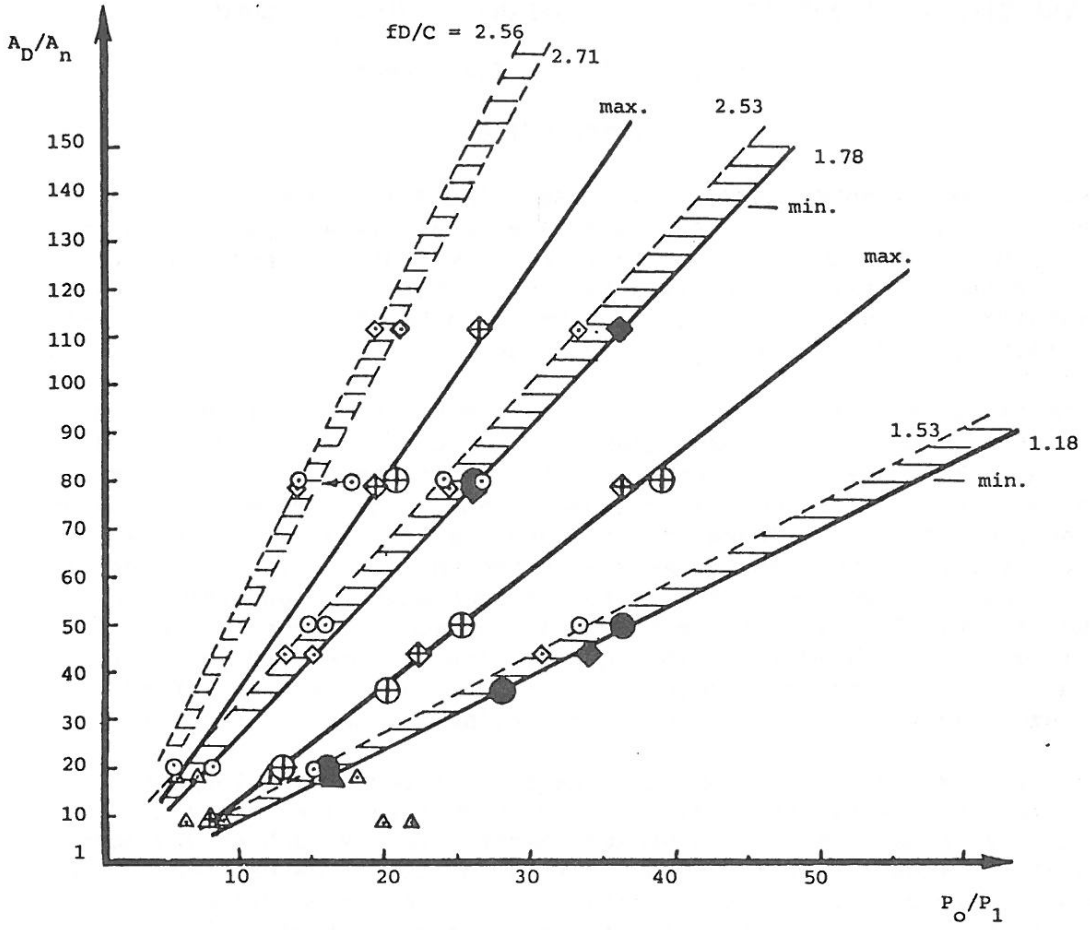

Figure 4: limits of frequency discontinuities obtained for different ejector configurations.

△ , D = 47.6 mm; ⊙ , D = 111.1 mm; ◇ , D = 165.1 mm; ⧋, ⊕, ⧈ , maximum duct thrust; ▲, ●, ◆ , minimum duct thrust.

Duct diameter mm	No of nodal circles (n) / No of nodal diameters(p)	0	1	2
47.6	0	0	8.70	15.93
111.1		0	3.73	6.83
165.1		0	2.51	4.60
47.6	1	4.18	12.11	19.4
111.1		1.79	5.19	8.32
165.1		1.20	3.49	5.60
47.6	2	6.93	15.22	22.63
111.1		2.97	6.52	9.70
165.1		2.00	4.39	6.53

TABLE 1 : Theoretical transverse resonant modes for the circular ducts used in the experiments.

THE START-UP BEHAVIOUR OF A GAS TURBINE - EJECTOR - LONG STACK SYSTEM

M Somogyi*, G E Pleasance*

INTRODUCTION

Emergency power generating units of power plants are usually driven by Diesel engines or gas turbines, which discharge their exhaust gases via short (6-7m high) stacks. The Commission's Loy Yang A Power Station emergency gas turbine units were to be installed between two boiler houses. For safety reasons, this necessitated ducting of the high temperature exhaust gases above the boiler house roof via a 120 m high 200 m long stack.

The general arrangement of a unit is shown in Figure 1. Two gas turbines drive the generator through a common gear box, all of which is housed in an acoustic enclosure. The exhaust from each turbine discharges into an ejector which draws cooling air from the enclosure and attemperates the exhaust gases. Cooling air enters the generator enclosure via filters and passes into the gas turbine enclosure through the generator and the oil cooler radiator fans. The outflow from the two ejectors pass to a common silencer and then to the long exhaust stack. On start-up the turbines achieve full speed in approximately 30 seconds with very rapidly increasing mass-flow at the end of this interval (Figure 4). The exhaust temperature peaks at about 20s and after a trough it rises again as more fuel is injected according to the loading of the generator.

Concern was expressed that the back pressure caused by the long stack would be too great to allow the ejectors to operate satisfactorily and there was a possibility of backflow of hot exhaust gases into the turbine enclosure. Calculations showed that for an acceptable stack diameter the system would operate satisfactorily under steady state operating conditions. To determine if the system would operate satisfactorily during start-up, a model was developed to describe the flow through the system of filters, fans, gas turbines, ejectors, silencer, and stack.

NOMENCLATURE

A	area	s	length
C	pressure loss coefficient	t	time
f	friction coefficient	T	temperature
g	gravitational acceleration	v	average velocity
h	height	v(r)	local velocity
m	rate of mass-flow	ϱ	average density
p	pressure	ϱ(r)	local density

Subscripts:

c	cooling air	t	turbine
e	enclosure	x	ejector outlet
f	filter	o	ambient
i	ejector inlet		

MATHEMATICAL MODELS

During the development, several models were formulated and programmed for solution on a PDP11/34 computer. A preliminary model was developed for a single pipe with known rate of inlet massflow. The system of two partial differential equations (momentum equation and continuity) was solved for velocity and pressure by finite difference techniques.

* State Electricity Commission of Victoria, Melbourne, Australia

The results did not preclude the possibility of satisfactory start-up operation and provided insight into what aspects could be neglected in a detailed model. In the second step described here the aim was to include more elements of the complex ducting system, whilst keeping the model simple, in accordance with the reliability and availability of input data. The most essential output from the model is the predicted cooling air flow rate which is treated as an iteration variable. At time t we assume that everything is known and at the new time t+dt we know the turbine exhaust mass-flow and temperature. It is assumed that the exhaust flow characteristics of the turbines (Figure 4) are not influenced by the system (e.g. by back-pressure). Starting with an estimated cooling air mass-flow (that can be negative), the pressure in the generator enclosure is -

$$p_e = p_o - \frac{\rho_o}{2} C_f \; v_f \; |v_f| \tag{1}$$

As the radiator fans in the enclosure are only switched on when the turbines are nearly up to speed, the pressure in the turbine enclosure can be regarded as being the same as in the generator enclosure.

The ejector inlet pressure for positive and negative cooling air flow is -

$$\begin{aligned} p_i &= p_e - (1+C_i)\,\frac{\rho_o}{2}\,v_c^2 \qquad \text{for } m_c > 0 \\ p_i &= p_e \qquad\qquad\qquad\qquad\quad \text{for } m_c \le 0 \end{aligned} \tag{2}$$

and is regarded as average for the whole inlet cross section. The pressure increase through the ejector can be calculated from the integral form of the momentum equation for the control volume shown in Figure 2. Neglecting the unsteady term and the wall friction (the ejector is two orders of magnitude shorter than the stack), and assuming top-hat velocity profiles, the average pressure at the outlet for positive or negative cooling air flow is -

$$p_x = p_i + \frac{m_t v_t + m_c v_c - m_x v_x}{A_x} \tag{3}$$

Since the inlet/outlet velocity profiles are very much like those shown in the bottom of Figure 3, all of the momentum terms should be corrected by appropriate profile form-factors of the form -

$$\frac{\iint \rho(r)\, v^2(r)\, dA}{\rho\, v^2\, A} \tag{4}$$

These form-factors are calculated from steady state velocity survey data and are considered constants during the start-up. The average temperature of the turbine exhaust - cooling air mix at the ejector outlet is -

$$T_x = \frac{m_t T_t + m_c T_c}{m_t + m_c} \tag{5}$$

There is no need to introduce temperature profile form-factors. The cooling air temperature is equal to the enclosure temperature in the case of positive cooling air flow, and is equal to the turbine exhaust temperature in the case of backflow. The latter assumption provides quick convergence of the iterations in the case of backflow.

Starting with the silencer, the stack is divided into small elements in which the density can be regarded constant. Accounting for the inertia forces, friction, and buoyancy, the pressure difference between neighbouring nodes is -

$$p_j - p_{j-1} = - \frac{dm_v}{dt} \frac{\Delta s}{A} - \frac{\varrho}{2} f \frac{\Delta s}{d} v|v| - \varrho g \Delta h \qquad (6)$$

The friction factor contains the pipe friction as well as the losses of elbows, etc. It is assumed that since the changes are relatively slow, losses, etc, can be calculated as if we were dealing with a succession of steady state flows. The local density and local velocity are calculated on the basis of the local temperature. Temperatures are calculated from a simplified energy equation -

$$\frac{\partial T}{\partial t} = - v \frac{\partial T}{\partial s} \qquad (7)$$

In neglecting heat losses to the walls of the ducting this equation overestimates the temperature. The error, however, is not thought to be very significant (the critical period is only about 35 seconds) and, since in our particular case a temperature drop would result in nearly the same drop in buoyancy as in friction losses, the accuracy of the solution is still commensurate with that of the input data.

The advantage of this form of the energy equation is that it can be given a geometrical meaning (Figure 3). If the "old" temperature distribution is known, we can create the "new" distribution by shifting each of the old nodes a distance that is the products of the local velocity and the time-step (see the arrows leading to the new points P1, P2, ... in Figure 3). The point P0 is the mixture temperature at the ejector outlet calculated from equation 5. We can now fit a spline through the points P0, P1, ..., and obtain the new temperature values at the old nodes. In this way essentialy bigger steps can be employed both in space and time; 20-30 nodes for the 200 m long stack, and time steps of 0.1-0.25 s. (This made possible the use of the PDP11/34 computer with software simulated floating point processor.)

With the repetitive use of equation 6 the pressure at the stack outlet can be calculated. If it is not equal to the ambient pressure at that level, the cooling air flow should be modified. Usually, the balancing cooling air flow can be found in 3 steps; more steps (5-6) are needed when the mass-flow is small and in the case of backflow.

RESULTS AND CONCLUSIONS

The computer program written to solve the governing equations generates intermediate nodes along the stack, fits splines on the input mass-flow and temperature points. On the output side it prints/plots all the primary variables along the stack at predefined times (see a typical temperature plot in Figure 5). The main purpose of the model is to predict the cooling air flow. The most adverse situation in practice is when start-up is with a cold stack. In such a case an initial backflow is predicted, followed by positive cooling air flow with a sharp dip at the time when the turbine mass-flow increases very rapidly towards the end of the run-up to speed (Figure 4). Depending on system parameters (e.g. filter pressure drop) backflow may occur at this stage of the start-up. Starting with a "preheated stack" (e.g. start after a trip-off), the resulting draft is enough to offset the backflows.

The system has been installed and commissioned but at the time of writing this paper there are no detailed measurements available with the long stack. However, observations confirmed that on cold winter days when starting from cold, positive enclosure pressure occurs in the first 5-10 seconds, and there appeared to be some backflow for a very short period of time at the end of the turbine acceleration period. Nevertheless, there has been no report of any damage due to overheating within the turbine enclosure. Under warmer atmospheric conditions or with a start following trip-off, backflows into the enclosure are most likely avoided.

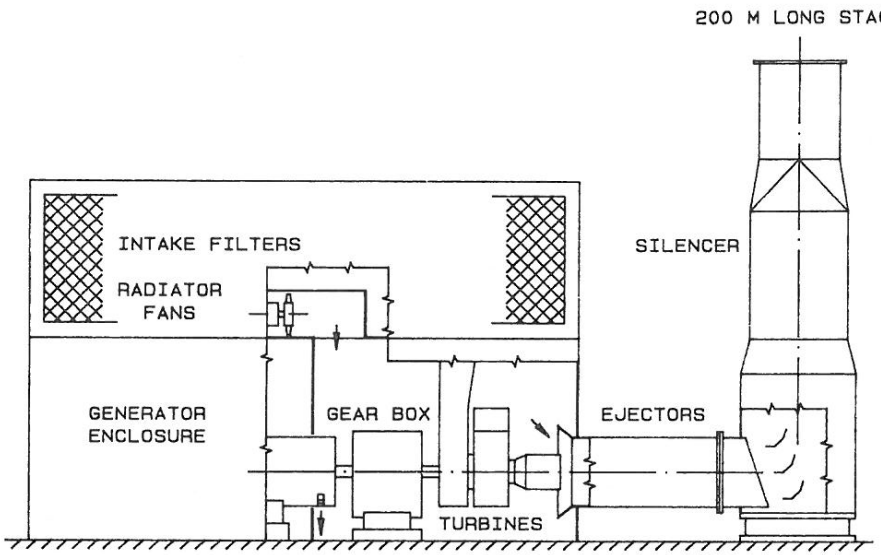

GENERAL LAYOUT
FIGURE 1

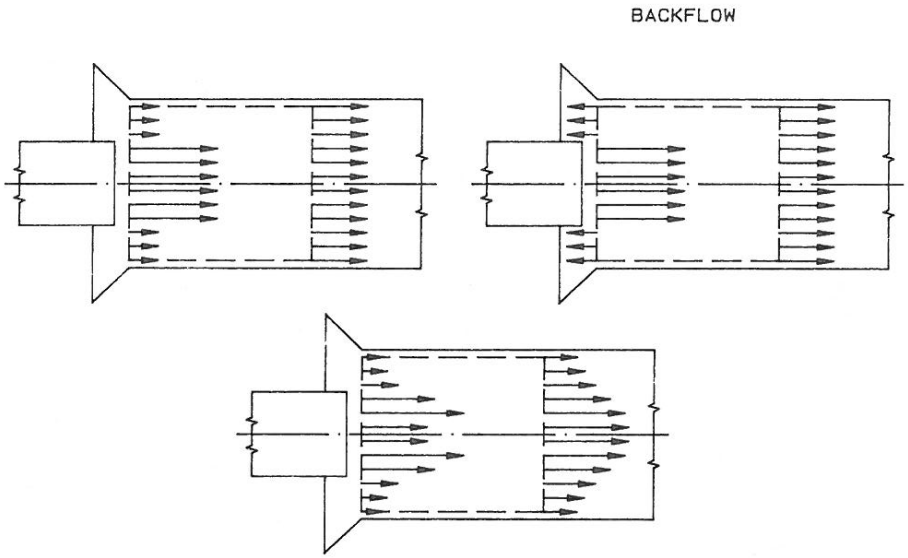

EJECTOR VELOCITY DISTRIBUTIONS
FIGURE 2

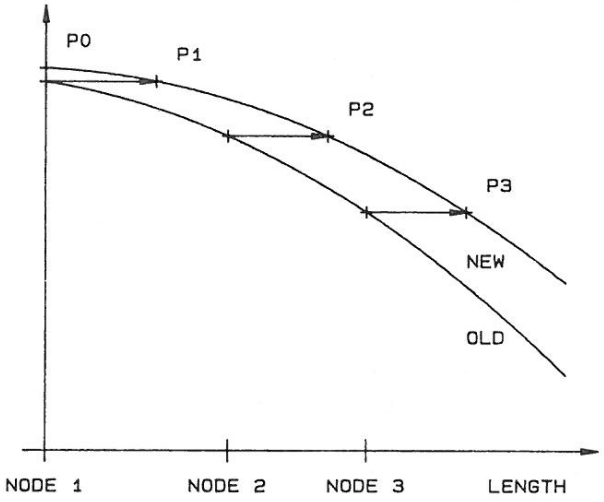

THE CALCULATION OF A NEW TEMPERATURE CURVE
FIGURE 3

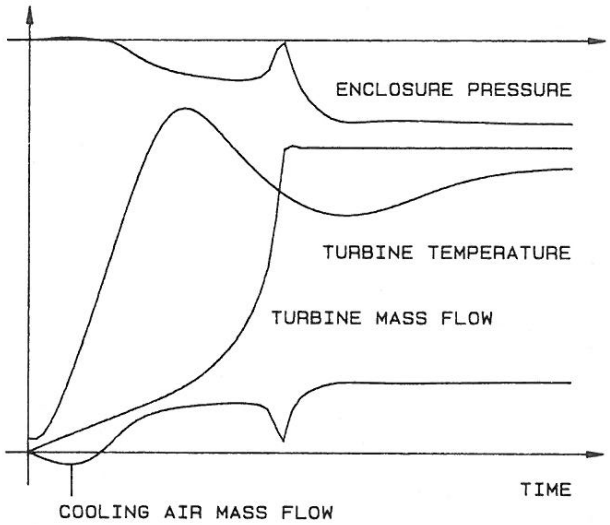

CHARACTERISTIC CURVES
FIGURE 4

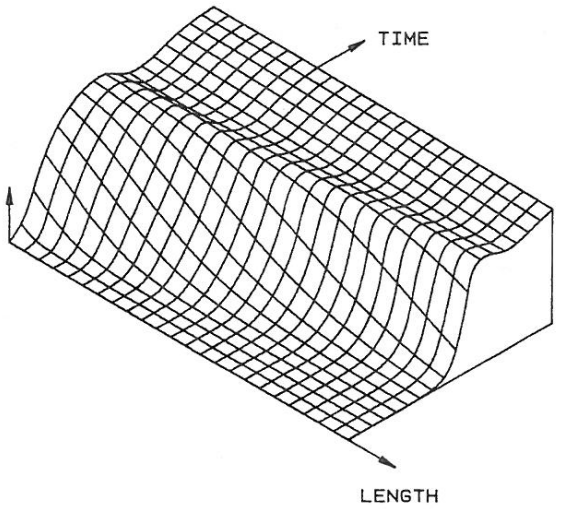

TEMPERATURE DISTRIBUTION ALONG THE STACK
FIGURE 5

MEASUREMENT OF REYNOLDS STRESSES IN DUCT FLOW BY HOT-WIRE ANEMOMETRY

J.D. Hooper*

Introduction

The determination of all components of the Reynolds stresses for turbulent in-line single phase flow through complex cross-section ducts is a major experimental task, even if limited to the developed flow region. The system outlined in this paper used hot-wire anemometry for the turbulence measurements, with fully automated probe traversing, signal processing and rig control by a PDP computer. The time required for a fixed Reynolds number study of the developed flow region was reduced from months, when manually performed, to continuous operation and completion in several days.

The automated system significantly improved the accuracy of the Reynolds stress measurement, by continuously monitoring the hot-wire probe performance. Changes in the small-signal sensitivity of the hot-wire sensors could readily be detected. A constant duct Reynolds number was maintained by monitoring the ambient air temperature and pressure, and by resetting the rig operating point to a new reference axial pressure drop when significant changes occurred.

Experimental Method

The duct mean axial velocity distribution was determined by pitot probe traverse, and the velocity data stored in reference files. The computer stored reference velocity profiles are to be scaled by

$$U(x,y) = U_r(x,y)\ (\upsilon/\upsilon_r) \tag{1}$$

to determine the local mean velocity when subsequently using hot wire probes. The selected rig axial pressure drop is calculated by

$$\Delta p = \Delta p_r.(\rho/\rho_r).(\upsilon/\upsilon_r)^2 \tag{2}$$

in order to maintain a constant duct Reynolds number. The kinematic air viscosity is υ, and subscript r refers to the reference mean velocity study.

A simple form of hot wire correlation (1) was selected, with the bridge voltage E of a wire normal to the mean flow U given by

$$E^2 = E_o^2 + B\ U^n \tag{3}$$

where both B and n are functions of the mean velocity. The inclined wire response is given by

$$E_\alpha^2 = E_{o\alpha}^2 + B\ U^n\ \cos^m(\alpha) \tag{4}$$

where α is the angle between the normal to the wire and the mean velocity. Davies and Davis [1] and Bruun [2] have shown that the functional relationship of the indicies m and n with velocity is constant for a limited range of probe slenderness ratios, wire material and probe overheat ratios if the sensor is isolated from the probe support forks. A standard single inclined wire and single normal wire probe was developed, using 2 mm long 5 μm tungsten wire sensors, which were isolated from the support forks by 2 mm of copper plating.

---

* CSIRO Division of Mineral Engineering, Lucas Heights, Sydney.

The use of equation (4) for the inclined wire response, rather than the correlations developed by Champagne et al. [3] which use an optically measured angle, requires that a yaw calibration be made to determine α. The inclined probe is yawed to known angles β in a low turbulence intensity parallel air jet at the same mean velocity as the experimental duct, and the effective inclined wire angle α calculated from

$$\alpha = \tan^{-1} \left[\cot\beta - \operatorname{cosec}\beta . \left[\frac{E_{\alpha+\beta}^{2} - E_{o\alpha}^{2}}{E_{\alpha}^{2} - E_{o\alpha}^{2}} \right]^{\frac{1}{m}} \right] \quad . \qquad (5)$$

Twelve individual estimates of α, using β in the range $\pm$ 15°, defined the effective probe angle α to a standard deviation of 0.5°.

The use of small signal expansions of the unlinearised probe steady state response equations (3) and (4), to calculate the Reynolds stresses, has been shown by [4] to generate Reynolds stress distributions in developed axi-symmetric pipe that are in close agreement with accepted data. Several redundant measurements were made by taking the normal and inclined wire signal variance, and the covariance of the signal cross-product, in a normally 7 segment axial probe rotation sequence. The probe was rotated in 45° increments, and the redundant equations used to test the accuracy of the small signal approximations.

The axial component of the Reynolds stress is

$$\overline{u^2} = 4\ E^2\ U^2/(n^2(E^2 - E_o^2)^2)\ .\ \overline{e^2} \qquad (6)$$

and application of the inclined wire equation

$$(u + m/n\ \tan(\alpha)\ v)^2 = \overline{e_\alpha^2}\ .\ 4\ E^2\ U^2/(n^2(E_\alpha^2 - E_{o\alpha}^2)^2) \qquad (7)$$

to five rotation positions determines the six Reynolds stresses.

Duct Measurements of Mean Velocity and Reynolds Stresses

In conclusion, a study simulating the fluid dynamics of a single phase coolant in a power reactor core is presented. The flow was fully developed (i.e. the axial derivative of the data presented is zero), and symmetry was used to further limit the measurement area shown in the duct cross section, figure 1. The axial mean velocity (fig. 2 (a)) is normalised by the average velocity for this area, the turbulence intensities (figs. 2 (b), (c) and (d)) by the mean wall friction velocity, and the Reynolds shear stresses (figs. 2 (e) and (f)) by the mean wall shear stress. Approximately 450 data points (about 150 hours of measurement) were used to generate these contour plots [5], with the experimental time being reduced by a factor of approximately fifty when compared to manual operation.

References

1. P.O.A.L. Davies and M.R. Davis, 'Factors Influencing the Heat Transfer from Cylindrical Anemometer Probes', Int.J.Heat and Mass Transfer, 15, 1659, 1972.

2. H. Bruun, 'Interpretation of a Hot Wire Signal Using a Universal Calibration Law', J.Phys.E. (Sci.Inst.), 4, 225, 1971.

3. F.H. Champagne, C.A. Sleicher and O.H. Whermann, 'Turbulence Measurements with Inclined Hot Wires (Part 1)', J.Fluid Mech., 28, 153, 1967.

4. J.D. Hooper, 'Fully Developed Turbulent Flow Through a Rod Cluster', Ph.D. Thesis, U. of N.S.W., 1980.

5. L. Vosahlo, 'Computer Programs for Evaluation of Turbulence Characteristics from Hot Wire Measurements', KfK Report 3743, Karlsruhe W. Germany, 1984.

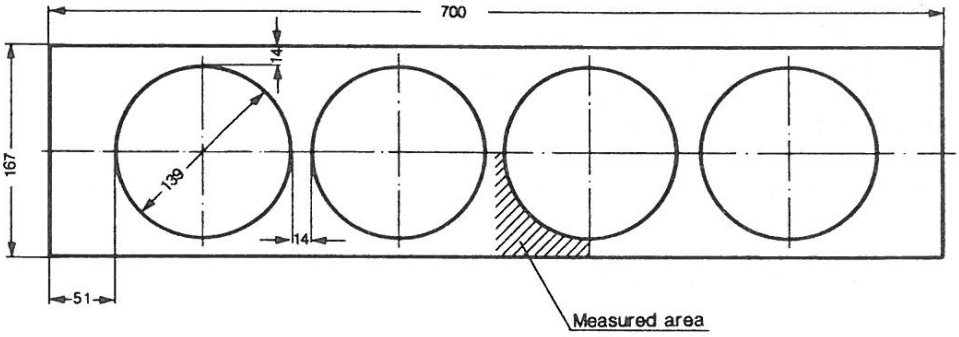

Figure 1: Cross-section of duct.

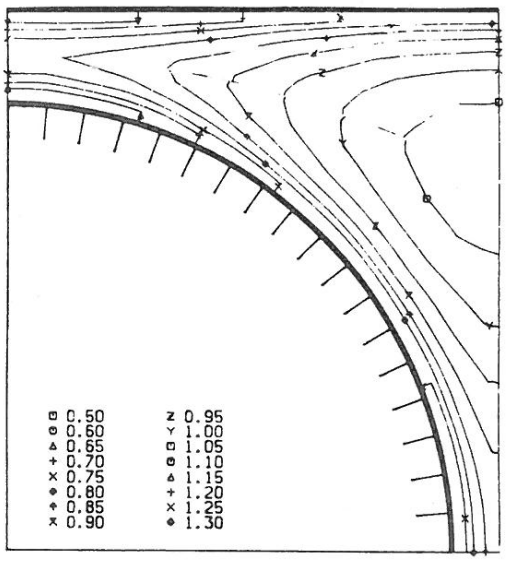

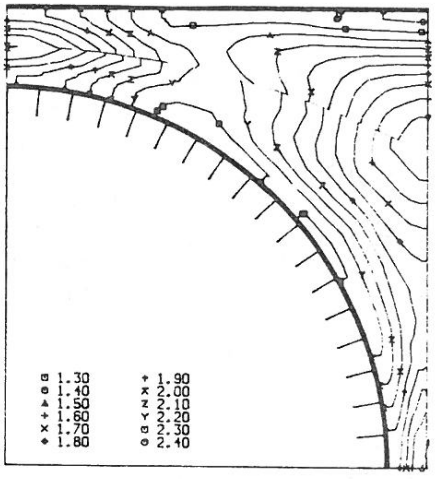

Figure 2: (a) Mean axial velocity (b) Axial turbulence intensity

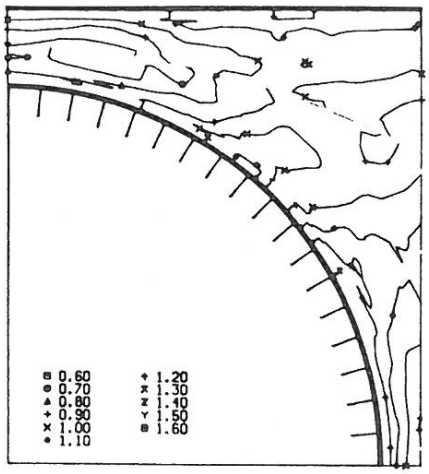

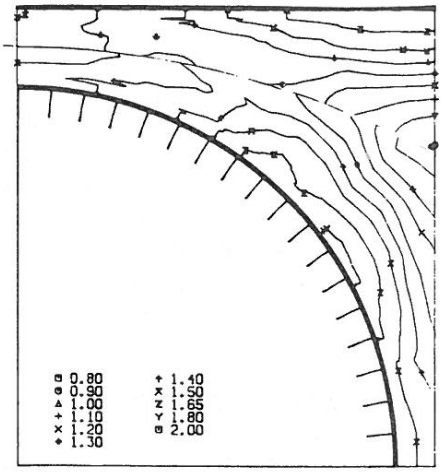

Figure 2: (c) Radial turbulence intensity. (d) Azimuthal turbulence intensity.

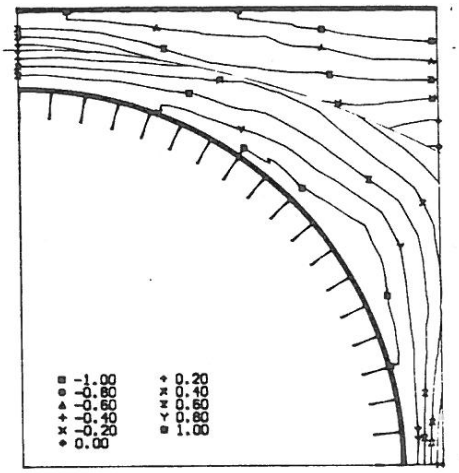

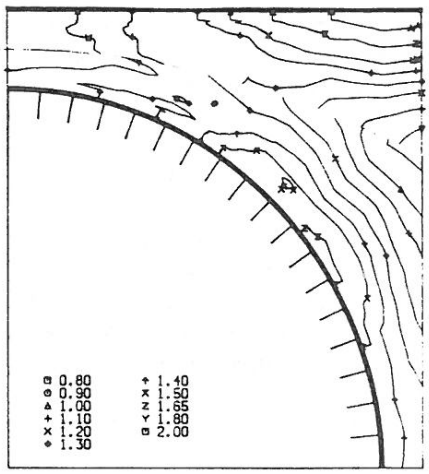

Figure 2: (e) Radial Reynolds shear stress. (f) Azimuthal Reynolds shear stress.

PRESSURE FLUCTUATION TRANSMISSION IN SMALL DIAMETER TUBES - COMPARISON OF THEORY AND EXPERIMENT

J.D. Holmes* and R.E. Lewis*

Introduction

Knowledge of the transmission characteristics for pressure fluctuations of small diameter tubes is important for many practical measurement situations in wind engineering, aerodynamics and aeroacoustics. Although the theoretical problem of propagation of sound waves in gases in cylindrical tubing is a classical one, associated with such famous names as Helmholtz, Kirchhoff and Rayleigh, most of the early approximate solutions (for low reduced frequencies) have been superseded by those developed by Iberall [1] and Bergh and Tijdeman [2]. A review of the many existing analytical solutions has been given by Tijdeman [3].

Recent experimental developments have been the introduction of very small diameter restrictor tubes [4], and pneumatic averagers involving parallel tube systems, [5]. Gumley [6, 7] extended the Bergh and Tijdeman theory to include the pneumatic averagers, and advocated the use of the theory for designing tubing systems in practical situations.

The interest of the Division of Building Research in the problem is essentially a practical one - the optimization of tubing systems for the measurement of fluctuating and peak pressures and area loads on wind tunnel models of buildings in simulated atmospheric boundary layers. The frequency response requirements for accurate measurements of peak pressures in these situations have been defined [8], and an experimental rig has been set up to carry out dynamic calibration of complete pressure measurement systems, including pressure transducers and associated volumes [9]. The present paper makes some comparisons between system responses measured with the calibration rig, and predicted by the theory, as formulated by Bergh and Tijdeman, and Gumley.

Assumptions of the Theory

The derivation of the theory is fairly lengthy, but described in detail in References [2] and [6]. The motion of the fluid in a tube of circular cross-section is described by the fundamental flow equations: the Navier-Stokes equations of momentum conservation, the equation of continuity, the equation of state, and the energy equation. The following assumptions are made:

(i) the sinusoidal pertubations in pressure, density, temperature and velocity are small in comparison to the mean values.

(ii) The length to diameter ratios of the tube sections are assumed large so that end effects are negligible.

(iii) The Reynolds Numbers are low enough so that the flow is laminar throughout the system.

(iv) The thermal conductivity of the wall of the tubes is assumed to be large, so that temperature fluctuations at the wall are zero.

(v) The material of the tube walls is assumed to be rigid.

---

* CSIRO Division of Building Research

(vi) The cross flow velocity at the entrance to the tubes is assumed small.

(vii) When the averaging manifold is included, it is assumed to have rigid walls, and that there are no spatial variations of fluid properties within the volume.

(viii) The pressure expansions in the tubing, manifold and transducer volume are assumed to be polytropic processes.

With these assumptions, Bergh and Tijdeman [2] derived a recursion equation for the complex ratio of pressure amplitudes across an element consisting of a tube and a volume. With the assumptions made, the equation is valid for values of reduced frequency $\omega D/a_0$ much less then unity, where ω is the circular frequency of pressure fluctations, D is the tube diameter and a_0 is the speed of sound. This condition is normally easily satisfied for most practical measurement conditions and frequency requirements. Gumley [6] derived a similar equation for an element consisting of m identical parallel tubes feeding a single volume. In this case, the equation gives the ratio of the *average* of the pressure amplitudes at the inlets to the m tubes, and the pressure amplitude in the volume.

The Bergh and Tijdeman element can be used to represent a series of tubes of different diameters, including restrictors, by setting all volumes except the last (adjacent to the transducer) equal to zero. The Gumley element can be used to represent a pneumatic averager (manifold) system at the input end of a series tube system [6]. For the present results, the theoretical equations were programmed in BASIC, and a microcomputer used to compute the response characteristics.

Single Tube Comparisons

Figure 1 shows the computed amplitude ratio and phase response for a simple constant diameter tube of 1.5 mm internal diameter and 500 mm length connected to a volume of 250 mm^3. The theoretical results were compared with experimental data obtained for a stainless steel tube connected to a cavity exposed to the diaphragm of a Setra 237 pressure transducer. The pressure fluctuation amplitudes in the reference or coupling cavity, at the input end of the tube, were measured by a Bruel and Kjaer 4147 low frequency microphone. The amplitude of the sinusoidal pressure fluctuations in the coupling cavity was approximately 70 Pascals. However other runs with amplitudes varying from 20 to 200 Pascals showed no significant difference in measured response characteristics.

Reasonable agreement with the experimental data is obtained when the experimental tube diameter of 1.5 mm is used in the theoretical equations, including the resonant frequencies of the 2nd and 3rd modes. However a better agreement with the magnitude of the resonant amplitude peaks and phase response, is achieved when the tube diameter is reduced by 10% in the theoretical calculations. Bergh and Tijdeman [2] observed a similar phenomenon in their comparisons and attributed the discrepancy to inaccurate measurement of the tube diameter. We do not believe that this is the reason for the differences in our case, as great care was taken to accurately measure the internal diameter of the tube.

Other comparisons have been made for series tubes involving flexible (p.v.c.) tubes, changes in diameter due to pressure taps, and restrictors. Generally, the theory has predicted the experimental data quite well in these cases, although it is not always possible to specify the diameter of the p.v.c. tubing accurately.

Manifold Tube Comparisons

A comparison for a system involving a 10 input manifold system, as well as flexible tubing, pressure taps and restrictors is shown in Figure 2.This is a near optimum system, with a flat amplitude response (± 5%) and near-linear phase lag up to nearly 300 Hz, that has been used for measurement of area-averaged loads on wind tunnel models of buildings. For such a complex system, the theory predicts the measured response quite well. No reduction of tube diameters was made in this case.

It should be noted that the input tubes to the manifold were assumed to be of constant diameter, in the theoretical calculations. In fact, in the experiment there were pressure taps of smaller diameter at the start and termination of these tubes. Although it is possible to account for these in the theoretical model, the computations become considerably more complicated [6] and were not justified for the small improvement in accuracy to be achieved.

Discussion and Conclusions

Like Gumley [6], we believe that the theoretical method can be used to optimize tubing systems required for measurements. However, it is essential that an experimental calibration be carried out subsequently. When this is done, fine tuning of the system, by, for example, moving the restrictor(s) along the tube is usually required for final optimization.

It should also be noted that tubing systems incorporating a 'Scanivalve' pressure scanning switch cannot be adequately be included in the theoretical predictions. The interior passages of such devices include right angled bends, and tapered tubes which are not catered for by the theory. We have found that experimental trial and error calibration must be used for systems involving these devices.

A paper describing an optimization procedure for pressure systems is in preparation. However, for most cases, both single tube and manifolded systems, it is found that the best results are obtained using restrictors whose optimum positions are fairly close to the pressure transducer. Figure 2 shows the response curves for such a system.

References

1. A.S. Iberall, 'Attenuation of Oscillatory Pressures in Instrument Lines', J. Res. Nat. Bur. Stand., 45, 85, 1950.

2. H. Bergh and H. Tijdeman, 'Theoretical and Experimental Results for the Dynamic Response of Pressure Measuring Systems', National Aero- and Astronautical Research Institute, Amsterdam, Report NLR-TRF.238, 1965.

3. H. Tijdeman, 'On the Propagation of Sound Waves in Cylindrical Tubes', J. Sound & Vib., 39, 1, 1975.

4. H.P.A.H. Irwin, K.R. Cooper and R. Girard, Correction of Distortion Effects Caused by Tubing Systems in Measurements of Fluctuating Pressures', J. Ind. Aerodyn., 5, 93, 1979.

5. D. Surry and T. Stathopoulos, 'An Experimental Approach to the Economical Measurement of Spatially-averaged Wind Loads', J. Ind. Aerodyn. 2, 1977.

6. S.J. Gumley, 'Tubing Systems for Pneumatic Averaging of Fluctuating Pressures', J. Wind. Engg. & Ind. Aerodyn., *12*, 189, 1983.

7. S.J. Gumley, 'A Detailed Design Method for Pneumatic Tubing Systems', 6th International Conference on Wind Engineering, Gold Coast, 1983.

8. J.D. Holmes, 'Effect of Frequency Response on Peak Pressure Measurements', J. Wind Engg. & Ind. Aerodyn., *17*, 1, 1984.

9. R.E. Lewis and J.D. Holmes, 'A Dynamic Calibration Rig for Pressure Tubing and Transducers', Workshop on Wind Engineering and Industrial Aerodynamics, Highett, 1984.

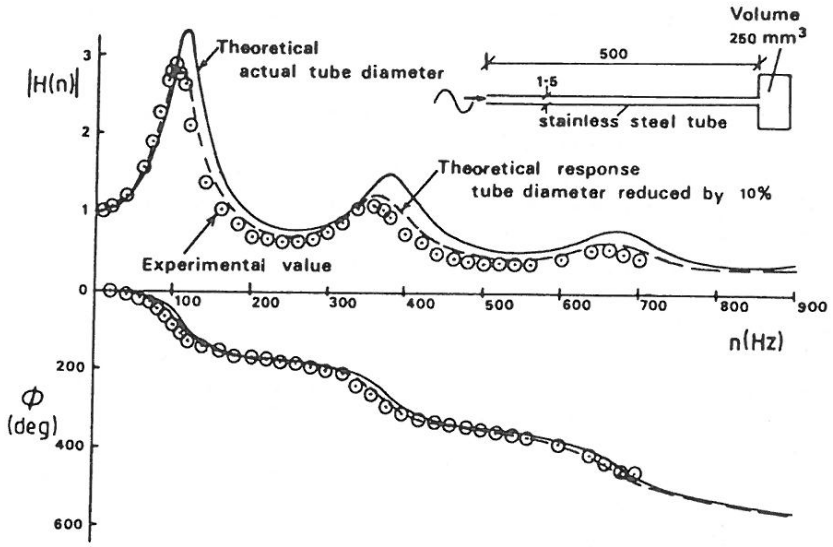

Figure 1. Comparison of responses - simple system

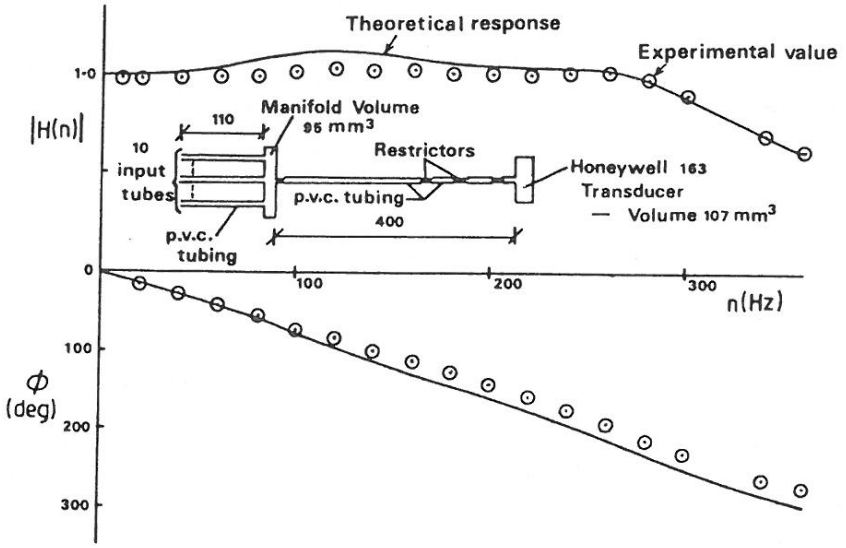

Figure 2. Comparison of responses - complex system

EFFECTS OF WIND TUNNEL BLOCKAGE ON STREAMWISE SURFACE PRESSURES

P.J. Saathoff and W.H. Melbourne*

Introduction

Studies of wind tunnel blockage effects have generally concentrated on obtaining corrections to bluff body drag (i.e. front face and base pressure) measurements. Little work has been published concerning effects of wall constraint on streamwise pressure measurements. As a result, these effects are usually ignored even at relatively high blockage ratios. (Blockage ratio is the ratio of effective model area, S, to tunnel cross-sectional area, C.) Some researchers [1 and 2] have attempted to remove blockage effects by altering the tunnel test section in some way. However, the effectiveness of these measures is open to question.

Awbi [3], from a study using two-dimensional rectangular cylinders in smooth flow, has shown that increasing the blockage ratio can lead to early reattachment of separated shear layers depending on the streamwise depth of the model. Hunt's [2] measurements on cubical building models in boundary layer flows indicated that for a relatively high blockage (S/C = 8%) fluctuating pressure coefficients, $C\sigma_p$, may be as much as 10% too large.

Experimental Procedure

Mean, fluctuating and peak pressures were measured on the streamwise surfaces of five axisymmetric cylinders with aspect ratio (L/D) of 1.0, where L is the streamwise depth and D is the cylinder diameter. Cylinder diameters ranged from 36 to 255 mm. Locations of pressure tappings are shown in Figure 1.

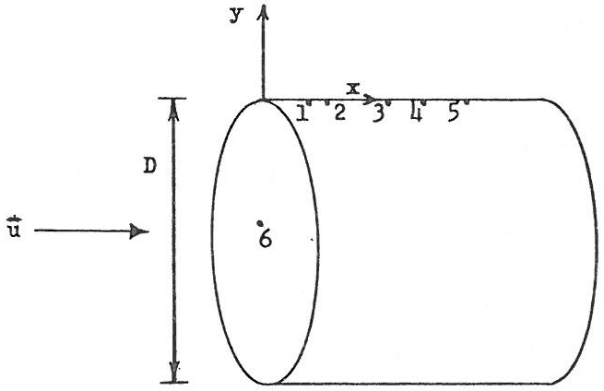

Pressure Tapping	Distance from Leading Edge (x/D)
1	0.09
2	0.19
3	0.39
4	0.59
5	0.78

Figure 1. Locations of pressure tappings

Experiments were performed in the 2 m x 2 m section of the 450 kW wind tunnel and in the 0.9 x 1.2 m 35 kW tunnel in the Department of Mechanical Engineering, Monash University. Blockage ratios ranged from 0.025% to 1.3% and 0.9% to 4.6% in the large and small tunnels, respectively. Most experiments were performed in grid-generated turbulence at a value of turbulence intensity ($\sigma_u/\bar{u}$) of approximately 8%. Measurements were also obtained in smooth flow in the small tunnel. Turbulence parameters associated with each tunnel configuration are given in Table 1.

* Department of Mechanical Engineering, Monash University

Table 1. Wind Tunnel Configurations

Tunnel	Grid	Bar width (mm)	Downstream distance (m)	Turbulence Intensity $\sigma_u/\bar{u}$	Integral Scale L_x(m)	Range of L_x/D
	A	35	2.0	8.0	0.08	0.3 - 2.1
450 kW	B	100	5.0	8.0	0.20	0.8 - 5.7
2 m x 2 m	C	303	11.7	8.3	0.55	2.2 - 15.3
	D	37	1.5	8.2	0.07	0.3 - 1.9
30 kW	E	70	3.0	8.2	0.13	0.5 - 3.7
0.9mx1.2m	Smooth Flow			0.7		

A SETRA Model 237 pressure transducer was used to measure mean, fluctuating and peak pressures. The reference static pressure was obtained with a pitot-static tube upstream of the cylinder. Static pressure was measured at the cylinder location to determine the correction factor and this factor was slightly adjusted to give $C_{\bar{p}}$ of 1.0 at the stagnation point (Tapping 6). A restrictor was used in the plastic tube connecting the transducer to the pressure tappings, providing a flat frequency response (±15%) up to 70 Hz and 100 Hz for the largest and smallest cylinders, respectively.

The experimental setup is shown in Figure 2. An additional pressure tapping was placed on the bottom surface of each cylinder at x/D = 0.09. The orientation of the cylinder was adjusted so that the difference in $C_{\bar{p}}$ on the top and bottom surfaces was less than 2%, so that approximately axisymmetric flow was ensured.

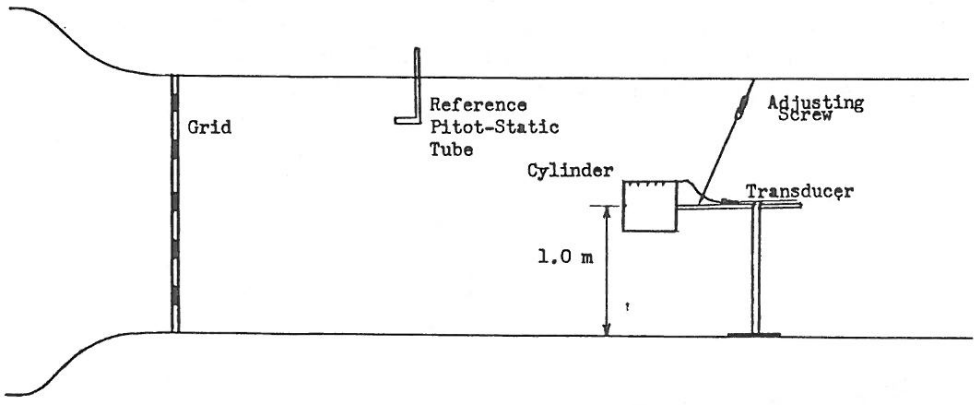

Figure 2. Experimental Configuration (not to scale)

Results

Space limitations permit only a small portion of the results to be discussed here. Figure 3 shows mean pressure coefficient at Tapping No.1 (x/D = 0.09) as a function of S/C for five flows having approximately the same turbulence intensity. For comparison, results obtained in smooth flow are also presented. The five flows at $\sigma_u/\bar{u}$ = 8% encompass a wide range of turbulence scales. However, as noted previously [4], little effect of scale is evident.

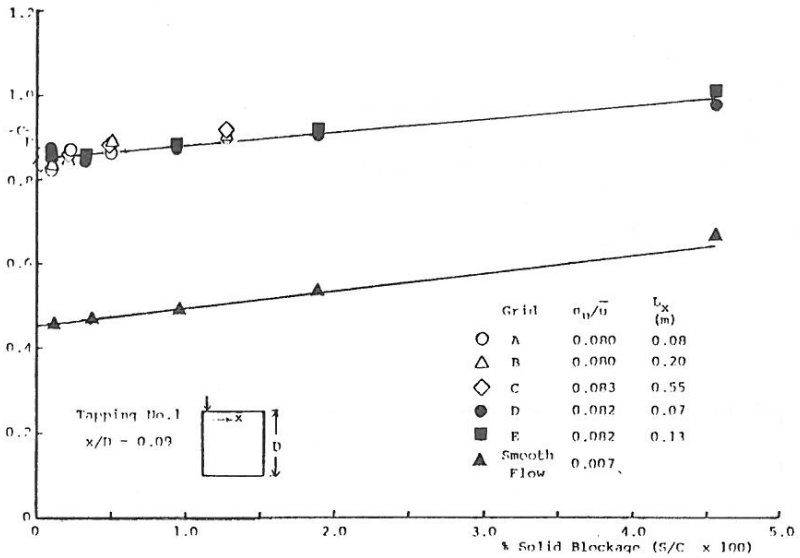

Figure 3. Mean pressure coefficient at Tapping No.1 as a function of wind tunnel blockage

The slopes of the blockage curves are approximately 3.0 and 4.0 for the turbulent and smooth flow cases, respectively. Flow reattachment did not occur in smooth flow, therefore blockage corrections are larger in this case. In the turbulent flow an increase in S/C from 0 to 4.6% increases $|C_{\bar{p}}|$ by approximately 15%. In coefficient form:

$$C_{\bar{p}_c} = C_{\bar{p}_m} + 3.0\ (S/C) \qquad (1)$$

where subscript c indicates the corrected value and subscript m indicates the measured value. Although Equ.(1) is applicable only at Tapping No.1, it is expected that at different $\sigma_u/\bar{u}$ the slope of the blockage curve would be the same, providing reattachment occurs.

Blockage corrections to fluctuataing pressures are complicated by the fact that $C\sigma_p$ is dependent on relative scale, L_x/D where L_x is the longitudinal integral scale of the turbulence. Figure 4 shows $C\sigma_p$ measured at Tapping No.1 as a function of S/C for five different flows with $\sigma_u/\bar{u} \approx 8\%$. Corresponding values of L_x/D are shown next to each data point.

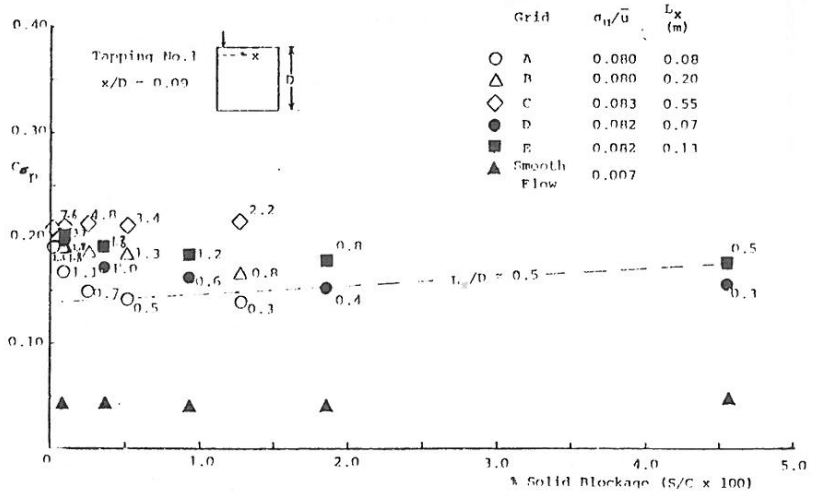

Figure 4. Fluctuating pressure coefficient at Tapping No.1 as a function of wind tunnel blockage and relative scale (L_x/D)

Although it is not possible to accurately determine the effect of S/C on $C\sigma_p$ especially at large L_x/D, it is clear that an increase in blockage produces an increase in $C\sigma_p$. For $L_x/D \approx 0.5$, an increase in S/C from 0 - 4.6% increases $C\sigma_p$ by approximately 20% . For this case:

$$C_{\sigma_{p_c}} = C_{\sigma_{p_m}} - 0.7\ (S/C) \qquad (2)$$

Considerable scatter is associated with peak pressure measurements. Therefore, blockage corrections cannot be directly obtained from the data. However, the significance of blockage effects on the peak pressure coefficient, $C_{\check{p}}$, can be inferred from the mean and fluctuating pressure data. The peak pressure coefficient can be obtained from the following:

$$C_{\check{p}} = C_{\bar{p}} - g\, C_{\sigma_p} \qquad (3)$$

where g is the peak factor.

For a normal distribution, the peak factor associated with a probability level of 10^{-4} is approximately 4.3 . At high turbulence intensities, fluctuating pressures near separation are negatively skewed and peak factors of 10 are not uncommon.

The effect of wind tunnel blockage on $C_{\check{p}}$ can be estimated using Equ.(3) . Assuming a peak factor of 6.0, S/C = 4.6% and L_x/D = 0.5, the uncorrected peak pressure coefficeint is:

$$C_{\check{p}} = -0.98 - 6.0(0.170) \approx -2.0$$

Substituting $C_{\bar{p}_c}$ and $C_{\sigma_{p_c}}$ into (3) the blockage corrected peak pressure coefficient is:

$$C_{\check{p}_c} = -0.85 - 6.0(0.140) \approx -1.7$$

Thus, a value of S/C of approximately 5% increases $|C_{\check{p}}|$ by approximately 15%.

Conclusions

Data obtained using axisymmetric cylinders suggest that a blockage ratio of 5% increases $|C_{\bar{p}}|$, C_{σ_p}, $|C_{\check{p}}|$ by approximately 15%. Although only data near separation was presented, corrections to other streamwise pressures will likely be of the same order of magnitude.

References

1. M. Kiya and K. Sasaki, 'Free-stream Turbulence Effects on a Separation Bubble", Jnl. Wind Eng. and Industrial Aerodynamics, 14, 375-386, 1983.

2. A. Hunt, 'Wind-Tunnel Measurements of Surface Pressures on Cubic Building Models at Several Scales', Jnl. Wind Eng. and Industrial Aerodynamics, 10, 137-163, 1982.

3. H.B. Awbi, 'Wind Tunnel Wall Constraint on Two-Dimensional Rectangular Section Prisms', Jnl. Wind Eng. and Industrial Aerodynamics, 3, 285-306, 1978.

4. R. Hillier and N.J. Cherry, 'The Effects of Stream Turbulence on Separation Bubbles', Jnl. Wind Eng. and Industrial Aerodynamics, 8, 49-58, 1981.

FLOW OVER A BLUNT FLAT PLATE

L.W. Welch, K. Hourigan and M.C. Welsh*

Introduction

It is now recognised that a high Reynolds-number flow around a bluff body separates from the leading edge corner, reattaches downstream and gives rise to regions of concentrated vorticity embedded in irrotational fluid. It has been also found that with such a flow the rate of heat transfer can be as much as 50% greater than that observed with an attached turbulent boundary layer [1].

There have been a number of papers arising from both numerical and experimental studies that have sought to further understand the mechanisms of improved heat transfer and the nature of the instantaneous flow velocities, [2,3,4]. Some of these studies have shown that the reattachment length can be reduced by changing the leading edge geometry, [5], by inclining the plate to the direction of flow, [6], or by the application of sound across the flow, [7]. Using the application of sound [8] it was found that the mean rate of heat transfer increased as the reattachment length was reduced, whilst [7] and [9] have shown that the point of reattachment of the separation bubble oscillates and that a large scale vortex is shed from the separation bubble each acoustic cycle.

Our studies, both numerical and experimental [10], have shown that at some sound pressure levels there is a strong tendency for the large scale vortices to pair. Our objectives are to determine the instantaneous flow velocities, the flow streamlines and to examine the mechanisms of heat transfer under these conditions. It is proposed to use LDA equipment and to phase relate the sampling to the acoustic cycle. Preliminary work has been carried out using hot-wire probes and this paper presents the findings that relate to the large-scale structures in the third or spanwise direction.

Experimental Apparatus

The major component of the test apparatus is a small blow down open jet wind tunnel, Fig.1. The centrifugal fan is powered by a direct current electric motor with variable speed thyristor control. A wide angle diffuser containing four perforated plates connects the fan outlet to a settling chamber which contains a honeycomb and four nylon screens. Air leaving the settling chamber is passed through an 8 to 1 contraction to create a 244mm square open jet working section.

The maximum velocity at the contraction outlet was $15ms^{-1}$ and the profile uniform, within 1%, between the boundary layers, approximately 5mm thick. The centre line longitudinal relative turbulence intensity is 0.3% with spectral components less than 100Hz. The major spectral component occurs at the rotational frequency of the fan. The total volume flow was monitored using a British Standard nozzle connected to the fan inlet.

* CSIRO Division of Energy Technology, Melbourne, Australia

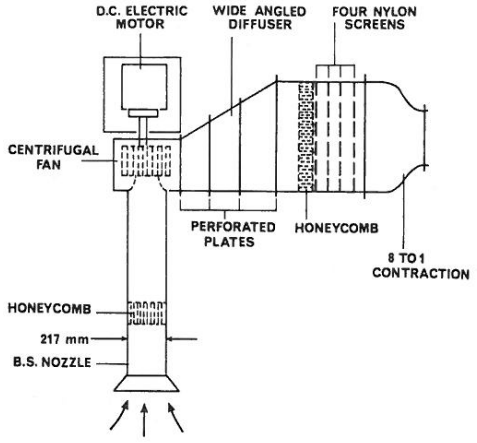

Fig.1 Open jet wind tunnel

The square edged test plate, 13mm thick, 135mm span and 130mm chord, was machined from a block of aluminium. The plate was located midway between the speakers, Fig. 2, and the plate/speaker assembly mounted on a machine table that allowed precise traversing of the assembly in each of the three major axes. The speakers were positioned 350mm apart and connected in anti-phase to generate the equivalent of an acoustic Parker β-mode near the plate [7]. This generated a maximum sound pressure level midway between leading and trailing edges which resulted in zero acoustic velocity at the mid-point of the plate and a maximum acoustic velocity at the leading and trailing edges. Glass endplates at the spanwise extremities ensured a two dimensional sound field.

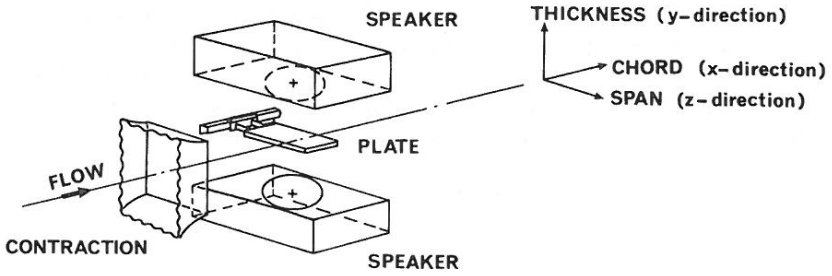

Fig.2 Plate and speakers

The fluctuating velocities were measured using single hot-wire probes which were aligned parallel to the leading edge and at right angles to the flow direction. The fluctuating signals from these probes were band passed, 10-3000Hz, and digitised at 9000Hz concurrently with the data required to determine the mean flow parameters. The data were subsequently processed on a PDP 11/44 mini-computer.

The experimental data presented in this paper were obtained with a mean freestream velocity, upstream infinity, of approximately $8ms^{-1}$. The probes were held at a height of 13mm above the plate with one fixed relative to the tunnel outlet and the other fixed relative to the plate/speaker assembly. The applied sound frequency was held at 135Hz and the sound pressure level set to 115dB just above the plate surface at its mid-point.

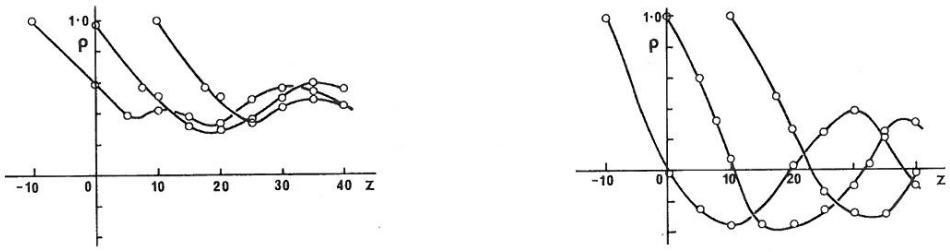

a) quarter chord b) half chord

Fig.5 Summary of cross-correlation coefficients - phase 0

Careful examination of simultaneous velocity time histories from any two spanwise locations reveals that one signal is either predominantly in-phase or out-of-phase with the other signal, see Fig.6, which shows time histories from two probes with a spanwise separation of 10mm, a zero cross-correlation condition.

A vortex distribution that is consistent with the above data may emerge as follows. An instability wave develops in the spanwise direction of a large-scale vortex structure. This wave 'breaks' the vortex up into a number of hairpin vortices with broad edges distributed in the span-wise direction. The spanwise phase angle of instability waves in subsequent vortices is set by the phase of the preceding vortex. This results in the formation of a train of hairpin vortices regularly spaced chordwise but alternately in anti-phase spanwise. A perturbation to the vortex shedding process may result in another train of hairpin vortices developing with a different spanwise phase. Due to the broad edged geometry of the vortices, time histories in the spanwise direction will therefore be solely in phase or anti-phase for each train. Over an extended period of time, the cross-correlation will have no phase shift and the amplitude will depend on the ratio of in-phase to out-of-phase data.

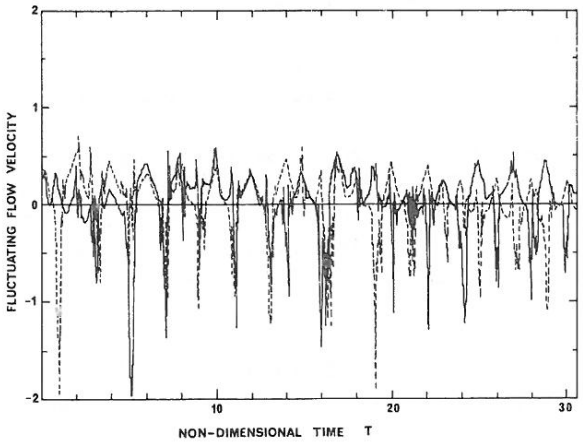

Fig.6 Mid-chord time histories - spanwise separation 10mm

Results and Discussion

The time histories without sound indicate the presence of asynchronous large scale structures, but when a sound field is applied these structures are shed in a regular manner. Above the leading edge the time history reflects the superimposed acoustic velocity, a low amplitude sinusoid at the frequency of the applied sound. Downstream of the point of reattachment a regular pattern occurs at half the sound frequency which is independent of the spanwise position, data recorded at positions to $\pm$ 40mm from the centre of the span. The auto-correlation of such data, see Fig.3 taken at mid-chord, shows a strong correlation at half the sound frequency.

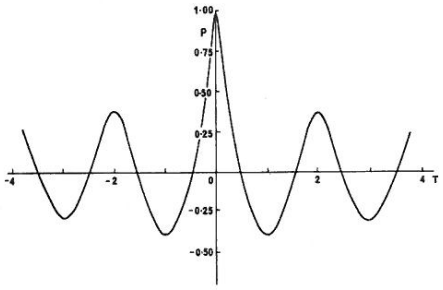

Fig.3 Auto-correlation
Mid-chord
ρ normalised coef.
τ non-dimensional time
(time/acoustic cycle)

Simultaneous recording of signals from two probes located at various positions above the plate have been used for a series of cross-correlations. Fig.4 shows cross-correlations for mid-chord spanwise separations of 10 and 20mm. The cross-correlations for positions 10 to 20mm apart show a change in amplitude from zero at 10mm to a minimum at 20mm, from 20 to 30mm the amplitude increases from the minimum back to zero and from 30 to 40mm the amplitude continues to increase to a new positive maximum at 40mm. There was no suggestion of phase shift.

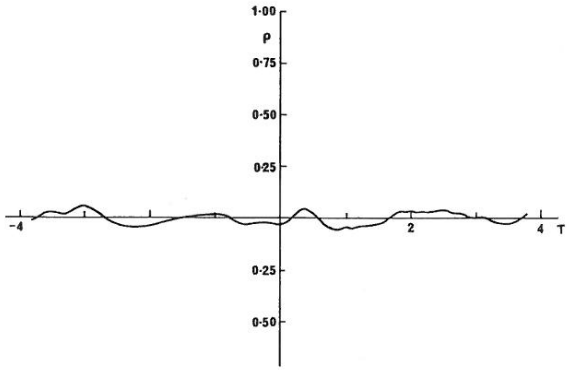

a) spanwise separation 10mm

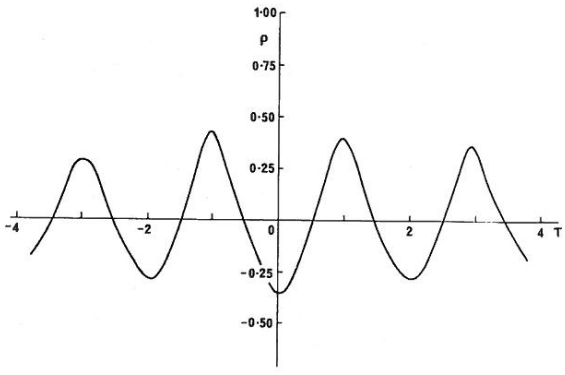

b) spanwise separation 20mm

Fig.4 Mid-chord Cross-correlations

At the leading edge the cross-correlation reflects the applied acoustic velocity and there is only a very small change in amplitude as the separation is increased. At the quarter chord position the cross-correlation coeficient changes in amplitude but is never less than zero. Downstream of mid-chord the resulting correlations are the same as at mid-chord. These findings are dependent only on the relative spanwise separation. The relationship between spanwise separation and cross-correlation is summarized in Fig.5.

This work suggests that the coherence of the flow induced by a sound field of medium intensity is restricted by instabilities in the third dimension. The presence of sound at high intensity levels (e.g. duct acoustic resonance [7]) appears, from flow visualisation, to promote a high degree of coherence. It is these levels that may be more appropriate to the use of phase-averaging techniques with LDA equipment.

References

1. Ota,T and Kon,N. "Heat Transfer in the Separated and Reattached Flow on a Blunt Flat Plate", J.Heat Transfer, Vol. 96, 1974, pp.459-462.

2. Ota,T and Itasaka,M. "A Separated Flow on a Blunt Flat Plate", J.Fluids Engineering, Vol. 98, 1976, pp.79-86.

3. Kiya,M. and Sasaki,K. "Structure of Large-Scale Vortices and Reversed Flow in the Reattaching Zone of a Turbulent Separation Bubble", J.Fluid Mechanics, Vol. 154, 1985, pp.463-491.

4. Cherry,N.J., Hillier,R. and Latour,M.E., "Unsteady Measurements in a Separated and Reattaching Flow", J.fluid Mechanics, Vol. 144, 1984, pp.13-46.

5. Ota,T and Kon,N., "Heat Transfer in the Separated and Reattached Flow over Blunt Flat Plates - Effects of Nose Shape", Int. J.Heat and Mass Transfer, Vol. 22, 1979, pp.197-206.

6. McCormick,D.C., Lessmann,R.C. and Test,F.L., "Heat Transfer to Separated Flow Regions from a Rectangular Prism in a Cross Stream", J.Heat Transfer, Vol. 106, 1984, pp.276-283.

7. Parker,R and Welsh,M.C., "Effects of Sound on Flow Separation from Blunt Flat Plates", Int. J.Heat and Fluid Flow", Vol. 4, 1983, pp.113-128.

8. Cooper,P.I., Sheridan,J.C.,Flood,G.J. and Welsh,M.C. "The Effect of Sound on Forced Convection from a Flat Plate", Proc. 8th. Aust. Fluid Mechanics Conf., Uni.of Newcastle, N.S.W. 1983.

9. Stokes,A.N. and Welsh,M.C., "Flow-Resonant Sound Interaction in a Duct Containing a Plate:- Square Leading Edge", J.Sound and Vibration, Vol. 103, No.1, 1985.

10. Hourigan,K., Welsh,M.C. and Welch,L.W., "Augmented Forced Convection Around a Heated Flat Plate", Proc. 23rd. A.I.Ch.E./A.S.M.E. National Heat Transfer Conference, Denver, Colorado, 1985, accepted for publication.

PRESSURES ON SURFACE-MOUNTED RECTANGULAR PLATES

J.D. Holmes*

Introduction

Measurements of normal pressures and form drag on flat plates, normal to an airstream at high Reynolds Number, date back to the classical early study of drag and wake structure of two-dimensional (infinite aspect ratio) plates by Fage and Johansen [1]. Fail, Lawford and Eyre [2] later investigated the drag and wake characteristics of rectangular plates with aspect ratios between 1 and 10. Maskell [3], in the process of deriving blockage corrections for bluff bodies and stalled wings in closed wind tunnels, examined the results from References [1] and [2], and contributed his own measurements on square plates. The corrected values of drag coefficient on rectangular plates in smooth flow, derived by Maskell, were about 1.15 for square plates, and 1.86 for two-dimensional plates.

Arie and Rouse [4] examined the pressures and forces on a two-dimensional plate, with a downwind splitter or tail-plate, to prevent oscillation of the wake; this was a first approximation to the effect of a surface or ground plane. They found a significant reduction in drag coefficient - to a value of about 1.4.

Drag on Plates in Turbulent Boundary Layers

Good and Joubert [5], and Sakamoto and Arie [6], describe measurements on two-dimensional and finite width plates mounted in smooth wall turbulent boundary layers of various depths. Sakamoto and Arie found a minimum drag coefficient at an aspect ratio of 5.

Ranga Ragu *et al.* [7] describe measurements on two-dimensional plates in turbulent boundary layers, and present a graph of drag coefficient, based on friction velocity, as a function of h/z_o, where h is the height of the plate, and z_o is the roughness length. This graph is reproduced in Fig. 1 of this paper. The data points are obtained from many tests in smooth and rough wall boundary layers, with values of h/δ, where h is the height of the fence or plate, and δ is the boundary layer thickness, varying from less than 0.05 to greater than unity.

The drag coefficient C_D^*, based on the friction velocity, u*, can be related to the drag coefficient C_{Dh}, based on the mean velocity at the height of the plate, for plates fully immersed in the region of the boundary layer in which the logarithmic mean velocity profile applies, by the following:

$$C_D^* = C_{Dh} \left[\frac{1}{k} \ln \left(\frac{h}{z_o}\right)\right]^2 \qquad (1)$$

where k is von Karman's constant.

Equation (1) with C_{Dh} equal to 1.1 is a good fit to the data of Ranga Raju *et al.* in the range of h/z_o from 40 to 1000. For h/z_o greater than 1000, the drag coefficients are up to 10% less. This may be due to the effect of low free stream turbulence, although Bearman [8] reports little effect of free stream turbulence on two-dimensional normal plates in unsheared flow.

CSIRO Measurements

Recently, measurements have been made by the Division of Building Research to determine wind pressures and forces on walls or solid fences for structural

---

* CSIRO Division of Building Research

design (Holmes [9]). An instrumented plate, of aspect ratio 1.5, was constructed with transmission channels machined within the thickness of the plate on both sides. A total of 48 pressure taps - 24 on each side were provided. The pressure taps were internally manifolded in groups of six, forming a total of eight separate panels - four on each side. Each panel was connected via p.v.c. tubing with small diameter 'restrictors' inserted in the line to a Honeywell 163 pressure transducer so that simultaneous fluctuating pressure measurements were possible. Each pressure measurement system was separately dynamically calibrated using a sinusoidal pressure generator and the restrictors were adjusted to give a flat amplitude frequency response to about 200 Hz. The phase responses were close to linear to 200 Hz and matched for the eight panels.

The panel pressures across the wall were subtracted and the four net panel pressures were added, to give sample records of the fluctuating normal force on the plate. In this way, peak and r.m.s. total forces, as well as mean values, could be determined.

The plate was mounted in a simulated atmospheric boundary layer created by the barrier-roughness technique described by Holmes and Osonphasop [10]. The barrier generates coherent eddy structures of a large scale, which are retained downwind well after the re-attachment of the shear layer shed from the barrier (e.g. Troutt, Scheelke and Norman [11]). At the position of the plate, the longitudinal turbulence scale at the height of the plate (64 mm) is about 400 mm, or more than six times the height of the plate. The value of h/z_o for the simulated boundary layer flow was about 160.

To represent walls of various aspect ratios, the plate was mounted on its own (aspect ratio, 1.5) and with non-instrumented side pieces to form walls of aspect ratios of 5, 10 and approaching infinity. In the latter case, the wall completely spanned the 2 m wide wind tunnel test section.

Table I shows the mean and peak normal pressure coefficients for the wind direction normal to the plate. Corrections for blockage were made using the method of McKeon and Melbourne [12].

Table I
Mean and Peak Pressure Coefficients
for wall section at CSIRO (θ = 0°)

Aspect Ratio b/h	$\bar{C}p$	$\hat{C}_p$
1.5	1.17	3.10
5	1.07	2.81
10	1.04	2.50
∞	1.21	2.53

As may be seen, minimum values of both $\bar{C}_p$ and $\hat{C}_p$ occur at the aspect ratio of 10. This can be compared with Sakamoto and Arie's minimum for the mean total wall drag at an aspect ratio of 5. The value of their minimum drag coefficient, $\bar{C}_{Dh}$, was 0.98, when adjusted to a reference mean wind speed at wall height.

The value of $\bar{C}_p$ for the two-dimensional wall at CSIRO, is also shown on Fig. 1, where it lies slightly above the measurements of Ranga Raju *et al.*, which presumably were made in turbulence of considerably lower intensity and

scale. However the present result lies within the scatter of measurements of Ranga Raju *et al*.

Conclusions

i) Minimum values of mean and peak normal pressure and drag for surface-mounted plates in turbulent boundary layers occur at aspect ratios of 5 to 10.

ii) Although an apparent collapse of data on drag coefficients or two-dimensional plates, immersed in turbulent boundary layers may be achieved by plotting C_D^* against h/z_o (Jensen Number), this correlation may disguise variations due to turbulence intensity and scale in the boundary layer. However these variations seem to be small, and over a large range of h/z_o, a constant value of C_{Dh}, based on the mean velocity at the plate height, can be assumed, for practical purposes.

References

1. A. Fage and F.C. Johansen, 'On the Flow of Air Behind an Inclined Flat Plate of Infinite Span' Proc. Roy. Soc. A, *116*, 170, 1927.

2. R. Fail, J.A. Lawford and R.C.W. Eyre, 'Low-speed Experiments on the Wake Characteristics of Flat Plates Normal to an Air Stream', Aeronautical Research Council, R & M 3120, 1957.

3. E.C. Maskell, 'A Theory of Blockage Effects on Bluff Bodies and Stalled Wings in a Closed Wind Tunnel', Aeronautical Research Coucnil, R & M 3400, 1963.

4. M. Arie and H. Rouse, 'Experiments on Two-dimensional Flow over a Normal Wall', J. Fluid Mech., 1, 129, 1956.

5. M.C. Good and P.N. Joubert, 'The Form Drag of Two-dimensional Bluff-plates Immersed in Turbulent Boundary Layers', J. Fluid Mech., *31*, 547, 1968,

6. H. Sakamoto and M. Arie, 'Flow Around a Normal Plate of Finite Width Immersed in a Turbulent Boundary Layer', J. Fluids Engg., *105*, 98, 1983.

7. K.G. Ranga Raju, J. Loeser, and E.J. Plate, 'Velocity Profiles and Fence Drag for a Turbulent Boundary Layer along Smooth and Rough Flat Plates', J. Fluid Mech., *76*, 383, 1976.

8. P.W. Bearman, 'Turbulence Effects on Bluff Body Mean Flow', 3rd U.S. National Conference on Wind Engineering, Gainesville, Florida, 1978.

9. J.D. Holmes, 'Wind Loading on Free-standing Walls', CSIRO Division of Building Research, Internal Report 85/13, 1985.

10. J.D. Holmes and C. Osonphasop, 'Flow Behind Two-dimensional Barriers on a Roughened Ground Plane, and Applications for Atmospheric Boundary Layer Modelling', 8th Australasian Fluid Mechanics Conference, Newcastle, 1983.

11. T.R. Troutt, B. Scheelke and T.R. Norman, 'Organized Structures in a Reattaching Separated Flow Field', J. Fluid Mech., 143, 413, 1984.

12. R.J. McKeon and W.H. Melbourne, 'Wind Tunnel Blockage Effects on Drag on Bluff Bodies in a Rough Wall Boundary Layer', 3rd International Conference on Wind Effects on Building and Structures, Tokyo, 1971.

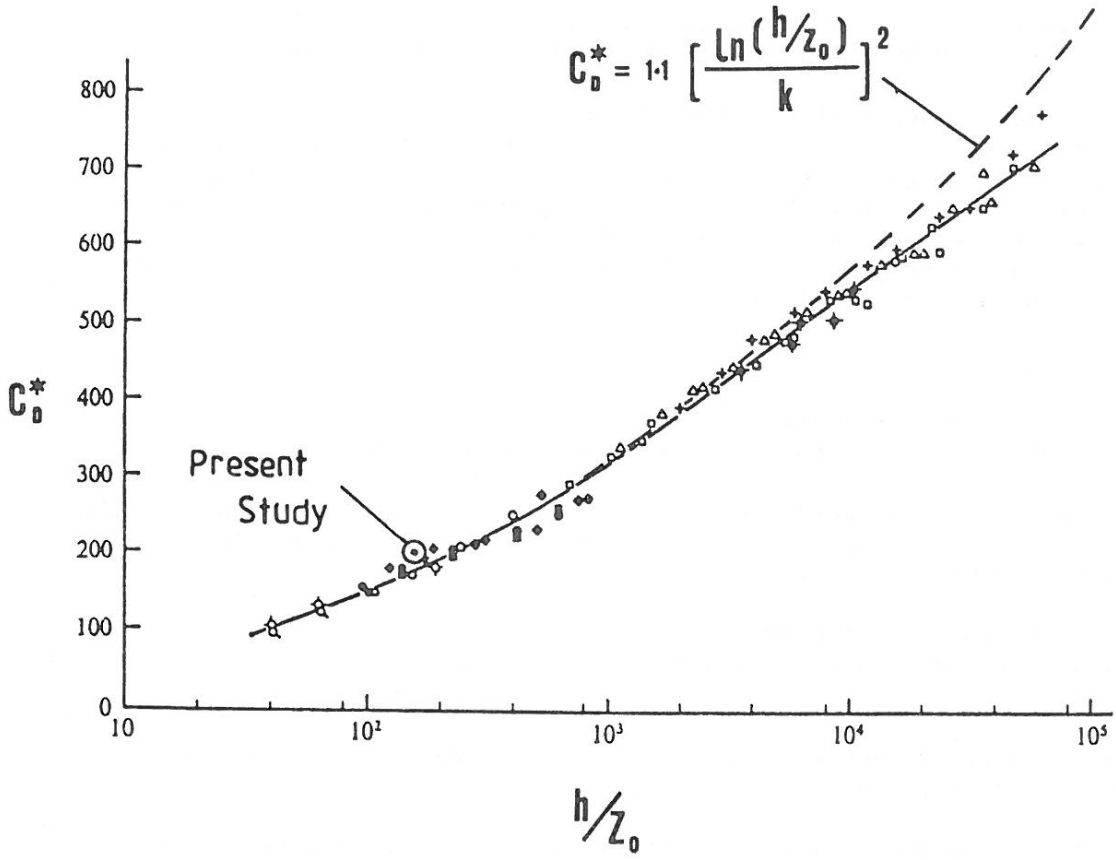

Figure 1. Drag coefficients for two-dimensional walls in turbulent boundary layers (from Reference [7])

THE INTERACTION OF SHEAR LAYERS WITH OBSTACLES IN A FLOW.

B.R. Morton *

Introduction

The interaction of shear layers in flow past either surface-mounted or free-standing obstacles gives rise to complex three-dimensional secondary flows, which may be observed both upstream of the obstacles and in their wakes. These flows have been quite widely studied, although the work is predominantly empirical and qualitative, but the flow behaviour remains poorly understood and difficult to predict. One obvious reason for this complexity is that the behaviour of flow past a cross-stream-symmetrical surface-mounted obstacle may depend on the gross height and width of the obstacle, representative radii of curvature in the vertical and horizontal at its leading edge, and the thickness of the incident boundary layer. Thus the flow may be characterised by as many as *five* Reynolds numbers, and we have only limited understanding of their relative importance. A surface mounted hemisphere might be regarded as one of the simpler types of obstacle as its representative lengths are all determined by the radius. Such hemispheres generate one or more pairs of trailing vortices in their wakes over a wide range of Reynolds numbers, whether the wakes be laminar or turbulent. In recent years there has been some disagreement as to whether the principal vortex pair has sense of rotation such as to produce upwash behind a hemisphere (or similar obstacle) or downwash. Although little of this discussion has been published, one opinion held that the sense depended on whether the flow was laminar or turbulent, Hanson [1] found predominant downwash in a wind tunnel study, while the results of Mason and Morton [2] suggest that downwash will dominate the wake when the ratio of boundary layer thickness to radius is small and boundary layer fluid is diverted primarily to the sides of the hemisphere, but that the wake vortices will be associated with upwash when this ratio is larger and diversion is primarily over the crest.

Much of the work on shear layer interaction with obstacles has related to the effects of small protuberances on boundary layer flows and on larger surface-mounted obstacles projecting through their boundary layers. The impetus for the former work arose primarily in aerodynamics and has been reviewed by Sedney [3], who noted that there had been little theoretical work and that insight into the complex flow patterns observed had come mainly from the visualisation of laboratory flows. One of the more detailed early studies was by Gregory and Walker [4], who described horseshoe shaped vortices which were seen wrapped around a low cylindrical obstacle, with arms trailing downstream. Studies of flow past taller obstacles have developed both in aerodynamics, where struts, fins and wings are believed to trap advected boundary layer vorticity, forming

---

* Department of Mathematics, Monash University, Clayton, Vic. 3168, Australia.

horseshoe vortices round the bases of the obstacles (Baker [5]; Bradshaw [6]) and in civil engineering where it has long been accepted that strong horseshoe vortices due to the trapping of boundary layer vorticity by bridge piers are responsible for bridge pier erosion of bed material upstream of the piers (Qadar [7]).

The horseshoe vortex paradox

On the traditional view, illustrated in Figure 1(i), a horseshoe vortex forms round the base of a cylinder in the boundary layer where cross-stream filaments of boundary layer vorticity are trapped ahead of the cylinder but carried past on either side. These filaments cannot be cut, and therefore collect into a U-shaped vortex round the cylinder with arms trailing off downstream. Advective stretching of the arms which tends to reduce the vortex core diameter and diffusive thickening which tends to increase it then settle into a balance, producing a strong, steady-in-the-mean horsehoe vortex lying parallel to the lower boundary and roughly within the boundary layer.

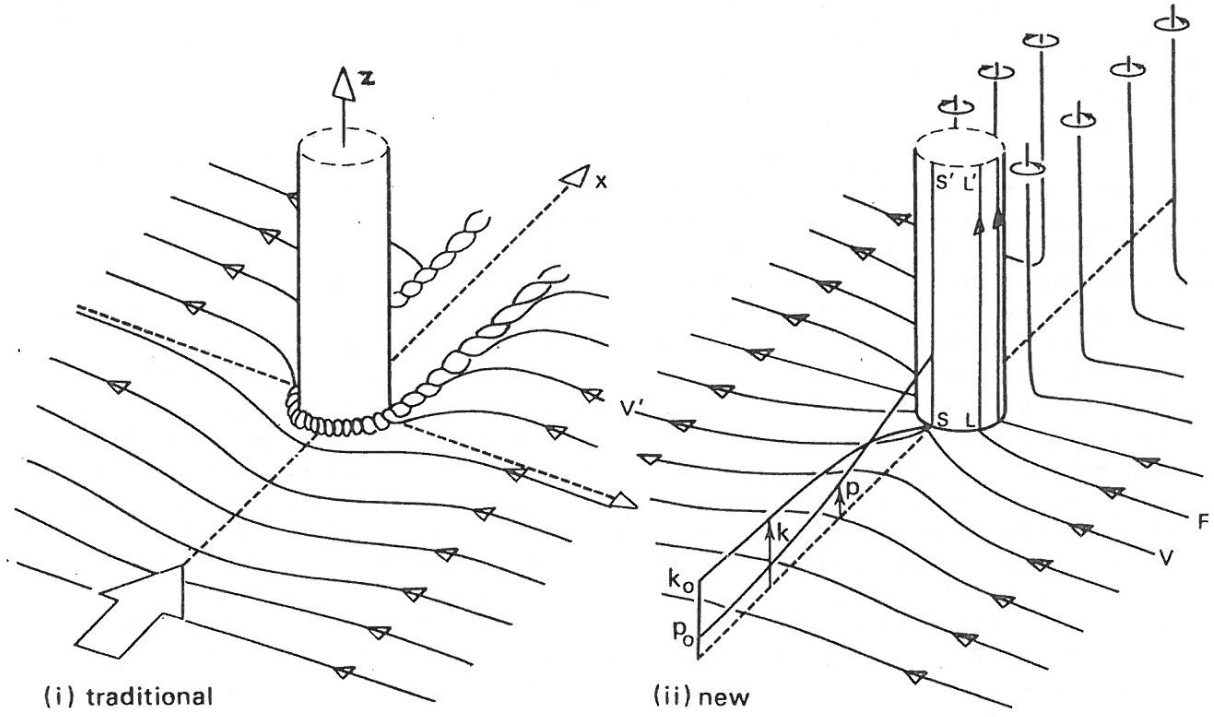

Figure 1 Schematic diagrams representing (i) the traditional and (ii) the proposed structure of vortex filaments where a boundary layer interacts with a cylinder. The diagrams represent a high Reynolds number, thin boundary layer limit.

The traditional view is unacceptable as it leads directly to a paradox. Suppose, in the configuration of Figure 1, a stream with uniform undisturbed velocity U in the x-direction and a boundary layer over the lower boundary interacting with a vertical cylinder mounted on the boundary. A measure of the gross vorticity in the boundary layer is provided by the circulation per unit streamwise length through the full depth of the layer, U; and a measure for the

mean speed of vorticity advection in the boundary layer is close to $\frac{1}{2}U$ for all likely profiles of velocity in the layer. It follows that the flux of vorticity in the boundary layer towards the cylinder has measure $\frac{1}{2}U^2$, and that *the trapped circulation after time t is approximately* $\frac{1}{2}U^2t$ *and is unbounded*! Moreover, this paradox cannot be resolved by viscous diffusion since in the upstream plane of symmetry all vorticity has the sense of that being advected in the boundary layer; nor can the trapped vortex filaments be advected up over the top of the cylinder, as no corresponding disturbance is observed on the upstream face of cylinders extending far above the boundary layer.

The interaction of a boundary layer with a cylinder

Further insight may be gained by flow visualisation of a stream U flowing over a horizontal lower boundary on which is mounted a vertical circular cylinder which extends through the boundary layer into the outer stream. Figure 2 shows a time exposure in the upstream plane of symmetry for flow past a circular cylinder. The flow is in a water channel with $0.2\times0.2m^2$ section in which the water is seeded with very small mica platelets and illuminated with a thin vertical sheet of light. Suitably oriented platelets reflect light horizontally to the camera, giving lines in the time exposure, but the platelets rotate in shear and so give streamlines and an indication only of velocity. The cylinder, just visible to the right, has height/diameter ratio h/d=0.36, height/boundary-layer-thickness ratio about 2, and Reynolds number 2700 (=Ud/ν). The outer edge

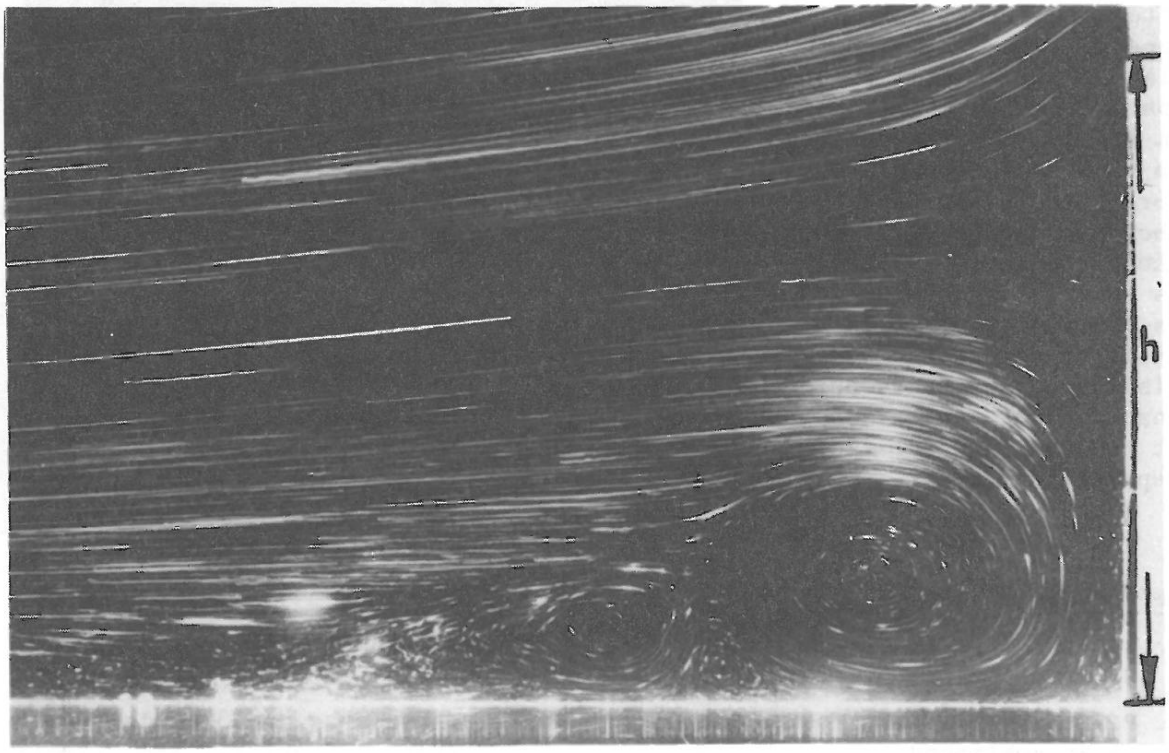

Figure 2 A visualisation in the upstream plane of symmetry for flow past a circular cylinder with h/d=0.36, h/$\delta\approx2$ and Re=2700.

of the boundary layer in Figure 2 corresponds to the stagnation point at about 3h/4, where h is the height of the cylinder. Above this stagnation point the flow is deflected over the top of the cylinder, while below it is a complex pattern of flow comprising in sequence from the right a large vortex with positive

sense of rotation (that of the boundary layer), a small lower "triangular" vortex with negative sense of rotation, an intermediate vortex of positive sense, and a flow separation which is poorly marked on account of the small speeds near the stagnation point.

The first point that should be made is that, although U-shaped vortices are certainly present round the base of the cylinder, they are surprisingly weak, with flow speeds far below those of the outer boundary layer and stream and vorticity well below that of the boundary layer.

Secondly, the small triangular vortex between the two larger positive (clockwise) vortices is quite definitely anticlockwise or negative in sense, and therefore consists of vorticity present nowhere else in this symmetry plane. For symmetry reasons, this vorticity cannot have been produced by turning boundary layer vorticity through angle π. The pattern is weaker and more complex than the anticipated classical horseshoe vortex and contains negative vorticity: it is therefore incompatible with the classical horseshoe model. This and other flows will be discussed at the meeting, especially in terms of the generation of vorticity at the boundaries and the proposed model of Fig.1(ii).

Wake and cylinder

Figure 3 shows the interaction of a wake generated from a splitter plate 40mm wide and 80mm upstream of the cylinder at Reynolds number 1200. In this case the advected vorticity is positive above and negative below the plate level. There is stretching as the flow is diverted past the cylinder resulting in a visible vortex pair, but insufficient generation at the cylinder for flow separation there.

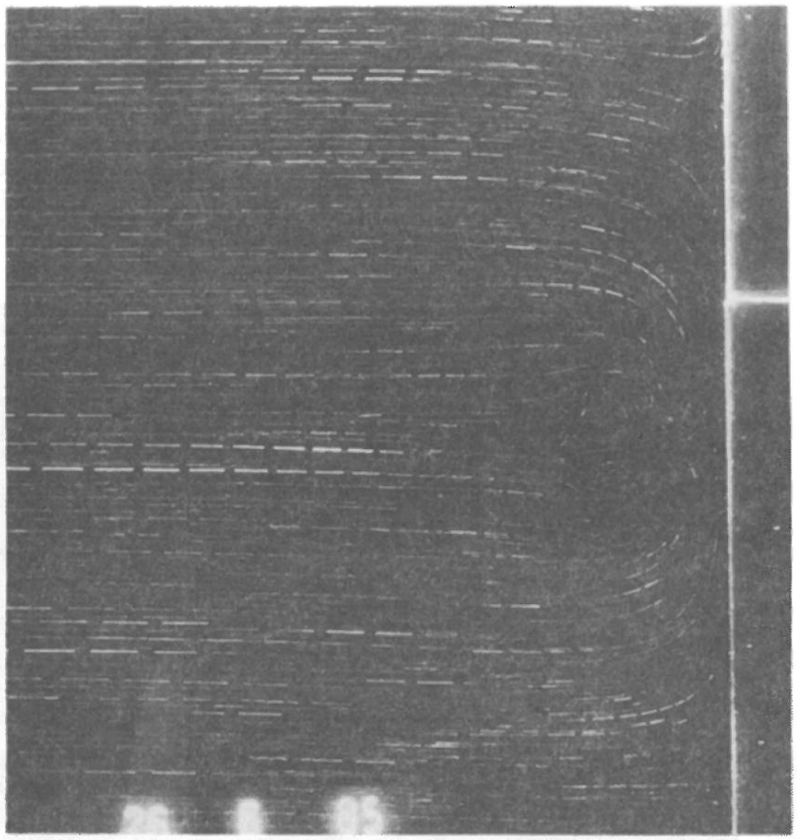

Figure 3 Interaction of wake and cylinder.

References

1. C.A. Hansen, 1975, PhD thesis, Colorado State University.
2. P.J. Ma son & B.R. Morton, 1985, to be published.
3. R. Sedney, 1973, AIAA J, 11, 782-792.
4. N. Gregory & W.S Walker, 1955, UK ARC R & M, 2779 Pt.1.
5. C.J. Baker, 1979, J. Fluid Mech., 95, 347-367.
6. P. Bradshaw, 1983, Mech. Engg. Trans., IE Austr., ME8, 192-199.
7. A. Qadar, 1981, Proc. Instn. Civ. Engrs., 71, 739-757.
8. B.R. Morton, 1984, Geophys. Astrophys. Fluid Dyn., 28, 277-308.

NUMERICAL SIMULATION OF SEPARATED AND REATTACHED FLOWS: EFFECT OF ACOUSTIC FIELD ON HEAT TRANSFER

Kerry Hourigan and Mark C. Thompson*

Introduction

Augmentation of the Nusselt number along a plate is found to occur when the flow is made to separate from the leading edge (Ota and Kon [1]). Further augmentation results when the mean reattachment length is decreased by changing the plate nose geometry (Ota and Kon [2]) or through application of an acoustic field. In fact, the time-mean local Nusselt number along the plate is chiefly a function of the mean reattachment length and is not sensitive to the perturbing mechanism (Cooper et al [3]). However, the application of sound is especially useful as an experimental technique in that it orders the large-scale vortex structures that are shed from the separation bubble (Parker and Welsh [4]). The increased coherence of the flow allows the use of conditional sampling with pressure probes, thermocouples and laser Doppler anemometers to construct an 'instantaneous' picture of the velocity and temperature fields. One aim of the present numerical work is to provide also the instantaneous fields, which can be used as guidelines for future experimental investigations.

Outline of the Numerical Model

The flow considered here is that past a rigid, two-dimensional, semi-infinite heated flat plate, which is aligned with a square leading edge normal to the flow. The flow at upstream infinity is taken to be of uniform velocity and temperature. The fluid is assumed to be inviscid, incompressible and irrotational everywhere except at points where simple inviscid line vortices are located. Attention is focussed on the shear layer separating from the top leading edge corner. The effect of the vorticity generated at the lower leading edge corner is assumed to be negligible.

The discrete-vortex model replaces the continuous sheet of vorticity entering the flow from the leading corner of the plate by a distribution of elemental line vortices. Vortices that recirculate upstream of the mean reattachment have their strengths reduced by a set fraction at each step to account for the generation of vorticity of opposite sign at the plate surface. In line with Morton [5], the amount of vorticity generated is matched to its generating mechanism - the tangential surface pressure gradient. A transverse fluctuating flow representing the acoustic field is also incorporated into the model.

The energy equation is solved using QUICKEST (Leonard [6]). This explicit scheme uses third order upstream differencing for the advection terms. The method approachs third order accuracy in both time and space as the Peclet number approaches infinity (but for a constant flow velocity).

A more detailed description of the discrete-vortex model and the finite-difference scheme used is contained in [7].

---

* CSIRO Division of Energy Technology, Melbourne, Australia

Results

A major reason for looking at this problem is to identify mechanisms responsible for changes in the heat transfer characteristics as the mean reattachment length is decreased through the application of sound. An important characteristic is the Nusselt number at the plate's surface. Figure 1 shows the mean Nusselt number along the surface of the plate for the following ratios of the acoustic particle velocity u_s to the approaching flow velocity v_∞: u_s/v_∞ = 0, 0.1 and 0.3. (The averaging is done over 1000 timesteps or 10 acoustic cycles. The Peclet number is 20). The mean separation bubble length shortens from 9H through 6H to 4H as the acoustic particle velocity is increased from zero through $0.1v_\infty$ to $0.3v_\infty$. (Here, H is the semi-thickness of the plate). The comparison of the curves indicates that an increase in the sound level results in a substantial increase in the peak value of the time-mean local Nusselt number.

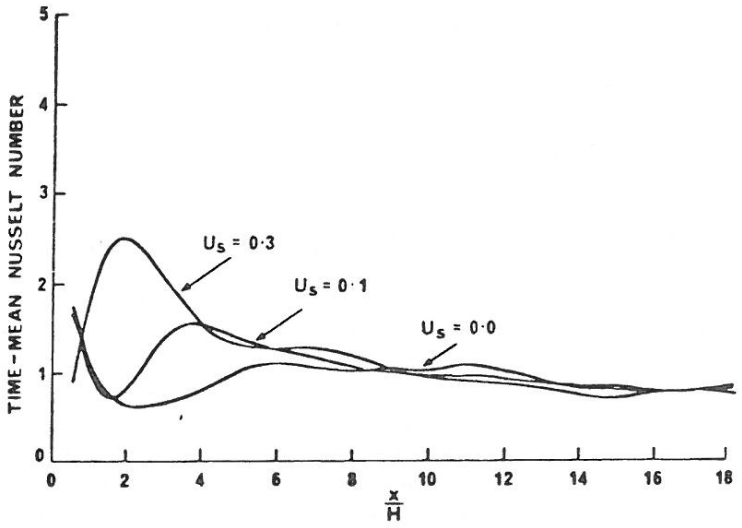

Figure 1. Predicted mean local Nusselt number for three different levels of acoustic perturbation.

Perhaps of more practical significance, reduction of the mean reattachment length is found to lead to a considerably greater time-mean Nusselt number averaged spatially over the plate. A quantitative comparison of the heat transfer characteristics at different sound levels can be made by averaging the Nusselt number over the first 10H of the length of the plate (this being typical of the plate lengths found in commercial heat exchangers) The values for the (spatially-averaged) time-mean Nusselt numbers are 0.95, 1.2 and 1.5 respectively. Thus the results indicate that by decreasing the reattachment length a substantial increase (up to 60% here) in the heat transfer can be achieved. This predicted trend is precisely in line with that found in experimental investigations (Cooper et al [3], Ota and Kon [2]).

An important feature of the present model is the prediction of the instantaneous flow. This allows further insight into the mechanisms responsible for the augmentation of the heat transfer rate. A 16mm movie film showing some of the numerical results has been made of the present simulations. Here, a 'snapshot' from the movie film is included in Figure 2 that characterise the flow structures and thermal field for a high sound case. The increased coherence of the flow through the locking of the vortex shedding to the acoustic field is clearly evident. Distortion of the isotherms near the large-scale vortex structures is seen. The local Nusselt number is found to be maximal immediately downstream of a vortex and to be minimal just upstream.

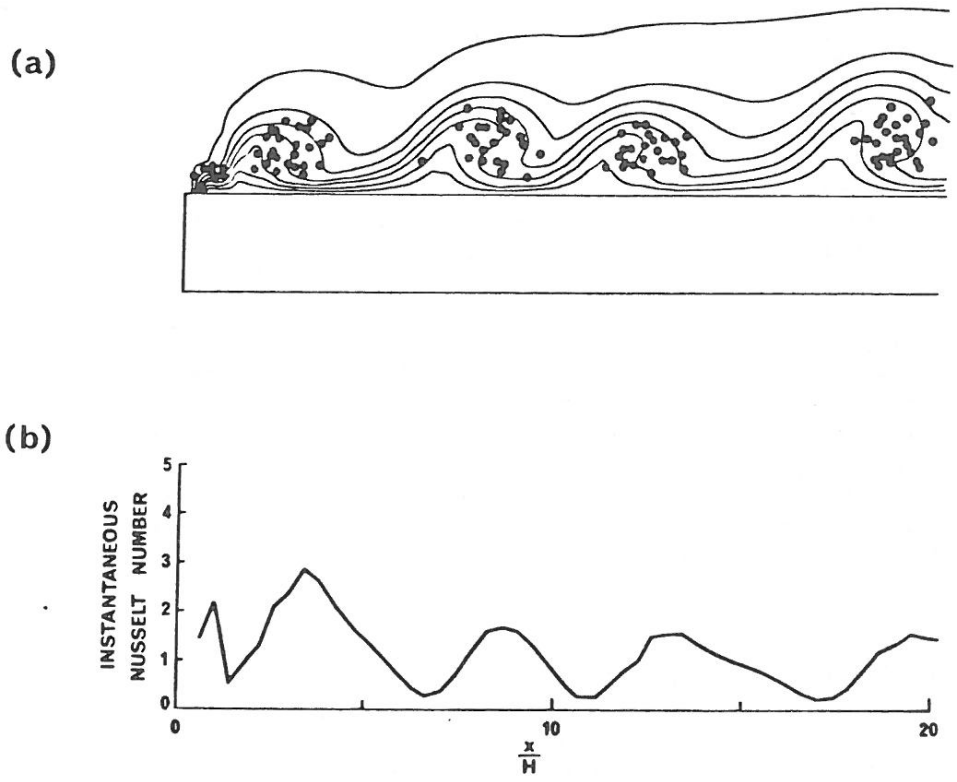

Figure 2. (a) Characteristic instantaneous isotherms for $u_s = 0.3v_\infty$. Small circles indicate positions of elemental vortices.
(b) Instantaneous local Nusselt number against distance along the plate surface.

The history of the temperature of a tracer particle released near the leading edge corner is shown in Figure 3. The repeated cooling and heating of the particle as it is moved towards and away from the plate's surface by the large-scale vortex structures is demonstrated.

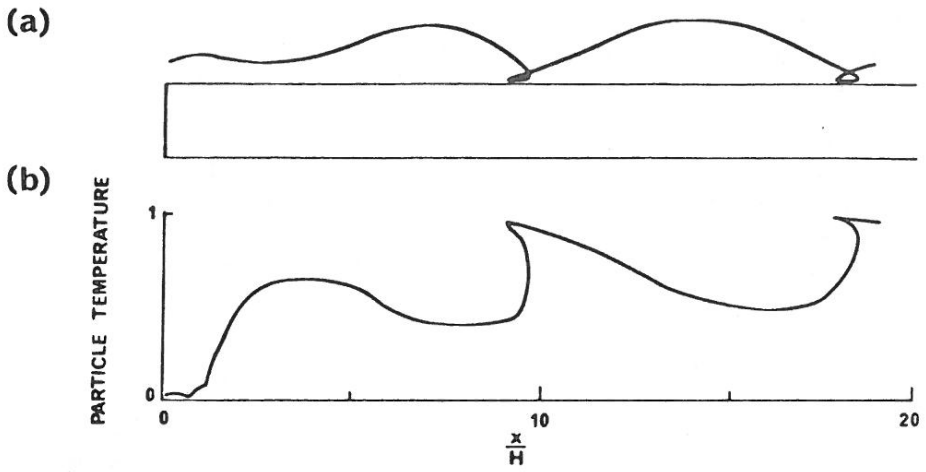

Figure 3. Thermal history of a passive tracer particle released near the leading edge. (a) particle trajectory and (b) temperature of the particle at the corresponding point on trajectory.

Another feature that was observed in the predictions of flows with high sound levels was the pressure distribution along the plate surface. During part of the sound cycle, a very large pressure drop close to the leading edge corner is recorded. This is related to the presence of a very concentrated growing vortex near this point. Modelling of the effect of smaller scale perturbations on the pressure distribution is being undertaken. It is hoped that this will provide insight into the effect of free stream turbulence on suctions on the plate surface.

References

[1] Ota, T. and Kon, N., Heat transfer in the separated and reattached flow on a blunt flat plate, Journal of Heat Transfer, 96 (1974) 459-462.

[2] Ota, T. and Kon, N., heat transfer in the separated and reattached flow over blunt flat plates - effects of nose shape, International Journal of Heat and Mass Transfer, 22 (1979) 197- 206.

[3] Cooper, P.I., Sheridan, J.C., Flood, G.J. and Welsh, M.C., The effect of sound on forced convection from a flat plate, Proceedings of the 8th Australian Fluid Mechanics Conference, University of Newcastle, Australia, (1983) 11C.9 - 11C.12.

[4] Parker, R. and Welsh, M.C., Effects of sound on flow separation from blunt flat plates, International Journal of Heat and Fluid Flow, 4 (1983) 113-128.

[5] Morton, B.R., The generation and decay of vorticity, Geophysical and Astrophysical Fluid Dynamics, 86 (1984) 277-308.

[6] Leonard, B.P., A stable and accurate convective modelling procedure based on quadratic upstream interpolation, Computer Methods in Applied Mechanics and Engineering, 19 (1979) 59-98.

[7] Thompson, M.C. and Hourigan, K., M.C., Combined finite-difference and discrete-vortex solution of acoustically perturbed two-dimensional separated flow around a heated plate, CTAC, The University of Melbourne, (1985) (provisionally accepted).

AEROELASTIC ANALYSIS OF SAILS

P.S. Jackson[1]

Introduction

The pressure distribution acting on a lifting surface depends on its shape, and usually this shape is fixed - that is, the aerodynamic loads do not cause significant changes in the shape of the lifting surface. However the shape of a sail under load depends strongly on the distribution of pressure over it, so that the shape determines the pressure but the pressure is determined by the shape. Therefore in order to predict this shape from first principles it is necessary to solve the aerodynamic and structural problems simultaneously. One way of doing this is to split the problem into two - that is, first assume a fixed shape for the sail and calculate the pressure distribution acting on it, then hold the pressure fixed and calculate the shape taken up by an elastic membrane under the action of the pressure loads, then repeat the whole process. This is the basis of a successful solution method which has been developed by the author (Jackson, 1982, 1985) together with his colleague Dr G.W. Christie.

Prediction of Sail Shape

The sail is modelled as a surface of constant-strain triangles connected at the nodes, allowing the state of strain of each triangle to be expressed in terms of the displacements of its nodes. If the nodes are displaced from an equilibrium position by a small distance, the virtual work done by the forces at the nodes is exactly balanced by the change in strain energy of the elements, and this statement can be expressed as a nonlinear relationship between the sail shape, the applied pressures, the material properties and the unknown nodal displacements. A detailed derivation of these equations is given by Oden and Sato (1969).

The calculation of the strain energy requires some statement about the stress/strain relationship of the sail fabric. As the strains in the sail membrane are small (not exceeding 0.5%), a linear constitutive law can be used. It is convenient to suppose that the fabric is isotropic. While it is not difficult to account for this, here only isotropic behaviour is assumed so that the elastic modulus E is all that is needed to describe the cloth stiffness. It is also necessary to model the inability of real membranes to withstand compressive in-plane stress - a membrane simply buckles, or wrinkles.

Dimensional analysis suggests that an important ratio is the aeroelastic number

$$æ = E\ t/L\ q\ ,$$

where q is the dynamic wind pressure, and t/L the ratio thickness to chord of the sail. Jackson (1985) has shown that this number represents the ratio of the elastic stiffness of the sail to its aerodynamic stiffness (the rate of change of aerodynamic force with sail displacement). In practice this number is large (at least 10^3), so that there is no need to actually calculate this aerodynamic stiffness. The physical significance of the

---

[1]Department of Mechanical Engineering, University of Auckland.

number is that any two sails with the same value of ff and the same boundary and upstream conditions will experience the same strains and generate the same lift coefficients at the same angle of attack.

As the system of equations for the nodal displacements is highly nonlinear, it is solved iteratively using the Newton-Raphson method. The applied pressures vary as the solution proceeds, and progressively approach the correct values as the membrane solution approaches its final shape. The solution method is discussed in more detail by Jackson (1985).

Pressure Prediction

The pressure forces are calculated using potential flow theory, in which boundary layers are effectively regarded as vortex sheets having zero thickness but with a finite jump in velocity across them. The sheet strength is found by requiring the sum of the flow induced by the sheet and the incident flow to be tangential to the sail surface. Since the finite element model needs only the average pressure on each element it is convenient to use a boundary element method in which the vorticity contained within each element is concentrated around its edges as a vortex loop - the vortex sheet then becomes a so-called vortex lattice. The strength of the loops is then found by applying the zero normal flow condition at the center of each element, giving as many equations as unknowns. This technique is well established in conventional aerodynamics.

The solution obtained is not unique unless the points at which the flow separates from the sail surface to form the wake are defined. The only situation for which this can be done accurately is that where the flow leaves the trailing edge of the sail smoothly, and this 'Kutta' condition is easily applied by extending the vortex loops adjacent to the trailing edge so that they trail off to infinity downstream of the sail.

The presence of the water surface is accounted for by including the image of every vortex loop in the surface. The approaching freestream flow is actually sheared and twisted by the vectorial addition of the wind boundary layer and the boat velocity, so that some vertical displacement of streamlines occurs as the wind approaches the sail. This displacement is ignored, but could be accounted for by yet more iterations. As there are no viscous effects included it is not possible to predict drag arising from skin friction, or the onset of stall.

Results for a Simple Sail

A rather idealised sail has been chosen as an example. The sail is triangular with no gap under the foot. It has no pretensioning and no initial camber, so in the absence of wind loading it is perfectly flat. The elastic constant for the membrane is ff = 1000, which means that if a 2-D membrane were loaded uniformly with a pressure of q it would deflect laterally to a displacement of about 4% of the chord. The corner nodes of the sail are totally constrained, as are those on the leading edge (luff). The trailing edge (leech) nodes are not restrained at all.

Figure 1 shows the equilibrium shape of the sail under wind loading at six equi spaced heights for an angle of attack of 10°. Since the flat sail must stretch under the action of *any* transverse loading, the loaded sail has acquired both camber and twist. Aerodynamic loading is strongly concentrated near the leading edge (it reduces to zero at the leech) so the camber tends to be larger there. However because the leech is unconstrained it has little resistance to transverse loads and thus allows the sail sections to twist so as to reduce the angle of attack. Initially this

effect is very pronounced but once the sail has acquired some geometric stiffness by virtue of curvature along the leech between the two restrained corners it becomes progressively more resistant to lateral loading. This is reflected in the change in lift coefficient with angle of attack, as shown in Figure 2.

The twist developed by the membrane sail means that its lift is less than that of a rigid sail of the same initial shape, which is also shown. The stresses in this sail for an angle of attack of 10 degrees are shown in Figure 3. Here the line segments are proportional to the principal stresses of the elements, and lie in the same directions. It can be seen that in many cases the elements do not show a minor principal stress, which means that they are wrinkled. If the aeroelastic number is now reduced by a factor of five the sail develops much more twist, as shown by the rear views of the sails for the two levels of stiffness shown in Figures 3 and 4. If this reduction in Æ has occurred because the sail is more stretchy then the levels of stress are also reduced because less lift and more curvature are developed - this can also be seen in these figures. However if the sail is the same but Æ is reduced by an increase in dynamic pressure, then the stresses as plotted must be increased by the same factor - this leads to an increase in stress, as expected. To demonstrate the effect of boundary conditions the edge restraints are now altered so that both the luff and foot slide along their respective axes. The stress distribution produced is that shown in Figure 5. While this is markedly different from Figure 3 the levels of indued camber and twist are about the same, as expressed by the small difference between lift coefficients for the two sails (Fig 2). The final example is more realistic shape with initial vertical and horizontal camber. Because the unloaded shape has curvature it also has a greater geometric stiffness, but as the same camber also greatly increases the lift the net level of stress is about the same as before. Figure 6 shows that the stress now tends to be concentrated along the leech.

Conclusions

One of the obstacles to rational sail desgin has been the absence of any means of engineering analysis. While it will now be possible to estimate the structural and aerodynamic performance of any given sail, it is hoped that this method will identify the most important of the numerous variables in sail design and thus lead to the development of a simpler model which can be used to predict optimum sail shapes directly.

References

Jackson, P.S. (1982); *'A 3-D aeroelastic sail model'*, Science of Sail Design, conf. proc. University of Western Ontario Boundary Layer Wind Tunnel Laboratory, June.

Jackson, P.S. (1985); *'The analysis of three-dimensional sails'*, CANCAM proceedings,

Oden, J.T. and T. Sato (1967); *'Finite strains and displacements of elastic membranes by the finite element method'*, Int. J. Solids Structures, 3, 471-488.

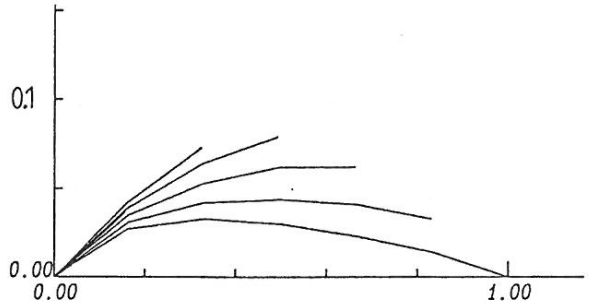

Figure 1 : Sections of loaded sail (Flat-1), initially flat.

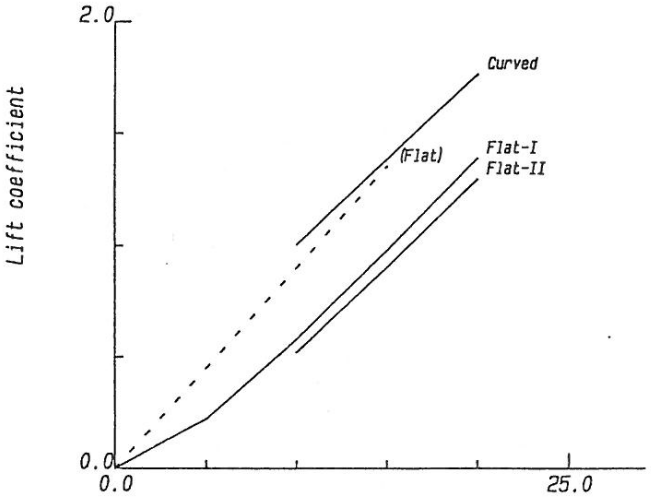

Figure 2

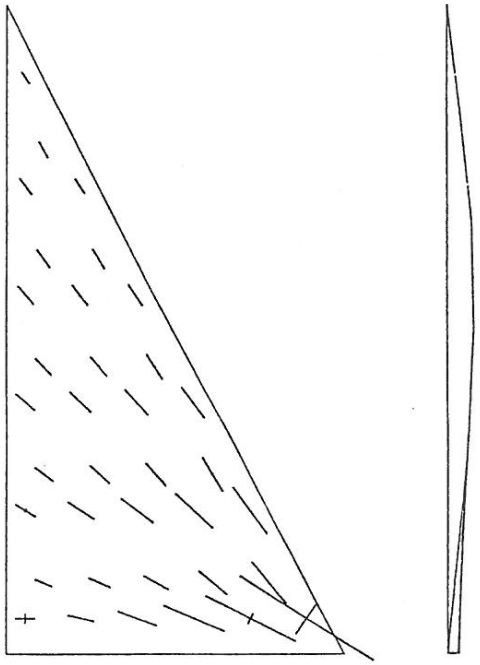

Figure 3 : Shape and stress of initially-flat sail (Flat-I) - fixed luff, Æ = 1000.

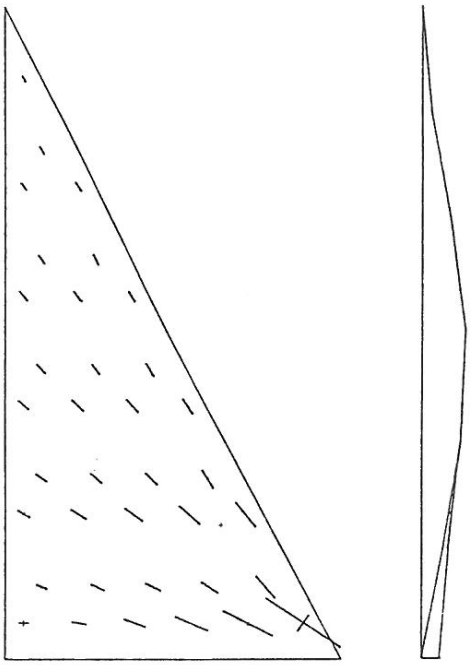

Figure 4 : Shape and stress of initially-flat sail (Æ = 200).

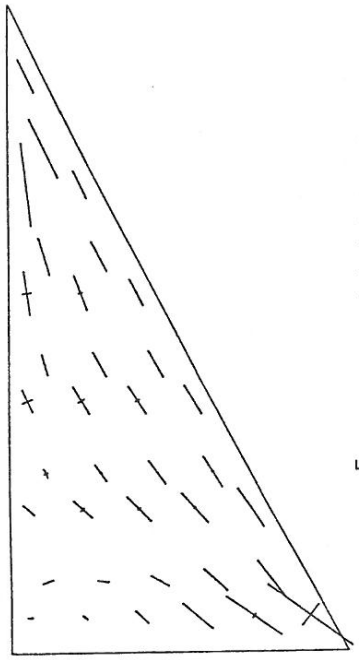

Figure 5 : Stress of initially-flat sail (sliding edges)

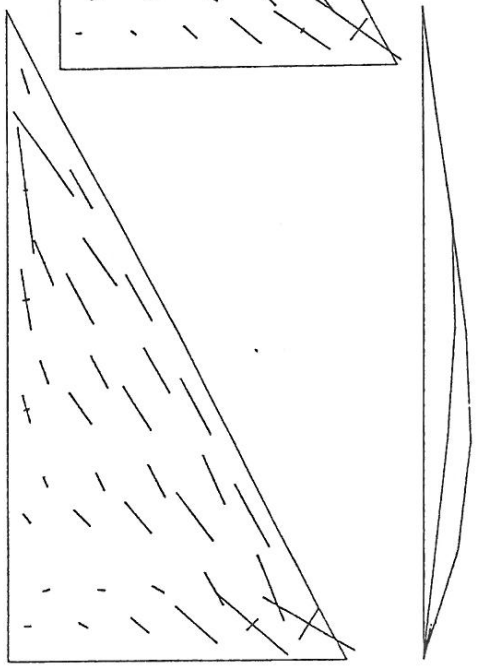

Figure 6 : Shape and stress of initially-curved sail.

WIND LOADS ON ATTACHED CANOPIES

E.D. Jancauskas[1] and J.D. Holmes[2]

Introduction

Despite the fact that the vast majority of canopy-type structures are installed in an attached configuration (that is, abutting an enclosed parent building) there has to date been no detailed study reported on the wind loads that such structures attract. This absence of information in the open literature is reflected in the Australian Wind Loading Code, AS1170 Part 2 - 1983, which provides no guidance on wind loads for attached canopies.

As a consequence of this absence of information, the Department of Civil & Systems Engineering at James Cook University and the CSIRO Division of Building Research embarked on a collaborative research project aimed at measuring the wind loads on this class of structure. This paper, which presents selected results from this project, describes the uplift forces on attached canopies as a function of the relative geometry of the canopy and the adjacent building. This data forms the basis of a codified description of attached canopy loads prepared by the authors for the upcoming revision of the Australian wind loading code.

Experimental Technique

The measurements reported in this paper were made in the boundary layer wind tunnels at James Cook University (Townsville) and CSIRO Division of Building Research (Melbourne). In both cases, a simulated boundary layer equivalent to flow over rural (Category 2) terrain was established using a combination of a plain barrier and carpet roughness. At a nominal scale of 1/75, the mean velocity and turbulence intensity profiles were a good fit to those of Deaves & Harris [1] with a roughness length (Zo) of 0.03 m.

The basic canopy dimensions, the canopy thickness and the dimensions of the parent building were identical for both laboratories. Figure 1 shows a schematic representation of the attached canopy configuration, together with the adopted nomenclature.

Although both laboratories measured the integrated peak loads exerted on the attached canopies, the experimental techniques employed were entirely different. At James Cook University the forces were measured directly using lightweight canopy models of various sizes mounted on a sensitive three-component force balance [2]. The clearance gap between the canopy and the parent building was sealed with a latex membrane. At the nominal scale of 1/75, the canopies had a frequency response equivalent to approximately 3.5 Hz in full scale.

The measurements performed at CSIRO were obtained using a pressure-based technique. Eight pressure transducers were used to simultaneously monitor pneumatically-averaged pressures from 48 pressure tappings on both sides of the canopy model. Manifolding was done internally within the canopy model, and the system had a frequency response equivalent to approximately 10 Hz in full scale (assuming a scale of 1/75).

Results

The canopy loads are given in terms of mean and peak nett vertical force coeffic-

---

1. James Cook University of North Queensland
2. CSIRO Division of Building Research.

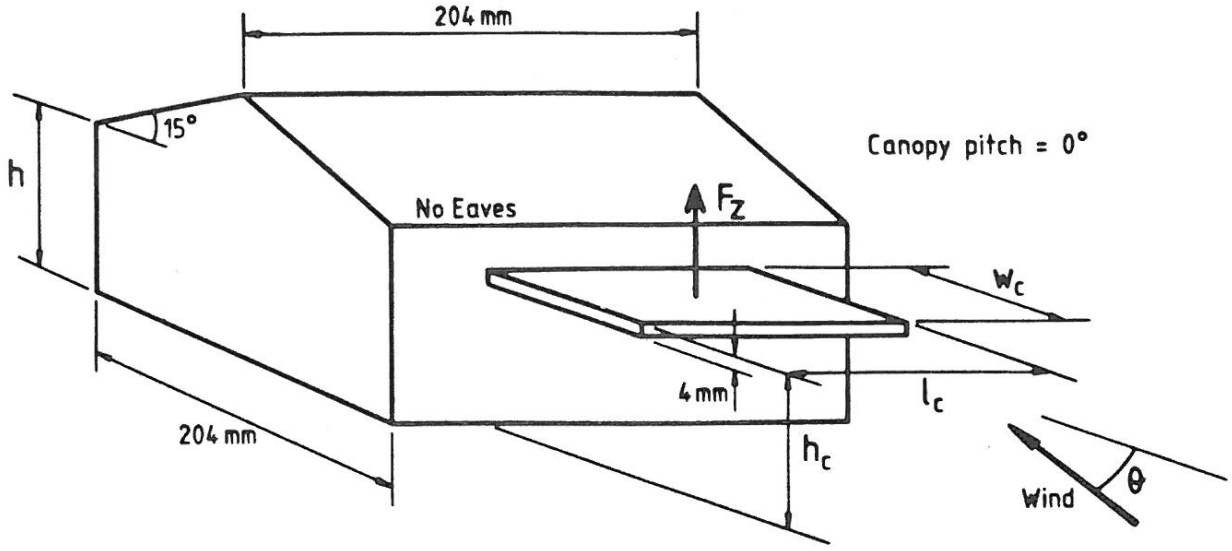

Figure 1 The attached canopy configuration.

ients, $C_{\bar{F}_z}$ and $C_{\hat{F}_z}$, defined as follows:

Mean coefficient $$C_{\bar{F}_z} = \frac{\bar{F}_z}{\frac{1}{2}\rho \bar{u}_c^2 A}$$

Peak coefficient $$C_{\hat{F}_z} = \frac{\hat{F}_z}{\frac{1}{2}\rho \bar{u}_c^2 A}$$

where $\bar{F}_z$ = mean nett vertical force on the canopy

$\hat{F}_z$ = peak nett vertical force on the canopy occurring within a time equivalent to 10 minutes full scale

$\bar{u}_c$ = mean wind velocity at canopy height

A = area of the canopy.

For the purpose of codification, the peak coefficients have been converted to quasi-steady (code-type) coefficients defined as

Quasi-steady Coefficient $$(C_{F_z})_o = \frac{\hat{F}_z}{\frac{1}{2}\rho \hat{u}_c^2 A}$$

where $\hat{u}_c$ = peak 2-3 second gust velocity at canopy height.

This conversion was based on pressure gust factors $\left(\frac{\hat{u}_c}{\bar{u}_c}\right)^2$ of 2.6, 2.7 and 2.85 at the three canopy heights of 84 mm, 63 mm and 42 mm respectively.

The canopy loads have been tabulated in Table 1 and plotted as a function of canopy height-to-width ratio in Figure 2.

Discussion

The first point that should be noted is that there was very good agreement between the measurements made using the two different experimental techniques. This was so not only with regard to the mean forces but also the peaks.

TABLE 1 MEASURED UPLIFT FORCES ON ATTACHED CANOPIES

Run	Wind Direction θ	h (mm)	hc (mm)	wc (mm)	lc (mm)	$\frac{hc}{h}$	$\frac{hc}{wc}$	UPLIFT C_{F_z}	UPLIFT $C_{\hat{F}_z}$	UPLIFT $(C_{F_z})_o$
JCU										
1	0°	84	84	64	96	1.0	1.31	+0.85	+2.28	+0.88
2	45°	84	84	64	96	1.0	1.31	+0.64	+2.11	+0.81
3	90°	84	84	64	96	1.0	1.31	-0.02	+1.06	+0.41
4	0°	84	84	36	96	1.0	2.33	+1.34	+3.58	+1.38
5	0°	84	84	36	192	1.0	2.33	+1.21	+3.16	+1.22
6	0°	84	84	52	96	1.0	1.62	+1.03	+2.71	+1.04
7	0°	84	84	96	96	1.0	0.88	+0.65	+1.69	+0.65
8	0°	63	63	64	96	1.0	0.98	+0.64	+1.88	+0.70
9	0°	42	42	64	96	1.0	0.66	+0.50	+1.43	+0.50
10	0°	84	63	64	96	0.75	0.98	+0.26	+1.06	+0.39
11	0°	84	42	64	96	0.50	0.66	-0.01	+0.51	+0.18
CSIRO										
12	0°	84	84	64	96	1.0	1.31	+0.87	+2.37	+0.91
13	0°	84	84	32	96	1.0	2.63	+1.35	+3.64	+1.40
14	0°	84	63	64	96	0.75	0.98	+0.38	+1.31	+0.49
15	0°	84	63	32	96	0.75	1.97	+0.37	+1.70	+0.63
16	0°	84	42	64	96	0.50	0.66	-0.01	+0.65	+0.23
17	0°	84	42	32	96	0.50	1.31	-0.21	+0.56	+0.20

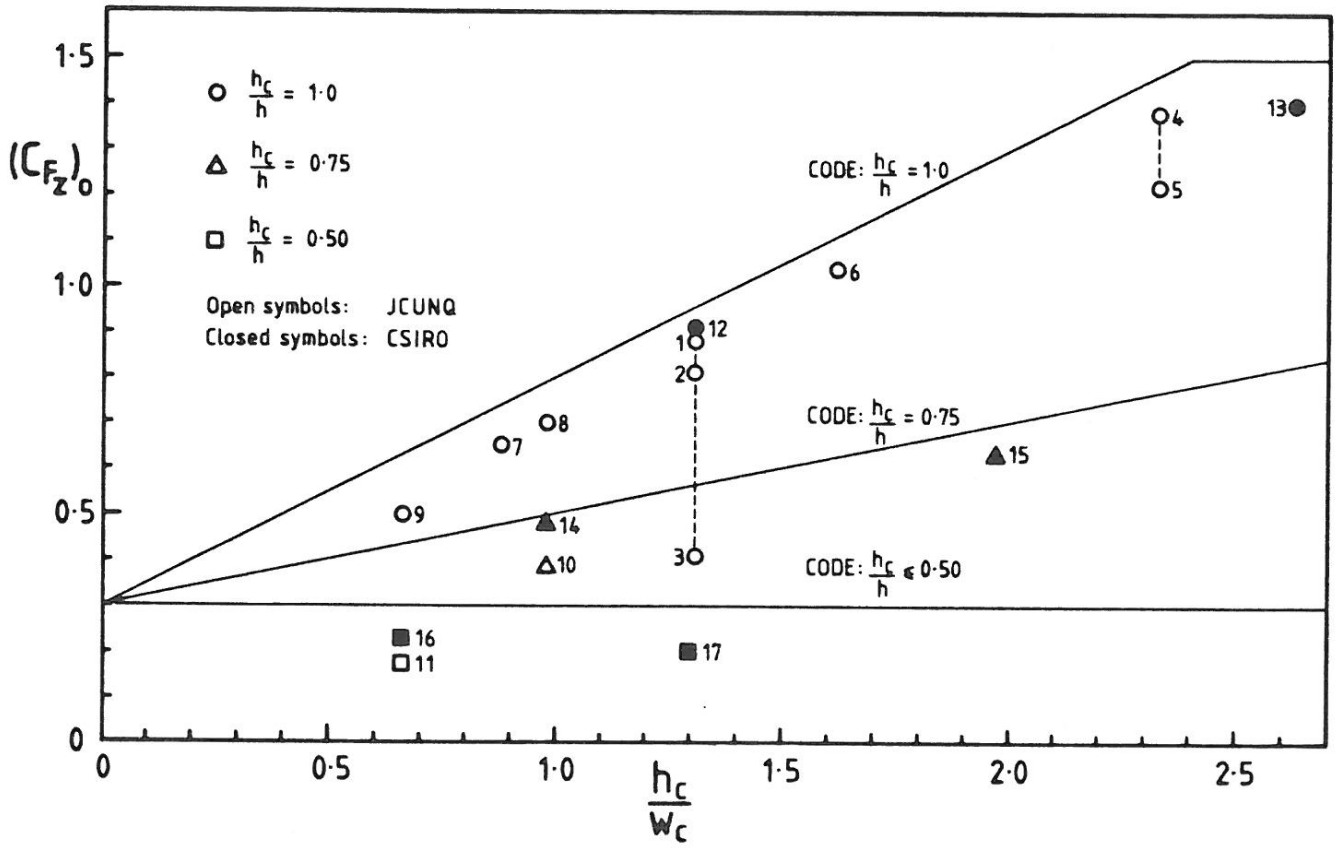

Figure 2 Measured uplift force as a function of canopy height-to-width ratio.

As a comparison between runs 1, 2 and 3 demonstrates, the uplift force on the attached canopy was greatest for a wind direction of $\theta = 0°$. This of course corresponds to the development of maximum stagnation pressure under the canopy.

Runs 4 and 5 indicate the effect of the canopy length, ℓ_c. As the length of the canopy is increased (keeping the canopy height and width constant), the uplift per unit area is decreased. This is due primarily to the decrease in the correlation of the forces over the increased span of the canopy.

The remainder of the runs investigate the dependence of the uplift forces on the

two ratios, $\frac{h_c}{h}$ and $\frac{h_c}{w_c}$. Decreasing either of these ratios decreases the uplift on the canopy. In the case of $\frac{h_c}{h}$, a decrease in the ratio corresponds to an increase in the amount of parent wall above the canopy. This produces increased stagnation of the flow above the canopy and a decrease in the nett uplift.

In the case of $\frac{h_c}{w_c}$, a decreased value corresponds to an increase in canopy width for a given canopy height. This results in a decrease in the proportion of the total upper surface of the canopy under the reattaching shear layer shed from the leading edge of the canopy. Consequently, the uplift per unit area is decreased.

Code Recommendation

On the basis of the above data, the authors offer the following codified description of the uplift forces on attached canopies:

For $\frac{h_c}{h} = 1.0$: $(C_{F_z})_o = 0.3 + 0.5\ (\frac{h_c}{w_c})$ or 1.5, whichever is the lesser

For $\frac{h_c}{h} = 0.75$: $(C_{F_z})_o = 0.3 + 0.2\ (\frac{h_c}{w_c})$ or 1.5, whichever is the lesser

For $\frac{h_c}{h} \leq 0.5$: $(C_{F_z})_o = 0.3$

Linear interpolation may be used to obtain values for $\frac{h_c}{h}$ ratios other than those shown.

These recommendations have been plotted in Figure 2. It can be seen that in all cases the code recommendations conservatively estimate the uplift forces on attached canopies.

Conclusions

- There was very good agreement between the measurements of peak uplift made at James Cook University and CSIRO using entirely different experimental techniques.
- The maximum uplifts on attached canopies occur for a wind direction of $\theta = 0°$.
- The wind loads on attached canopies are primarily dependent on the two ratios $\frac{h_c}{h}$ and $\frac{h_c}{w_c}$.
- The code recommendation offered by the authors conservatively estimates the uplift forces on attached canopies.

Acknowledgements

This research was funded by a grant from the CSIRO/James Cook University Collaborative Research Fund. The technical assistance of Mr. G. McNealy is gratefully acknowledged.

References

1. Deaves, D. and Harris, R.I. "The Structure of Strong Winds", Cranfield Institute of Technology Report, 1981.

2. Roy, R.J. "Total Force and Moment Measurement on Wind Tunnel Models of Low Rise Buildings", M.Eng.Sc. Thesis, James Cook University, 1982.

WIND-INDUCED FORCES AT THE TRUSS-WALL CONNECTIONS IN A LOW-RISE BUILDING

E.D. Jancauskas[1] and J.A. Harris[1]

Introduction

Failure of the tie-down connections between roof trusses and wall frames remains a common mode of failure of low-rise structures in severe wind storms. This paper describes the results of a wind tunnel investigation into the wind loads induced at the truss-wall connections in a typical single-story tropical house.

Experimental Technique

The measurements reported in this paper were made in the boundary layer wind tunnel at James Cook University. The measurements were made on a 1/50 scale model of a typical single-story tropical house. The house had a full-scale plan of 14 m x 7 m, an eaves height of 3 m, a gable roof with a pitch of 10°, large (1.2 m) eaves and 0.45 m verges. This geometry was identical to that tested by Best & Holmes [1] and Holmes [2]. The dimensions of the model are shown in Figure 1.

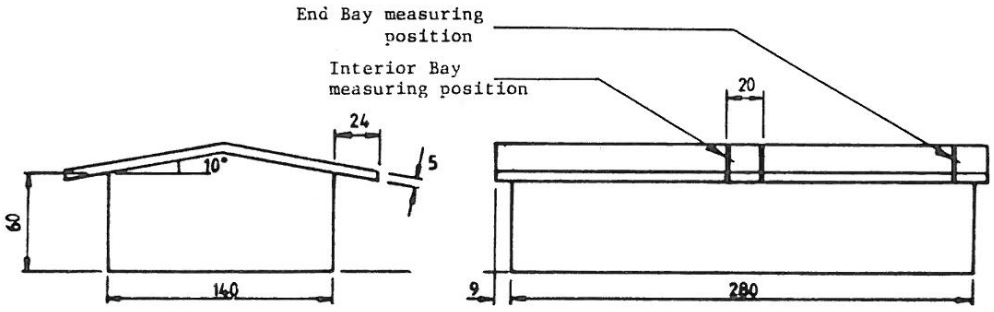

Figure 1 Dimensions of the wind tunnel model

A section of the roof equivalent to the typical area of influence of a single roof truss (1.0 m wide in full-scale for this type of structure) was isolated from the rest of the house and mounted on a sensitive three-component force balance [3]. The fluctuating lift force and moment outputs from the force balance were converted to fluctuating loads at the two truss-wall connections using simple static relationships.

As shown in Figure 2, the measuring panel was constructed so that it could be configured as either an interior bay or an end bay. Very fine latex rubber was used to seal the clearance gaps between the measuring panel and the adjoining segments. The pressure inside the house (underneath the measuring panel) was vented to the static pressure in the wind tunnel. This measurement system had a frequency response equivalent to approximately 6 Hz in full scale.

Boundary Layer Simulation

All tests were performed in a simulated boundary layer equivalent to flow over rural (Category 2) terrain. The boundary layer was generated using a combination of carpet roughness and a 350 mm high plain barrier located 12 m upstream of the model. Both the mean velocity and turbulence intensity profiles were a good fit to those of Deaves & Harris [4] with a roughness length (Z_o) of 0.02 m.

---

1. James Cook University of North Queensland.

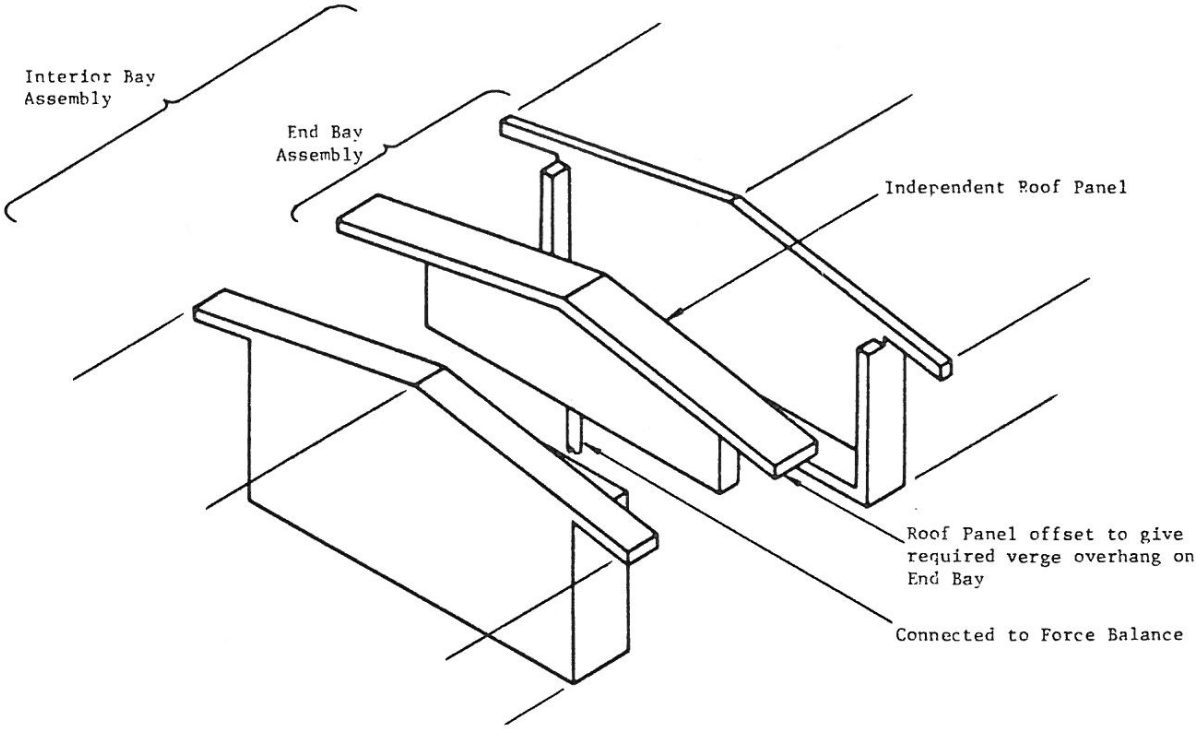

Figure 2 Arrangement of the measuring panel

Results

The measured forces at the truss-wall connections were reduced to coefficients using the dynamic pressure based on the mean velocity at eaves height:

$$C_{R1} = \frac{R1}{\frac{1}{2}\rho\bar{u}^2 A_R}$$

$$C_{R2} = \frac{R2}{\frac{1}{2}\rho\bar{u}^2 A_R}$$

where R1 = force on the windward truss-wall connection
R2 = force on the leeward truss-wall connection
$\bar{u}$ = mean velocity at eaves height
A_R = plan area of roof bay

The symbols $-$ and $\hat{}$ have been used to denote mean and peak forces, respectively. The peak forces correspond to those occurring within a time equivalent to 10 minutes in full scale, and were obtained from an average of at least 16 runs.

Table 1 shows the measured mean and peak force coefficients for the 4 different configurations tested:

- Centre Bay for $\theta = 0°$
- End Bay for $\theta = 0°$
- End Bay for $\theta = 60°$
- End Bay for $\theta = 90°$

Using appropriate influence coefficients, corresponding truss-wall force coefficients were computed from three other sources:

1. Australian Wind Loading Code, AS1170 Part 2 - 1983
   Peak coefficients were calculated on the basis of a pressure gust factor $\frac{\hat{u}^2}{\bar{u}^2}$ of 3.14 (obtained from Deaves & Harris' model [4]).

Table 1 Measured and Predicted Loads at the Truss-Wall Connections

Configuration	Coefficient	Measured	AS1170 Pt. 2 1983		Best & Holmes (Point Pressures)	Holmes (Covariance Integration)
			No L.P.F.	With L.P.F.		
Centre Bay, $\theta = 0°$	$C_{\overline{R1}}$	-0.55	-0.48		-0.43	-0.43
	$C_{\hat{R1}}$	-1.56	-1.51		-1.42	-0.86
	$C_{\overline{R2}}$	-0.23	-0.20		-0.22	-0.16
	$C_{\hat{R2}}$	-0.64	-0.63		-0.52	-0.32
End Bay, $\theta = 0°$	$C_{\overline{R1}}$	-0.36	-0.38		-0.22	
	$C_{\hat{R1}}$	-1.45	-1.19		-0.91	
	$C_{\overline{R2}}$	-0.15	-0.10		-0.18	
	$C_{\hat{R2}}$	-1.10	-0.31		-0.95	
End Bay, $\theta = 60°$	$C_{\overline{R1}}$	-1.04			-0.65	
	$C_{\hat{R1}}$	-2.19			-2.69	
	$C_{\overline{R2}}$	-0.82			-0.61	
	$C_{\hat{R2}}$	-2.27			-2.42	
End Bay, $\theta = 90°$	$C_{\overline{R1}}$	-0.80	-0.55	-0.85	-0.60	
	$C_{\hat{R1}}$	-2.36	-1.64	-2.67	-2.64	
	$C_{\overline{R2}}$	-0.84	-0.55	-0.85	-0.60	
	$C_{\hat{R2}}$	-2.60	-1.64	-2.67	-2.46	

2. Mean and peak point pressure measurements made by Best & Holmes [1] on an identical model.
3. Truss-wall force coefficients computed by Holmes [2] using the covariance integration technique.

These estimates are also presented in Table 1.

Discussion

Agreement between the measured coefficients and those calculated from the pressure distributions of Best & Holmes [1] was, on the whole, reasonably good. Poorest agreement occurred for the loads on the windward connection in the two configurations having a wind direction of $\theta = 0°$. A possible explanation for the lower coefficients of Best & Holmes is the low density of pressure taps close to the leading edge of their model roof.

A comparison with the covariance integration work of Holmes [2] was only possible for the centre bay configuration with $\theta = 0°$. As can be seen from Table 1, while there was reasonable agreement between the mean values, Holmes' peak coefficients were significantly below those measured. This was primarily a result of the relatively low pressure gust factor used by Holmes (2.0 compared to 3.14 in this study).

The most interesting comparisons, however, were between the measured loads and those predicted by the Code. For the centre bay configuration, the agreement was excellent. For the end bay configurations, however, the agreement was not so comforting. For $\theta = 0°$, while there was good agreement between the mean coefficients, the peak Code coefficients were significantly below those measured, particularly for the leeward truss-wall connection. This deficiency relates to one of the known limitations of the quasi-steady approach, namely the calculation of peak forces using mean coefficients which are close to zero.

The most important comparison of this study, however, was for the end bay loads at $\theta = 90°$. For this configuration, the Code underestimated the measured truss-wall forces by approximately 35%. The loads on the end bay for this wind dir-

ection are dominated by the high suctions developed under the reattaching shear layer shed from the gable edge of the roof. While the Code recognises the increased pressures that result from this mechanism (through the provision of local pressure factors), it does not require application of these factors to an area as large as a bay; the assumption being that these increased pressures will not be well correlated over such an area. This assumption is obviously not justified for the case of a relatively narrow end bay for a wind direction of $\theta = 90°$. As Table 1 shows, if the local pressure factors are included in the calculation of the truss-wall connection forces, the Code produces a (conservative) result very close to the measured loads.

Conclusion

Loads at the truss-wall connections of a single-storey tropical house have been measured. The results demonstrate that for the case of a typical domestic end bay the loads predicted by the Australian Wind Loading Code are unconservative.

Acknowledgements

These measurements were undertaken as part of a wider project on wind-induced fatigue, and were funded by the Australian Research Grants Scheme.

References

1. R.J. Best and J.D. Holmes. "Model Study of Wind Pressures on an Isolated Single-Storey House", James Cook University Wind Engineering Report 3/78, September 1978.

2. J.D. Holmes. "Wind Pressures and Forces on Tropical Houses", Final Report of Project No. 17 of the Australian Housing Research Council, February 1980.

3. R.J. Roy. "Total Force and Moment Measurement on Wind Tunnel Models of Low Rise Buildings", M.Eng.Sc. Thesis, James Cook University, 1982.

4. R.I. Harris and D. Deaves. "The Structure of Strong Winds", Cranfield Institute of Technology Report, 1981.